POWER CONVERSION SYSTEM DESIGN FOR A LOW COST DOMESTIC PV SYSTEM

Lingling Sun

A thesis submitted for the degree of
Master of Engineering
in
Electrical and Computer Engineering
at the
University of Canterbury
Christchurch, New Zealand.

March, 2016

ABSTRACT

In the new global economy, renewable energy is central to solving the energy crisis. As a widely used renewable energy, the technologies of solar energy and energy storage are mature. The energy storage systems of PV system can transfer the generated energy and match the domestic load profile. Nearly 1/3 domestic energy consumption is household water heating system in temperate climates. As the energy storage medium with the most effectiveness, hot water is to be used in this project. Because of the cheap implementation and low maintenance cost, the hot water storage system has also been an important component of a typical household energy budget.

This PV conversion is designed for the household hot water heating system which is supplied by PV panels. MPPT method will be employed. The hot water cylinder and solar panels will also be optimized. 75% budget of required domestic hot water can be provided by this PV conversion system.

Key words: household water heater, photovoltaic (PV) system, MPPT, PV inverter.

ACKNOWLEDGEMENTS

Firstly, I am heartily thankful to my supervisor, Dr Alan Wood, who introduced me to the world of Power Conversion System Design for a Low Cost Domestic PV System. His encouragement, guidance and assistance from the initial to the final level of my work, enabled me to develop an understanding of the subject. His permanent patience and rigorous academic attitude has my uttermost gratitude and respect. Without his help and pioneering work, completion of this thesis will not be possible. At the second, I would like to thank technical staff, Mr Edsel Villa Mr Jac Woudberg, Mr Michael Cusdin, and Mr Philipp Hof (in order by first name). Thanks for their help and encouragement.

I also would like to thank my parents for their countless emotional and financial support. I thank my dear sister, Miss Xiao Han, who always stayed with me and took care of me.

CONTENTS

LIST OF TABLES

LIST OF FIGURES

Chapter 1

INTRODUCTION

With the immense amounts of luminous power from the sun reaching the earth, solar energy will be one of the best alternative energy sources in the future [1]. Because solar energy is widely available, the electricity bill in the home could be cut down via PV energy conversion into electricity energy [2]. This benign alternative energy leads to very little environmental issues. Nuclear reactions or chemicals are not involved in the utilization procedure, and then there are no emitting radionuclides and emission chemicals. This environmental advantage makes the solar energy an environmentally friendly power source [1].

As a renewable resource, solar energy is an ideal substitute for fossil fuels. PV power systems are low maintenance, and this reliable energy source is silent. If solar energy can be used by 1,000,000 houses, 4.3 million tons emissions of CO_2 would be reduced, which is equivalent to about 850,000 cars removed from the road [3].

The total electric energy consumption of household hot water heating is a significant component of domestic in energy usage in New Zealand [4]; water heating consumes approximately one-third of one home's electricity usage [5]. Because of the total electricity consumption of domestic water heaters in New Zealand, this usage proportion has made water heating a focus of strategies, policies and interventions in power efficiency. For instance, the website of EECA (Energy Efficiency and Conservation Authority) in New Zealand contains a lot of information on high efficiency domestic water heaters. Extra subsidies can be attracted by the installation both of solar energy systems and hot water heater systems [6]. The PV conversion system proposed in this thesis is an energy generation system to supply the household water heater, and this project could use the extra subsidies from both of these two sides. Because the solar energy system could be installed

and used immediately, this PV conversion system could become a popular household appliance.

In this project, a PV conversion system will be designed and tested. By the algorithm of MPPT (Maximum Power Point Tracking) controller, the MPP (Maximum Power Point) will be tracked and the maximum generation electricity will be output by PV panels. The characteristic of this PV conversion system is that the output is not the pure sinusoidal waveform. This simplifies the conversion system and reduces its cost.

1.1 Thesis Structure

- Chapter 1 presents a background and brief introduction of the PV conversion system and the thesis structure.
- In chapter 2, the method and knowledge is summarized and categorised into three classes, solar energy, hot water heating, and DC/AC inverter.
- In chapter 3, the PV conversion system is assessed. Software PVsyst is used to preliminarily design the PV system. The generation balance and money returned will be analysed and calculated based on the simulated results of PVsyst.
- The fourth chapter presents the main body frame of the PV conversion system. The system model is built part by part, the control method and some significant components are also illustrated in this chapter.
- In chapter five, software MATLAB is used to simulate the designed system. The system design model is modified with the help of the simulation results of MATLAB.
- The sixth chapter illustrates the schematics of PV inverter and the layout diagram of PCB. Most of components are decided and placed. Software Altium Designer helps to finish the system design of schematics and PCB.
- In chapter 7, as the controller, Arduino boards are used to run the control programs in this project. The the main parameters is shown on the LCD display.
- In chapter 8, the operating results of the PV inverter are shown and analysed.
- The discussion summary and conclusion is also presented in chapter 9.

Chapter 2

LITERATURE REVIEW

2.1 PV Power System

2.1.1 PV Generation

Photovoltaics is a technology to convert the light to electricity power directly at the atomic level. Semiconductor materials are used to produce the PV cell in the microelectronics industry, for example the widely used material silicon [7]. The semiconductor material, silicon, absorbs the power of photons and releases the electrons by the property of the photoelectric effect. An electric field is formed by the thin silicon wafer treated specially, one side is positive and another is negative [8].

Electrons are lost and released from the atoms of semiconductor silicon when the photons of light strike the PV cell. An electrical circuit is formed when the positive side and the negative are attached to the electrical conductors, the captured electrons flow in this electrical circuit, and then the electric current is generated. This free electric current products can be used as electricity energy to supply a load [8]. In this project, the load is a household water heater.

2.1.2 PV Application

A PV System can be classed into two main styles by the utilisation of energy, grid connected PV system connects to the utility grid and standard PV system only connect with loads (off-grid system). In these two different styles of PV power system, four primary applications can be used to provide energy in domestic [9].

- Pico PV system is a small PV off-grid system with a few Watts from a small panel to power small electronic loads.
- Standard domestic PV system provides power to lower power household loads and not connect with the utility grid. Relatively mature technologies have been used to satisfy the partly or mostly energy demand of a house.
- Hybrid systems combines the PV panels with the diesel generator. They are another kind of off-grid PV system in mini grids.
- Grid connected PV system can sell the extra PV generated power to grid to partly offset the electricity bill.

2.1.3 MPPT

The factors that affect the output energy of solar array are the effective irradiance, ambient temperature and shadowing [10-11]. Because fluctuating irradiance is the main factor affecting the output power of solar array, MPPT is necessary for PV power systems [12]. To capture the maximum generation of solar energy, the electronic circuits should be well-designed and the algorithm of control system needs be efficient. MPPT control describes a number of techniques to extract the maximum power of PV panels. To locate the MPP, the Perturb and Observe algorithm (P&O) (Hill Climbing algorithm) is suitable for the dynamically varying point [13]. In this project, Improved Perturb and Observe algorithm (ImP&O) is used to track MPP. The details of ImP&O will be analysed in section 4.3.1.

2.2 Water Heater

Hot water heaters are simply a resistor and a thermostat controller [14]. In according to the rule of thumb, the tank capacity of domestic water heaters should be accorded to the amount of hot water on the time with peak demand in every home. Generally the minimum volume of hot water is 50 L/day/person at the temperature between 50°C and 60°C [15]. In this project, 180 litres is chosen as a typical domestic water heater volume.

2.3 DC/AC Inverter Conversion

2.3.1 Pulse Width Modulation (PWM)

PWM (Pulse Width Modulation) is extensively used in electronic power conversion systems. By this means, a DC source is inverted to an AC energy to operate devices, and it is usually called DC/AC inverter [16]. PWM control signals are used to control the switching equipment of H-bridge. In this project, they are MOSFETs.

In this PV conversion system, the output PWM is not a pure sinusoidal waveform (PSW), it is a modified sinusoidal waveform (MSW). The duty cycle of a pure sinusoidal PWM is changed following the sinusoidal wave, the duty cycle of modified PWM is constant in a period [16]. The MSW signal can be used to switch H-bridge because of the resistive load, for which power quality is not important. An AC waveform is required; however, as all water heating elements are required to have a thermal cut-out. These are rated to operate with AC, and they may fail to operate if supplied by a DC voltage. Doing this reduces the filtering requirements for the DC bus, and makes the converter cheaper.

2.3.2 H-Bridge

The bridge structure is widely used in power electronic applications. Full-bridge and half-bridge structures are common switching configurations. The full bridge is also called H-bridge; four switches are placed at two sides of load [16]. Switching component MOSFETs are the significant elements. Compared with bipolar transistors, MOSFET has three terminals, drain, gate and source. MOSFET usually is in the off state, load can be controlled/switched at the place of the drain or source terminal of MOSFET. The turn-on voltage is applied by gate driver to the gate terminal with respect to terminal source [17].

Snubber circuits are necessary to prevent overvoltage for H-bridge MOSFETs. The snubber circuit effectively restricts the value of overvoltage across every MOSFET. Snubbers are the required for switches to cut down voltage stresses [18].

Advantages and necessities of snubber circuit are

- lower the voltage stresses of MOSFETs,
- lower the power dissipations of switches,
- improve the capabilities on over load and short-circuit protection,

The over-voltage snubber circuit is chosen to be used in this PV conversion system.

Chapter 3

SYSTEM ASSESSMENT

3.1 Introduction

The decision as to whether a PV power system should be grid connected or stand-alone must be partly decided by the local electricity rates. For most power companies, the buy-back tariffs of renewable energy are different in summer and winter. The tariffs for Meridian Energy are respectively 10c and 7c for every kWh in the winter (from 1 May to 30 September) and in the summer (1 October to 30 April) [19]. The power companies Contact Energy and Mercury will credit 9 and 8 cents per kilowatt hour in whole year. All of these tariffs are excluding GST [20]. Although power companies change tariffs from time to time, compared with other power companies in New Zealand, these three companies are the best.

Compare with the average residential cost per unit (28.86 c/kWh) [19], the buyback price of the electricity is low (refer to Table 1).

Table 1: Residential electricity cost and solar power buy back rate

cost price	28.86 c/kWh	
Buy-back price	Contact	9 c/kWh
	Meridian Energy	10 c/kWh (in the winter)
		7 c/kWh (in the summer)
	Mercury	8 c/kWh

In this project, the energy storage ability of a domestic water cylinder is used to maximise the locally used energy, avoiding the retail cost of energy and also avoiding the low buy-back rates. The proposed system is also cheaper than a typical grid connected system, further improving the return on investment.

The aim of this project is to develop an interface between an array of PV panels and a resistive domestic water heating element. For the PV system, the software 'PVsyst' is used for modelling and analysis of power generation at MPP. The water heater load is estimated by AS/NZS 4234. In this chapter, the generation data and load data is calculated and compared. Matching these two, the economic efficiency is analysed. The schematic simulation model of the system is detailed in chapter 5.

3.2 Modelling Tool 'PVsyst'

PVsyst is software for solar power system design. PVsyst is able to import meteorological data, components from many different sources, and user-supplied data. The system design procedure is simple and quick; specify the available area or the desired power of PV panels, choose the PV module and the inverter from the internal database, and so on. The simulation results can be represented by PVsyst in forms, graphs and tables, and all the data can be exported. There are specific graphs, like hourly simulation of local irradiance, the I/V curve of the PV array, together with the MPPT range, and so on. The distribution of annual energy is also calculated by PVsyst. All results of a detailed study are printed in a complete report [21].

3.2.1 Irradiance Data

All of the main cities and locations of the world can be found in the internal database. The name of city or area is the only needed information, the irradiance and meteorological detail can be shown. Beam shading factors are linearly calculated by PVsyst, and the monthly Iso-shadings curve is represented when the plane orientation is equal to 30 degree (Figure 1). The distribution of annual irradiance is statistically analyzed. In Christchurch, New Zealand, the times when the irradiance is higher than 600W/m^2 is more than 1700 hours (Figure 2).

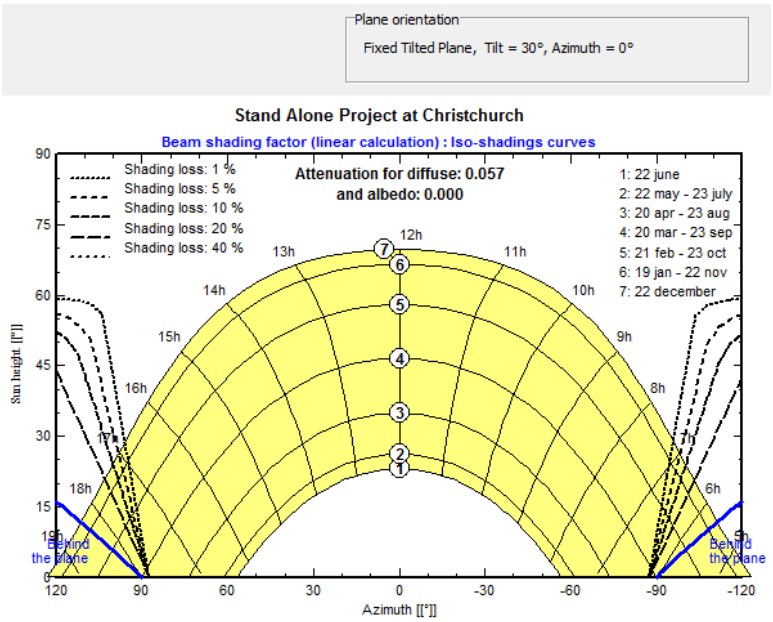

Figure 1: Iso-shadings curve of the standard PV system in Christchurch

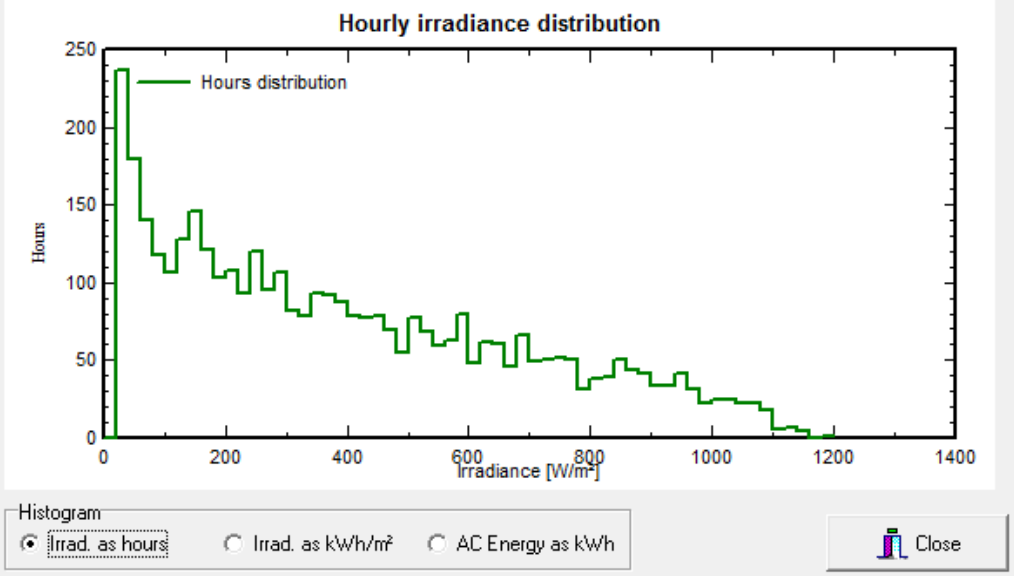

Figure 2: Hourly irradiance distribution for a standard PV system in Christchurch, New Zealand.

3.2.2 PV array

3.2.2.1 PV panel array

In this project, the panel DJ-195D/A which is made by NESL is used to generate the electricity (Appendix 1). DJ-195D/A is a monocrystalline PV panel, the power tolerance is guaranteed within 0-3% which is the peak power of modules, the peak power is guaranteed equal or more than the average power of single module and the life time is guaranteed not less than 25 years on minimum power output [22].

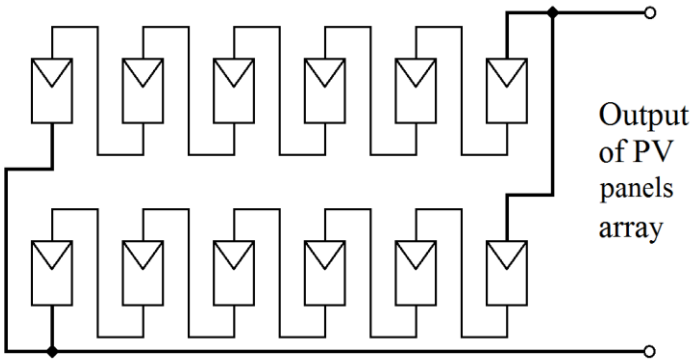

Figure 3: Connection diagram of PV array

The electrical data and mechanical data are given in Appendix 1. The PV panel array includes 12 solar panels, two rows are parallel connected such that in each row there are 6 panels in series as shown in Figure 3. The output voltage of the PV panels array V_{array} is shown in following equation.

$$V_{array} = V_{panel} * 6 = V_{mp} * 6 = 38.59 * 6 = 231.54\, Volt$$

The output voltage (231.54 Volt) is nearly the voltage of the supply grid (230 Volt). The proposed converter can only step panel voltage down, and the rated power of the array, at 2340 Watts, requires the element voltage to be stepped down to 203 Volts. 2.3 kW is around the optimal power for a system, as reported in Table A1-3 (Appendix 1). On the MPP, the PV panels array could generate up to 2.34 kW to supply household water heater.

$$I_{array} = I_{panel} * 2 = I_{mp} * 2 = 5.05 * 2 = 10.1\ Amp$$

$$P_{array} = P_{panel} * 12 = P_{max} * 12 = 195 * 12 = 2{,}340\ Watt$$

3.2.2.2 Shadow

The surroundings conditions are the source of shadow for PV panel array. After the surroundings import, PVsyst can simulate and show the shadow detail of any time in a year. It is assumed that there is only a building with PV array on its roof and nothing to shade the light, such as shown in Figure 4. The PV panels array, 2 parallel strings of 6 panels, is installed on the roof and faced north (Figure 5). In accordance with all of these settings, shadow details of solar array can be simulated and shown for any time. Figure 6 shows the shadow on the solar array in summer (17th January 2016, 13.00pm & 16.45pm) and winter (17th July 2015, 12.30pm & 16.45pm).

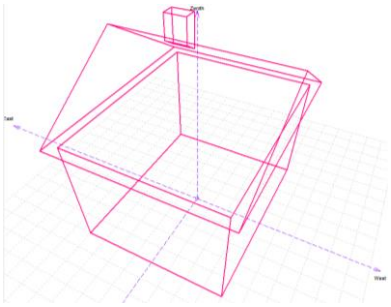

Figure 4: Surround conductions of solar array

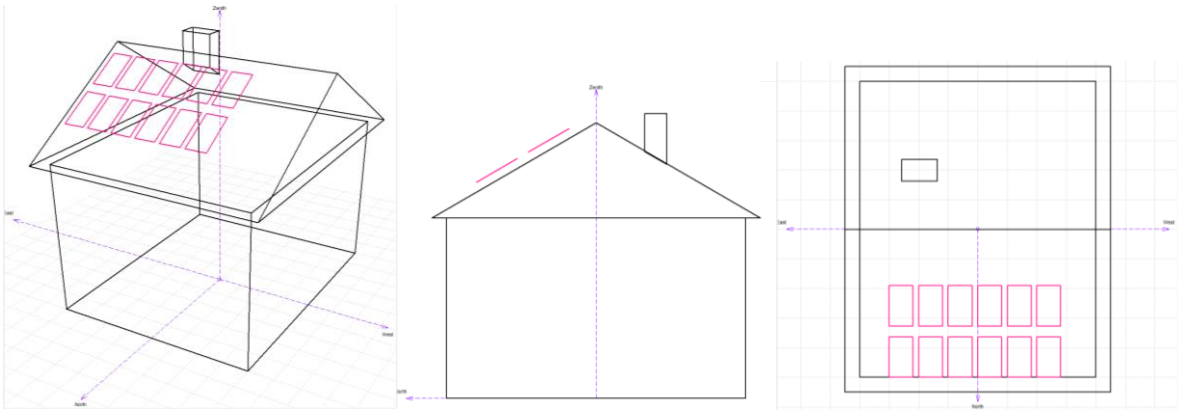

Figure 5: Layout of solar array

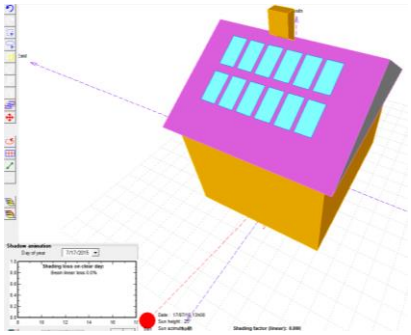

17 July 2015, 13.00

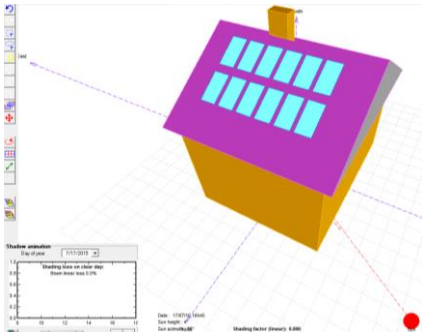

17 July 2015, 16.45

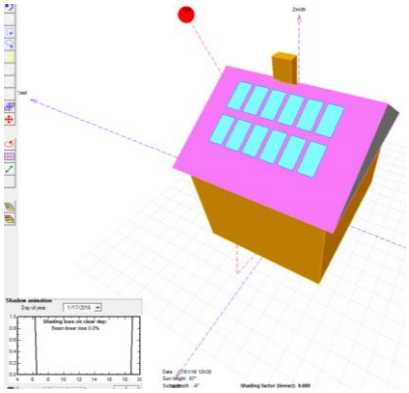

17 January 2016, 12.30

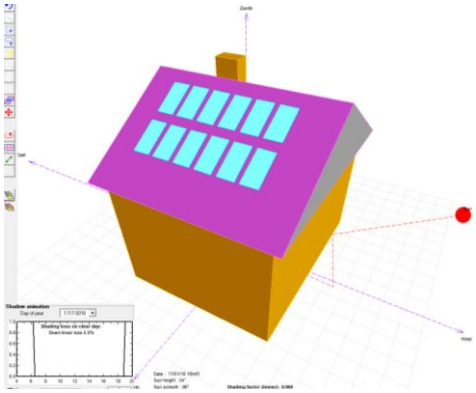

17 January 2016, 16.45

Figure 6: Shadow of solar array at different dates and times

3.2.3 Power Generation

Although the system is set to grid connected style, the solar panels actually only supply the household water heater and do not connect with the public grid. The grid connected system is just to show the total energy generated by the solar panel array. Based on the average data of the irradiation in Christchurch, the 12 PV panels (DJ-195D/A) array is set to a standard PV system with free horizon and grid-connected.

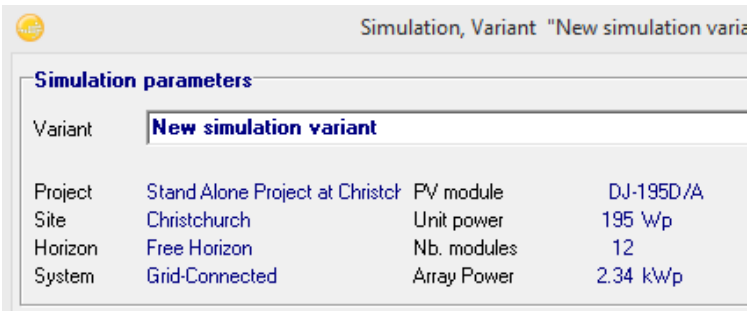

Figure 7: The Simulation parameters of the PV panels array

Referring to Figure 8, the rated output power of the array is 2.34kWp, and the voltage and the current values for a single panel on the MPP are 37.9V and 5.2A (Figure 8). The daily output energy in PV power is shown in Figure 9.

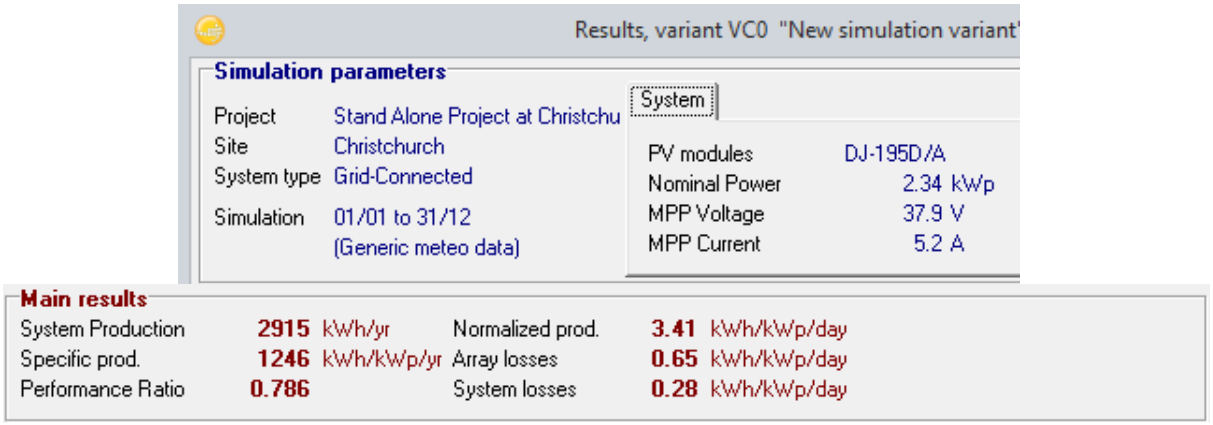

Figure 8: The main results of the array simulation.

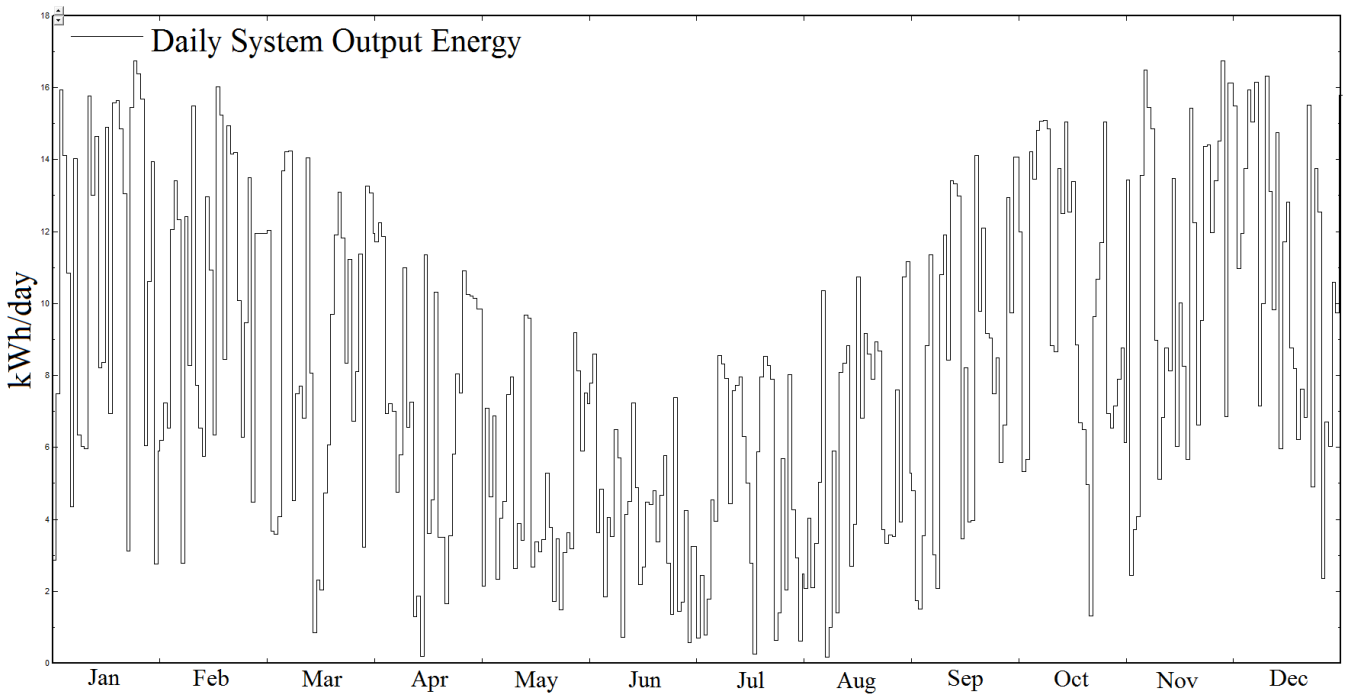

Figure 9: Daily output energy in PV power

3.3 Water Heater Load

In New Zealand, the tank size of a general household water heater is less than 200 L [23]. The normal household water heater stores 180 litres of water [24]. In this project, the default tank volume is V = 180 L. The energy (E) to heat the water in the tank is

$$\mathrm{E} = \Delta\mathrm{T} * \mathrm{M} * c_{water} + E_{loss}$$

Where ΔT is the difference temperature between the outdoor cold water (T_{cw}) and the thermostat temperature (T_{th}) in the water heater, ΔT = T_{th} -T_{cw};

M is the amount mass of water which is storage in the tank;

c_{water} is the specific heat capacity of water;

E_{loss} is the heat loss of the water heater tank.

Here, the tank heat loss E_{loss} is assumed to be 1.76 kWh/day (Table 2).

$$\mathrm{M} = \mathrm{V} * \rho = 180\,\mathrm{L} * 1000\,\mathrm{kg}/m^3 = 0.18\,m^3 * 1000\,\mathrm{kg}/m^3 = 180\,\mathrm{kg}$$

Where V is the volume of water which is storage in the tank, ρ is the density of water.

$$c_{water} = 4.2\,\frac{kJ}{kg * K}$$

Then the energy E of water heating per day is

$$\mathrm{E} = (T_{th} - T_{cw}) * 180\,\mathrm{kg} * 4.2\,\frac{kJ}{kg * K} + 1.76\,\mathrm{kWh/day}$$

If the thermostat temperature T_{th} in the tank is set at a fixed value, the water heating energy E of a house will change with the temperature of cold water, then the extreme value of E is in summer (January) and winter (July), $T_{cw,JAN} = 16\,^{\circ}C$, $T_{cw,JUL} = 5\,^{\circ}C$ (21). As examples, E will be calculated in January and July. Setting T_{th} is set at 65°C.

In January,

$$E_{JAN} = (T_{th} - T_{cw,JAN}) * 180\,\mathrm{kg} * 4.2\,\frac{kJ}{kg*K} / 3{,}600{,}000\,\mathrm{J/kWh} + 1.76\,\mathrm{kWh/day} = 12.05\,\mathrm{kWh/day}$$

In July,

$$E_{JUL} = (T_{th} - T_{cw,JUL}) * 180\,\mathrm{kg} * 4.2\,\frac{kJ}{kg*K} / 3{,}600{,}000\,\mathrm{J/kWh} + 1.76\,\mathrm{kWh/day} = 14.36\,\mathrm{kWh/day}$$

This is the daily energy required to heat 180 litres of water up to 65°C. However, this is not the daily energy requirement, as households tend to use more hot water in the winter than in the summer.

Based on the seasonal load profile C_{load}, it is found that the peak winter daily load P_{peak} is in August. Peak required daily energy in August is

$$E_8 = C_{load,AUG} * \frac{P_{peak}}{3{,}600{,}000\ J/kWh} = 1.0 * \frac{39\ \text{MJ/day}}{3{,}600{,}000\ J/kWh} = 10.83\ kWh/day$$

The energy for heating water is the 33% of the all energy of the household loads in a house. In this project, the daily average value of energy dissipation for household water heater is calculated on a monthly basis, following Table 4.

Table 2 shows the reference parameters for a normal electric water heater [24]. The difference temperature (ΔT) is the monthly average temperature between the natural water system and the normal thermostat in the tank (180L) of water heater (65 ºC). The cold water temperature in Christchurch (T_{cw}) [24] and the difference temperature (ΔT) are collected monthly in Table 3. Based on the typical volume of hot water used grid and its heat loss, the power consumption for heating water in Christchurch is given in Table 4.

Table 2: Characteristics of reference electric water heater (continuous boost)

Tank size (L)	Tank heat loss (kWh/day)	Thermostat temperature (ºC)	Thermostat differential (K)	Peak winter daily load P_{peak} (MJ/day)
180	1.76	65	10	39

Table 3: Cold water temperature in Christchurch, New Zealand

Month	Cold water temp (T_{cw})	Difference temp (ΔT)
January	16 ºC	49 ºC
February	16 ºC	49 ºC
March	15 ºC	50 ºC
April	11 ºC	54 ºC
May	9 ºC	56 ºC
June	6 ºC	59 ºC
July	5 ºC	60 ºC
August	6 ºC	59 ºC
September	8 ºC	57 ºC
October	11 ºC	54 ºC
November	13 ºC	52 ºC
December	15 ºC	50 ºC

NOTE: The cold water temperature and the thermostat temperature in the table shall be used as the water inlet temperature to the storage tank.

Table 4: Daily energy dissipation for heating water

Month	Seasonal load profile C_{load} [24]	Daily power required for heating water
January	0.51	5.52 kWh/day
February	0.58	6.28 kWh/day
March	0.60	6.50 kWh/day
April	0.72	7.80 kWh/day
May	0.83	8.99 kWh/day
June	0.89	9.64 kWh/day
July	0.99	10.72 kWh/day
August	1.00	10.83 kWh/day
September	0.90	9.75 kWh/day
October	0.83	8.99 kWh/day
November	0.76	8.23 kWh/day
December	0.65	7.04 kWh/day

In summer a typical family would use around 90 litres of hot water per day, whereas in winter the usage is close to 140 L/day. Based on the above Table 4, the step diagram of the daily power consumption for heating water is shown in the below Figure 10.

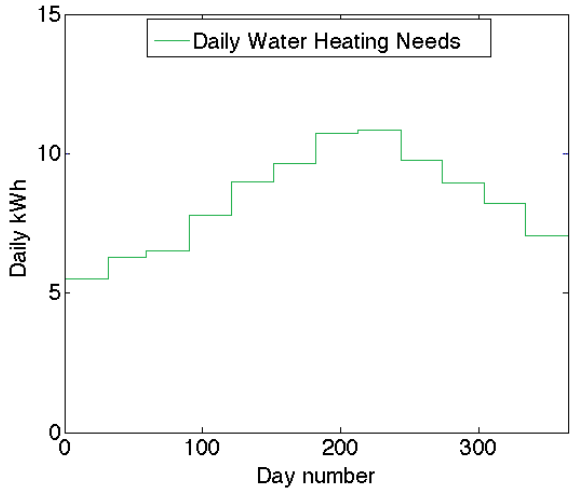

Figure 10: Average values diagram of the daily energy dissipation for heating the hot water

3.4 Energy Balance & Return

3.4.1 PV Conversion System

The daily generated energy by the PV system is calculated by PVsyst, the daily energy required by the household water heater has been shown in Table 4. Comparing the daily generated energy and used energy, the difference is used to analyse the system value. The average value diagram of the daily energy usage is merged into the daily generated energy by PV panels to compare and calculate the value of the difference energy, referring to Figure 11. The maximum value and the minimum values of the difference energy are in January and July, these two situation are enlarged as examples in Figure 12 and Figure 13.

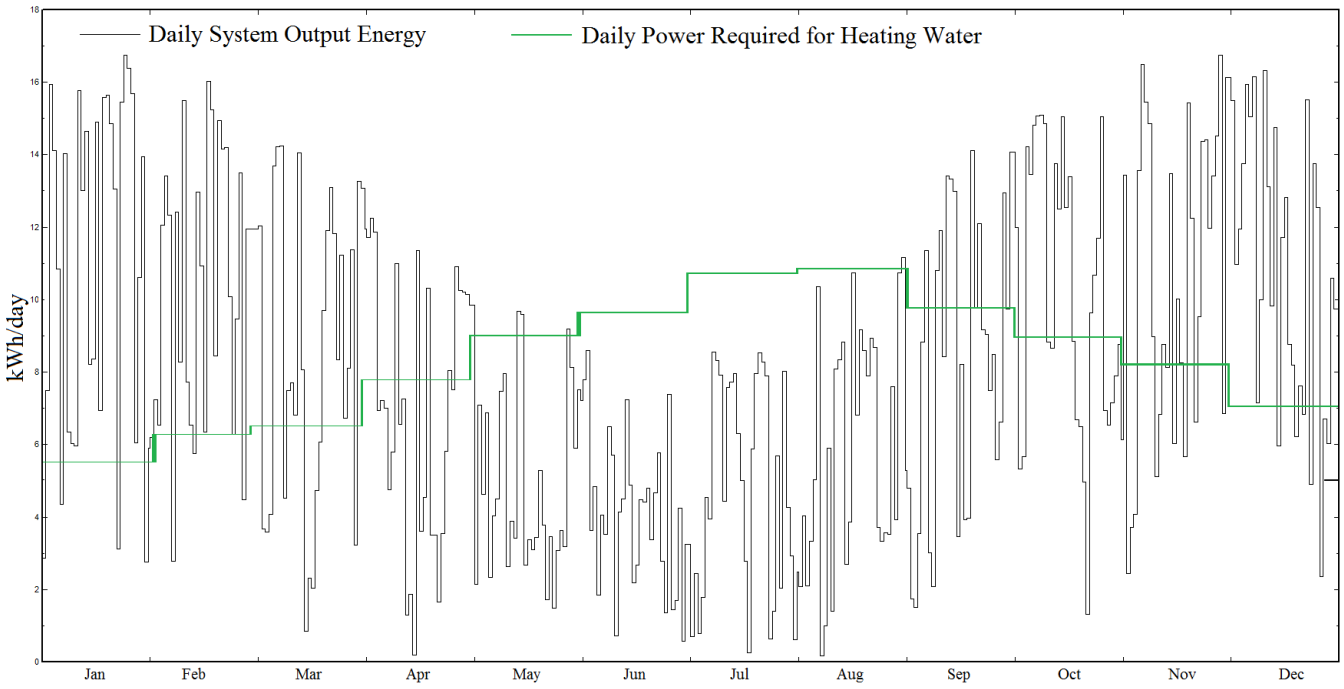

Figure 11: Difference energy between the daily output energy in PV power and monthly load of water heating.

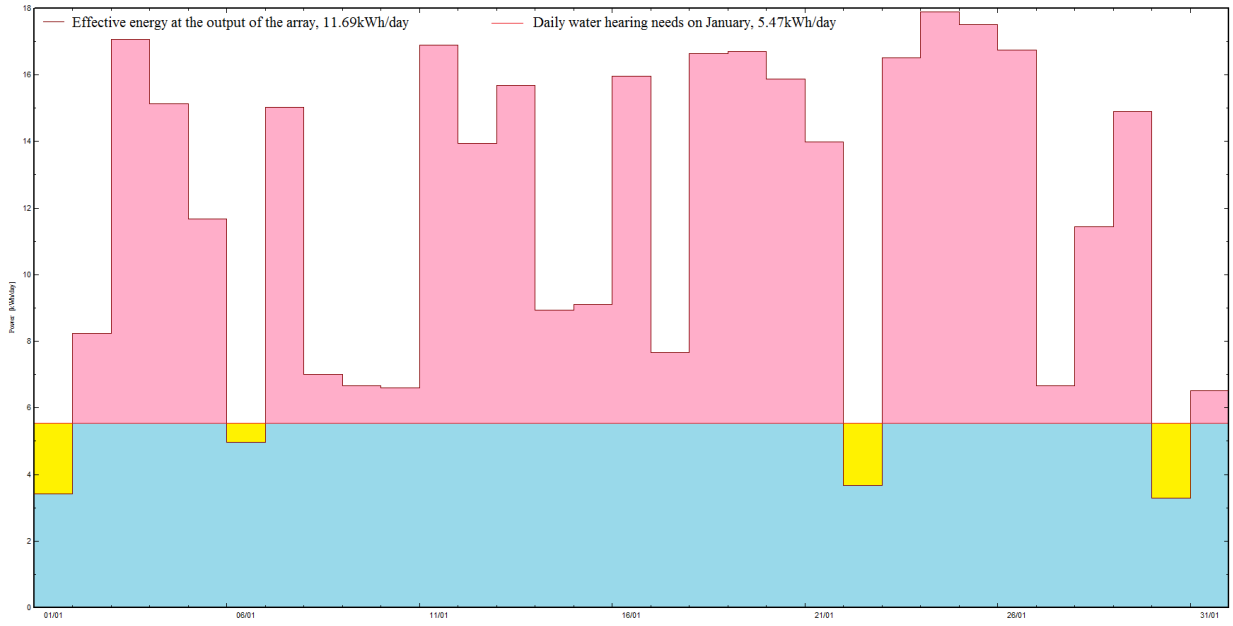

Figure 12: Enlarged diagram of the maximum difference energy in January.

From the difference energy diagram in January, Figure 12, the generated energy on four days is less than the daily water heating needs. The energy potentially generated by the PV system over the month is

$$P_{PV} = \sum P_{out} = 362.3\ kWh$$

The shortfall in energy, when grid energy is needed to heat the water (yellow area), is

$$\Delta P = \sum_{output<heating} (P_{heating} - P_{out})$$

$$\Delta P = 6.72 \text{ kWh}$$

and the un-harvested energy is the difference energy on January except for four days,

$$P_{loss} = \sum_{heating<output} (P_{out} - P_{heating}) = 161.9\ kWh$$

The used energy (blue area) to supply water heater is

$$P_{supply} = \sum_{31} P_{used} = 164.4\ kWh$$

It is clear that in January, slightly less than half of the available PV power is actually used. The residential average price of the electricity power is 28.86 c/kWh, the cost of electricity from the grid in January is

$$\$cost = \Delta P * 28.86\ c/kWh = 6.72*28.86 = 193.94\ c = \$1.94$$

The saving is

$$\$saving\ =\ P_{supply} * 28.86\ c/kWh = 164.4 * 28.86\ =\ \$47.45$$

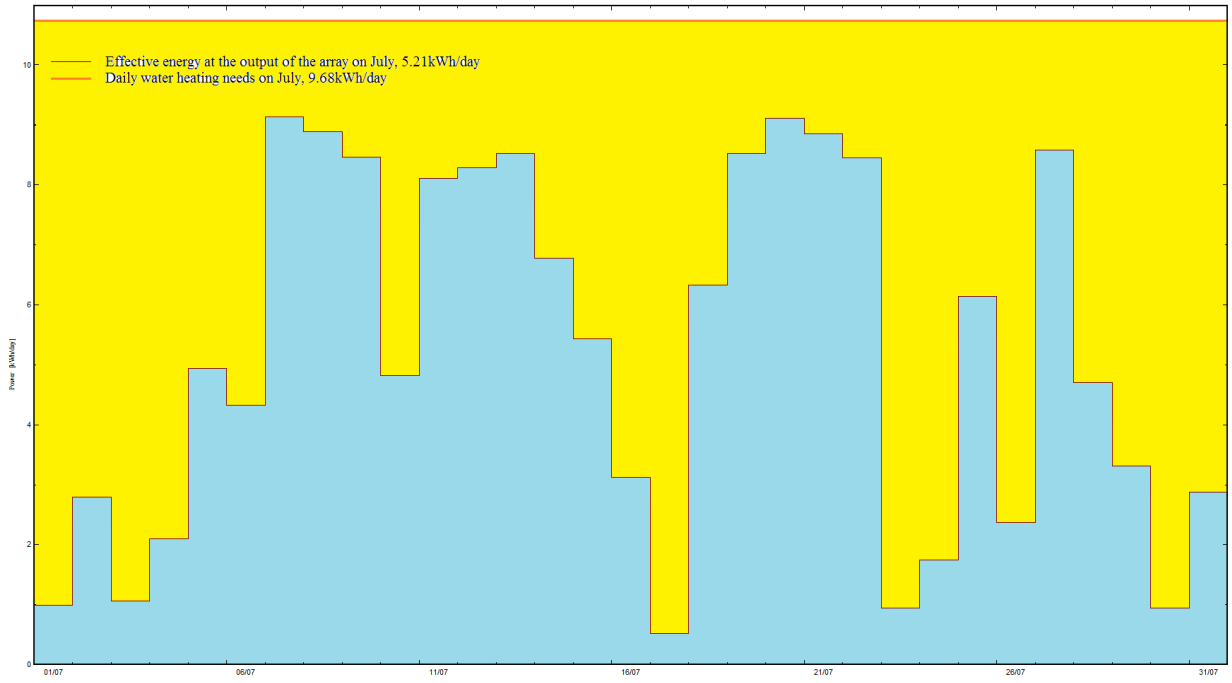

Figure 13: Enlarged diagram of the minimum difference energy in July.

From the difference energy diagram in July, Figure 13, the generated energy is less than the daily water heating needs every day. The generated energy is

$$P_{PV} = \sum P_{out} = 161.5\ kWh$$

Then the energy shortfall, which must be provided by the grid (yellow area), is

$$\Delta P = \sum_{output<heating} (P_{heating} - P_{out}) = 136.71\ kWh$$

The total required energy (blue area) of the household water heater is

$$P_{supply} = \sum_{31} P_{used} = P_{PV} = 161.51\ kWh$$

As the generated power in PV panels is less than the needed energy to supply the water heater, it means all of the generated electricity is used, so the lost energy (pink area) is zero,

$$P_{loss} = 0\ kWh$$

and the electricity cost and savings is

$$\$cost = \Delta P * 28.86\ c/kWh = 136.71*28.86 = \$39.45$$

$$\$saving = P_{supply} * 28.86\ c/kWh = 161.51 * 28.86 = \$46.61$$

It is clear that in July, the PV system supplies less than 60% of the water heating requirements. Table 5 summarises for a full year the water heating energy requirements, the potential PV generation, and the savings generated. For the overall system, nearly 75% of the water heating costs are covered by the PV system, and over $651 is saved.

Table 5: Calculated values of power and price

Month	Water Heater Required, P_{heater} (kWh)	Generated energy in PV power, P_{PV} (kWh)	Shortfall energy ΔP (kWh)	Generated energy to supply heating, P_{supply} (kWh)	Un-harvested energy, P_{loss} (kWh)	Cost of electricity from grid ($cost)	Saving price ($saving)
January	171.12	326.3	6.72	164.4	161.9	1.94	47.45
February	175.84	307.8	4.38	171.46	136.34	1.26	49.48
March	201.5	285	27.22	174.28	110.72	7.85	50.3
April	234	227.3	50.41	183.59	43.71	14.55	52.98
May	278.69	166.3	121.14	157.55	8.75	34.96	45.47
June	289.2	134.7	154.47	134.7	0	44.58	38.87
July	332.32	161.5	136.71	161.5	0	39.45	46.61
August	335.73	196.4	142.13	193.6	2.8	41.02	55.87
September	292.5	265.7	66.57	225.93	39.77	19.21	65.2
October	278.69	337.9	27.19	251.5	86.4	7.85	72.58
November	246.9	342.5	21.42	225.48	117.02	6.12	65.07
December	218.24	363.6	6.37	211.87	151.73	1.84	61.15
Amount	3054.73	3115	764.73	2255.86	859.14	220.63	651.03

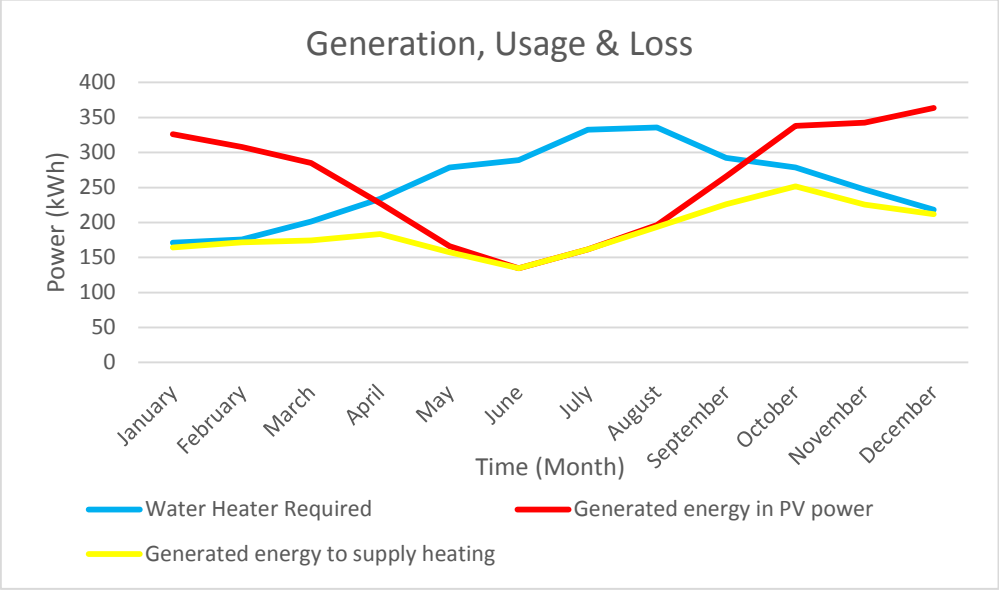

Figure 14: Possible generated energy, used energy and lost energy for this PV water heater system

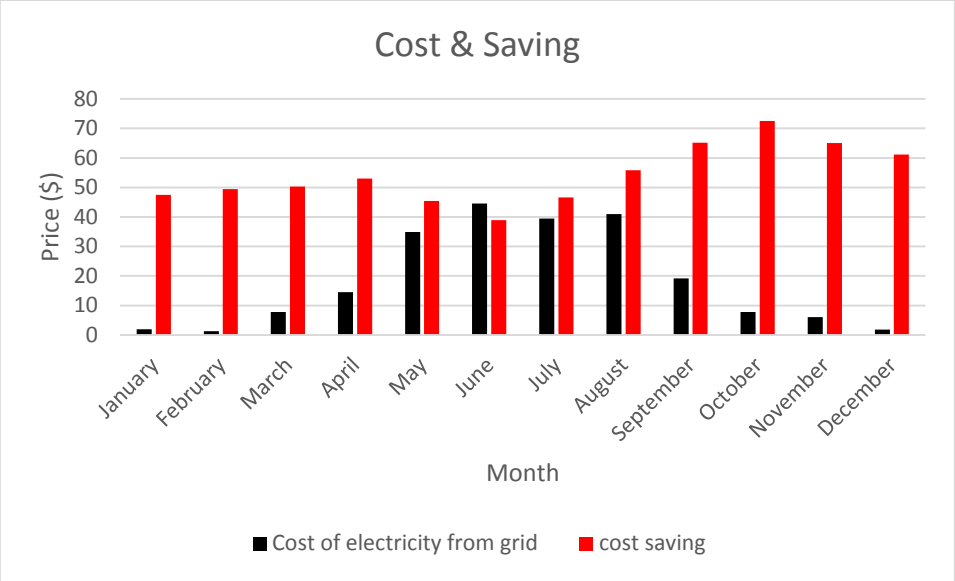

Figure 15: Cost and saving price for this PV water heater system

Figure 14 and Figure 15 are drawn from Table 5. Because of the seasonal irradiance variation, the peak summer generated power by PV panels is about 2.7 times the lowest winter generation. The demand for hot water in winter is much more than in summer. In summer, the generated energy to supply heating is limited by the required energy of water heater, the PV generation decides the energy supplied for heating in winter. The rest of the cost of electricity from grid follows the water heater required energy, it in winter is higher than in summer. Savings are decided by the energy to supply heating, and except in June, the saving price is always higher than electricity cost from grid.

Current price for a PV system in New Zealand runs at 1 $/W for the panel, 0.5 $/W for the racking, around 1 $/W for inverter and 1 $/W for wiring installation, compliance, inspection, metering etc. In this project the converter is self-designed, it will cost less than $400. For the PV solar heating system, the inverter-compliance costs are substantially reduced, to around 0.17 $/W for the inverter and 0.5 $/W for wiring, compliance etc. A 2340 Watts system should cost approximately 2.2 $/W or around $5,100, a savings of 651 $/year results in a simple payback of 8 years. For a PV power system, it could work more than 20-25 years, it means more than $10,000 will be saved by the end of the system lifetime.

3.4.2 Compare with Grid Connected System

For a grid connected system, the self-use of generated energy is best for the return to the home-owner. Average daytime load during sunshine hours (9am – 5pm) is 600 Watts in the Christchurch area (Figure 16) and this is used as the household load during the day. Table 6 and Table 7 shows the money and energy balance for a PV grid connected system under these conditions, in according with the simulation results by software PVsyst, Figure 17 & Figure 18 & Figure 19 is made.

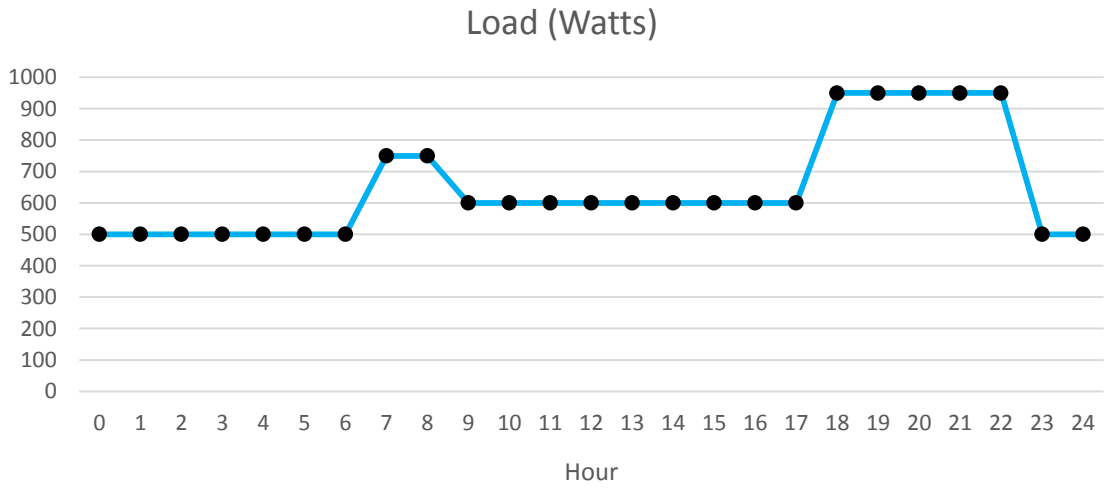

Figure 16: Simulation conditions of load setting of grid connected system

Table 6: Price data of grid connected system with different capacity

Panels quantity	Built costing price ($)	Panels generate energy sale ($)	Saving price ($)	Balance of PV power system ($)	Cost back time of PV system building (year)
6	3,853	18	400.3	418.3	9.2
12	7,720	121.14	516.6	637.7	12.1
18	11,540	251.82	569.4	821.2	14.1
30	19,624	536.22	621.4	1157.6	17
48	30,452	958.68	647.9	1606.6	19

Table 7: Power data of grid connected system with different capacity

Panel No	Solar array production energy (kWh/year)	Load used energy (kWh/year)	Sold energy (kWh/year)
6	1587	1387	200
12	3136	1790	1346
18	4772	1973	2798
30	8111	2153	5958
48	12898	2245	10652

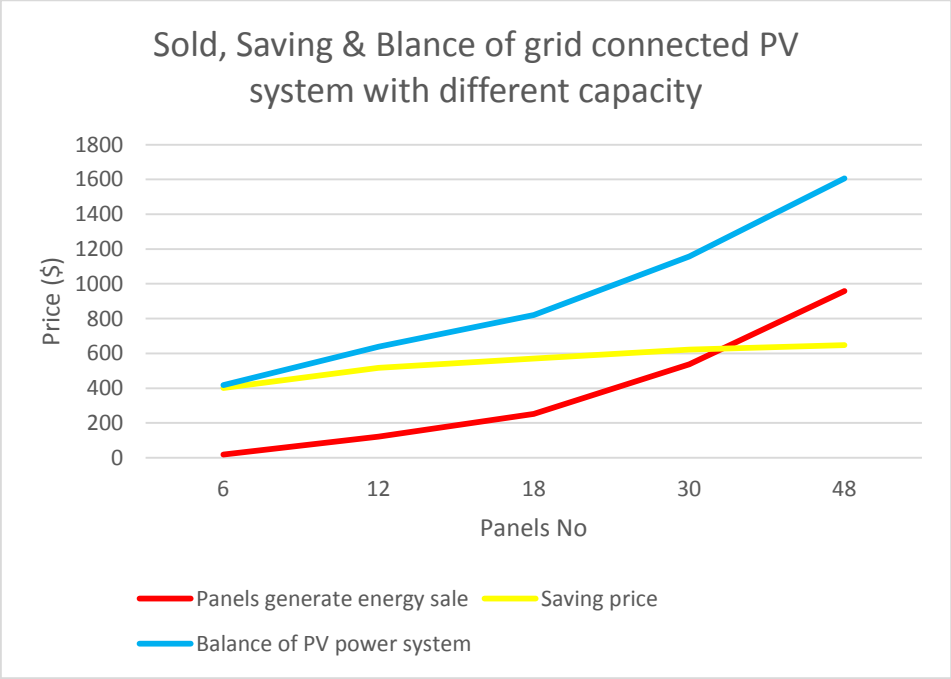

Figure 17: Costing, saving & Balance of grid connected PV system with different capacity

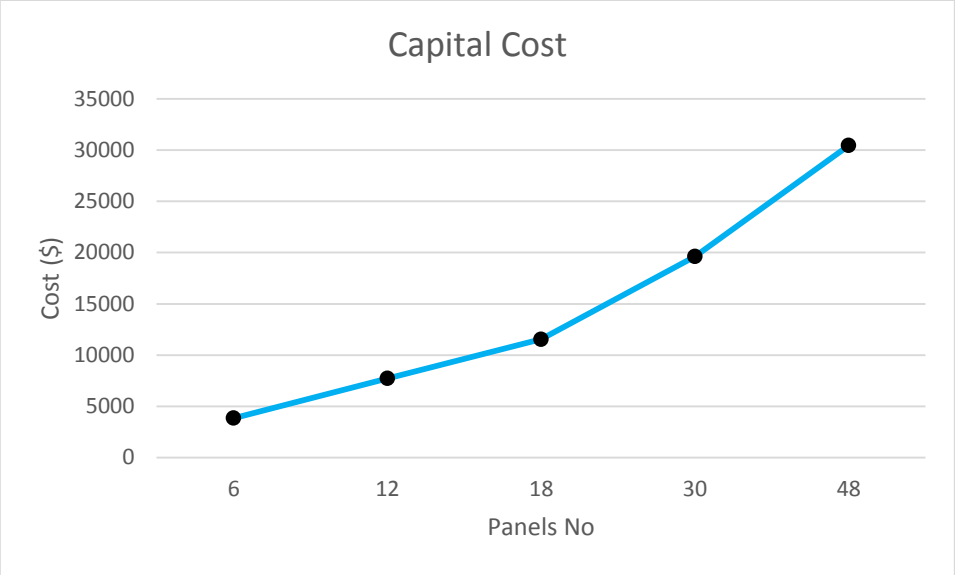

Figure 18: Costing price to build a grid connected PV system with different capacity

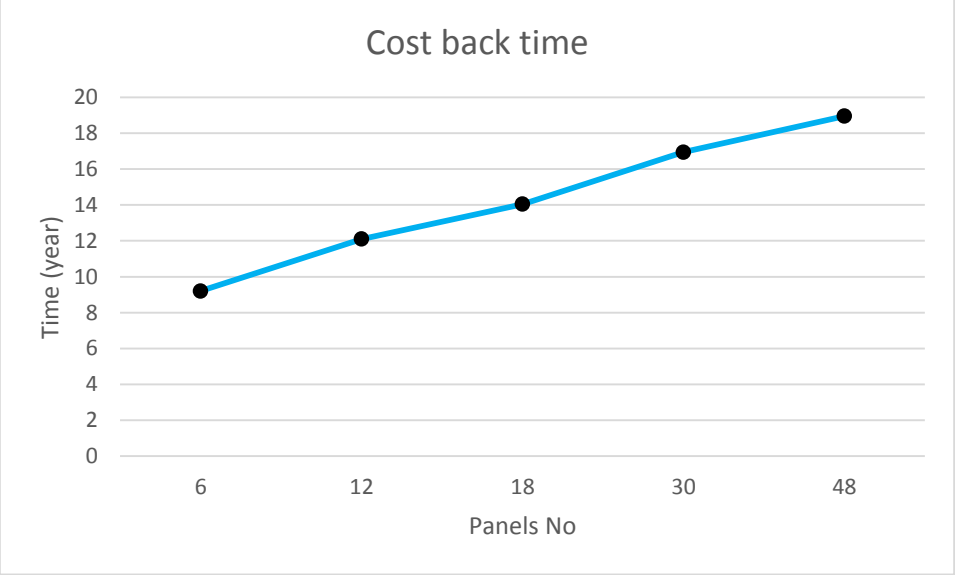

Figure 19: Investment saved back time of grid connected PV system with different capacity

The generated energy sold price, saving price and balance of PV system are all rising with the increasing number of PV panels (Figure 17). Although the savings and income go up with more PV panels, the cost to build grid connected system with higher system capacity is also more expensive. This is why simple payback time with low capacity is shorter than with high capacity (Figure 19). This PV water heater system with 48 panels needs more than 30

thousand dollar, after 19 years the price to build PV system will be saved by this PV system. For a solar system life time, 20-25 years, most of the time is used to save the building cost.

In accordance with above table and figures, the advantages of grid connected PV system are

- There is no PV energy left un-harvested;
- The generated energy can also be used by other household electronics;
- Money will be earned when there is nobody in the house.

The disadvantages are,

- The investment of grid connected PV system is more expensive than a water heating PV system, for a general family, it is not easy to spend so much money to build a PV system;
- The simple payback time for a grid connected system is longer than the water heating system.

In this project, the water heater PV power system only supplies the household water heater, the output of converter need not be pure sine wave, and the converter is cheaper. So this is a very good choice for a general family to save money.

Chapter 4

PV WATER HEATER

4.0 Introduction

In this chapter, the functional specification of the PV water heater is outlined, and the design process is described. The water heater controller has a number of tasks briefly outlined below.

- The controller must draw a steady current from the solar panel array that keeps the panels at their maximum power point.
- The controller must supply a voltage/current to the water heating element that has regular zero crossings, so that the element thermostat and thermal cut-off will safely operate.
- The controller must manage the hot water cylinder temperature, so that
  - A pre-specified maximum temperature is not exceeded;
  - Under conditions of insufficient sunshine, hot water supply is maintained.
- The controller must report energy saving to the owner.

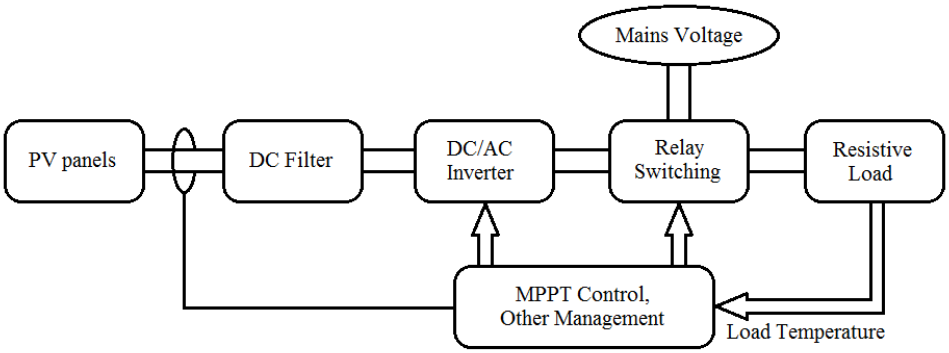

Figure 20: Block diagram of the household PV conversion system.

Figure 20 shows the basic layout of the PV hot water control system. This chapter presents a brief solar module model, the power circuitry used, and the control strategy.

4.1 PV Panel Model

A PV cell is the element of electricity generation element. PV panels can generate electrical energy when they exposed under the sun. The solar energy is absorbed by solar array and converted directly to DC power [25]. The circuit representation shown in Figure 21 is one of the most popular models of a solar cell [26-27].

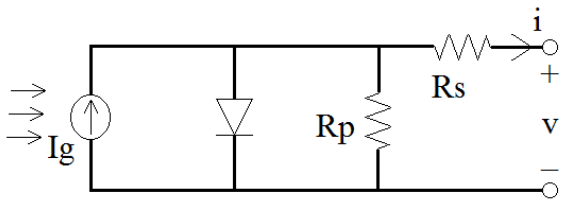

Figure 21: A circuit representation with two resistors of a PV cell.

For, the equation of photo-induced current (I_{ph}) is

$$I_{ph} = I_{ph,STC}\frac{G}{G_{STC}}[1 + \alpha_1(T - T_{STC})]$$

where $I_{ph,STC}$ the photo-induced current for Standard Test Conditions (STCs);

T_{STC} the cell temperature under STC;

T, the actual cell temperature;

G_{STC} the irradiation, G=1000 W/m^2;

α_1 the temperature coefficient of current, $\alpha_1 = \frac{dI}{dV}|_{STC}$;

I_{ph} is the current of a simple PV cell with two resistors

The best layout of the PV array (with hold 2.34k Watts) is 2 strings, parallel connected, of 6 panels in series (Figure 3). The array voltage at maximum power point is higher than

maximum expected heating element voltage (231.54V>230V), so that converter can operate in buck mode.

4.2 Power Circuit

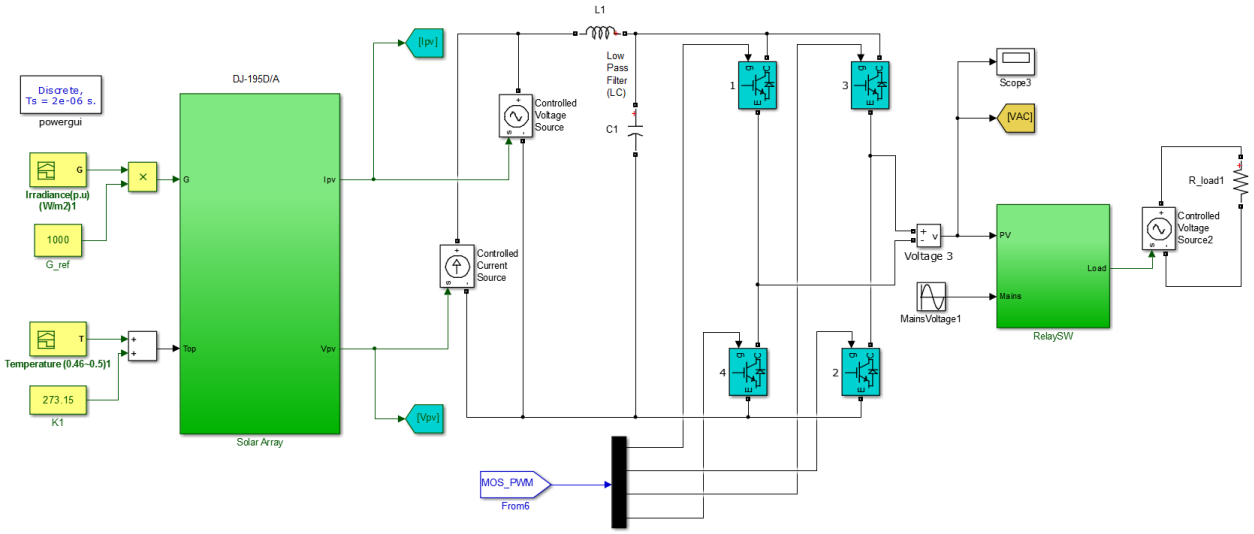

Figure 22: PV water heater system schematic

The H-bridge is switched as a buck converter, operating with either S2 ON and S1 PWM controlled, or S4 ON and S3 PWM controlled. In this way the low-pass filter only has to filter the switching frequency and its harmonics, while S2 and S4 can be switched at a much lower rate (50Hz) to provide current zero crossings for the resistive heating element. DC power is inverted to AC by these four MOSFETs. The voltage waveform is shown in Figure 23, Figure 24 shows one period waveform of Figure 23 (0.15s – 0.17s). The amplitude of output voltage is controlled by the duty cycle of high frequency switching.

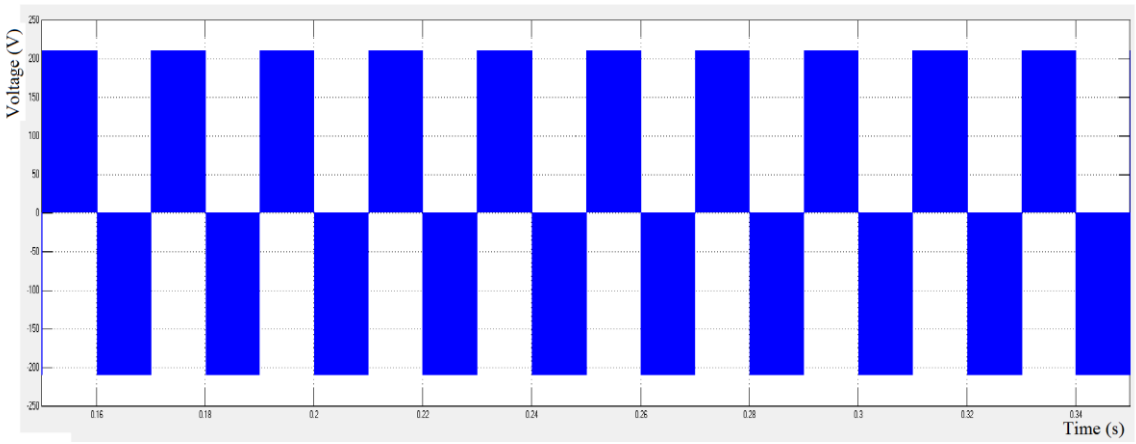

Figure 23: Output waveform of AC voltage (Voltage/ Time) on resistive load (R-Load)

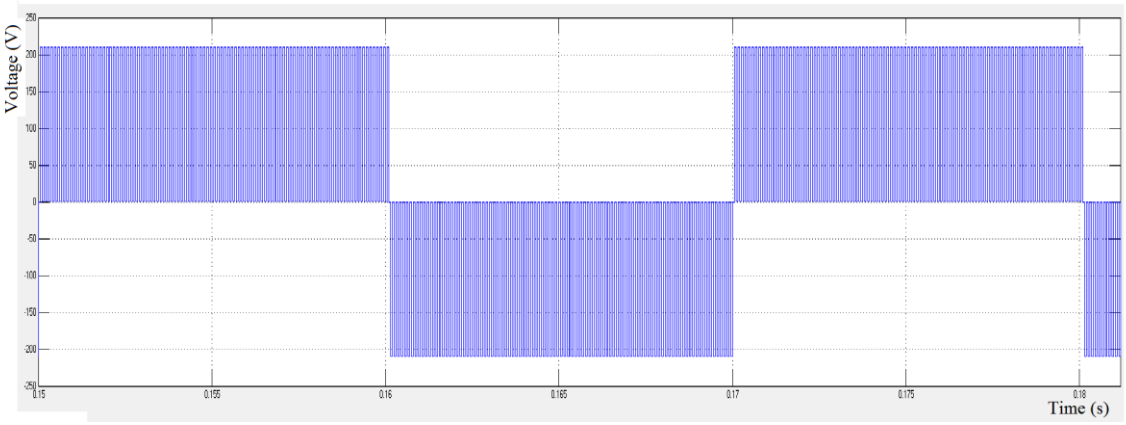

Figure 24: Output waveform of AC voltage (Voltage/ Time) on R-Load in one period

4.2.1 H-Bridge

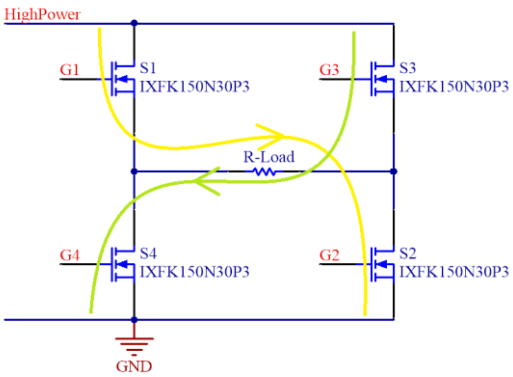

Figure 25: H-Bridge with 4 MOSFETs

In this project, H-Bridge with four MOSFETs was used to invert DC to AC, and this is shown in Figure 25. The output voltage is positive when the MOSFETs S1 and S2 turn on (yellow line), the output voltage becomes to be negative when S3 and S4 turn on (green line). The transistor chosen was the manufacturer name IXFK150N30P3, in particular due to its high drain-to-source breakdown voltage ($V_{ds} = 300\,Volts$) and low static drain-to-source on-resistance ($R_{ds(on)} = 19\,mOhms$) (Appendix 3). The very low $R_{ds(on)}$ minimises conduction losses, which minimises expensive heatsink requirements. As a result the current rating of the MOSFET, at 105 Amps, is much greater than required by the application.

4.2.1.1 MOSFET Losses

There are two main power losses of MOSFET, switching power loss P_{sw} and conduction power loss P_r. P_r could also be called resistive loss. Power losses P_r directly affect the temperature of the MOSFETs; the temperature is controlled by the heatsink.

For MOSFETs, calculation of switching losses P_{sw} involves the through power, the switching frequency and the switching times [28].

$$P_{sw} = P_{pv} * f_{sw} * \left(\frac{t_r + t_f}{2}\right)$$

where the power through the MOSFET is the power generated by the solar array,

$$P_{pv} = I_{arry} * V_{arry} = 10.1 * 231.5 = 2338\,Watts$$

the high side frequency is the switching frequency to calculate P_{sw},

$$f_{sw} = 30kHz$$

the switching times of MOSFET are the rise time t_r and the fall time t_f,

$$P_{sw} = 10.1A * 231.54V * 30kHz * \left(\frac{30ns + 12ns}{2}\right) = 1.473Watt$$

This is very low power, easily dissipated to air, with respect to the flowing power P_{pv}, P_{sw} is small enough to be negligible.

The most heat is dissipated in the H-Bridge from the four MOSFETs. Because to a great extent, the power dissipation of MOSFET is related to the current in the static drain-to-source on-resistance, the on-resistance loss calculation is a useful starting point. The following calculation assumes worst case conditions.

Assume MOSFET junction temperature is the worst case maximum value of operating junction temperature,

$$T_{hot} = T_{j,max} = 150°C$$

Calculate the MOSFET on-resistance at the assumed junction temperature, setting T_{spec} is the specification temperature, equal to 25°C

$$R_{ds(on)hot} = R_{ds(on)} * (1 + 0.05 * (T_{hot} - T_{spec}))$$

$$R_{ds(on)hot} = 19mOhm * (1 + 0.05 * (150°C - 25°C))$$

$$R_{ds(on)hot} = 137.75mOhm = 0.13775\ Ohm$$

Calculate the power dissipation $P = 2 * P_r + P_{sw}$, where Pr is the canduction power loss, the switching power loss Psw had been calculated on above.

$$P_{sw} = 1.5\ Watt$$

$$P_r = I_{array}^2 * R_{ds(on)hot} = 10.1^2 * 0.13775 = 14.052\ Watt$$

$$P = 2 * P_r + P_{sw} = 2 * 14 + 1.5 = 29.5\ Watt$$

4.2.1.2 Thermal Design

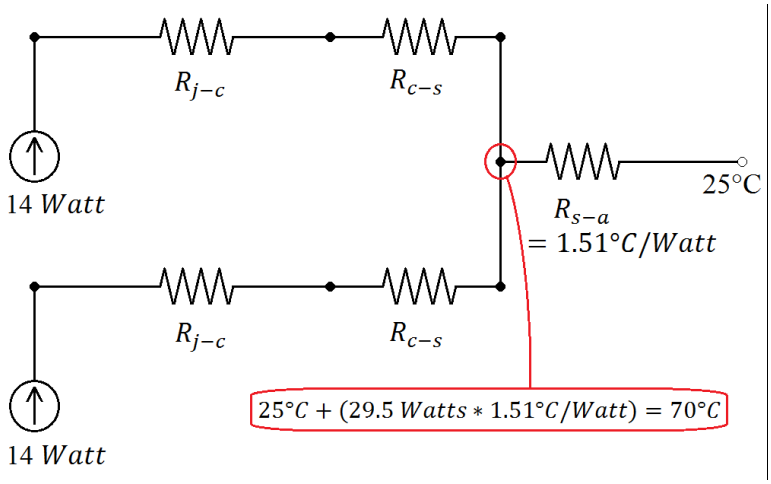

Figure 26: Schematic of energy transfer between switching devices and heat sink

The main parameter of heat sink is the thermal resistance θ_{th}. Calculate the maximum thermal resistance of heat sink to ambient temperature [29].

$$\theta_{th} = \frac{T_j}{P}$$

$$T_{j,max} = T_{ambient,max} = 125°C < T_{hot} = 150°C$$

$$\theta_{th} < \frac{T_{hot}}{P} = \frac{150}{29.5} = 5.1°C/W$$

This is the absolute minimum acceptable heat sink thermal resistance, the actual resistance must be considerably less than this. In this project, the heat sink 394-24B with 1.51°C/W thermal resistance will be used (Appendix 4), this θ_{th} will only be checked in this paper. The thermal resistance will be iterated to the above function, when the junction temperature is lower than the peak operating temperature, this heat sink could be used in this PV system.

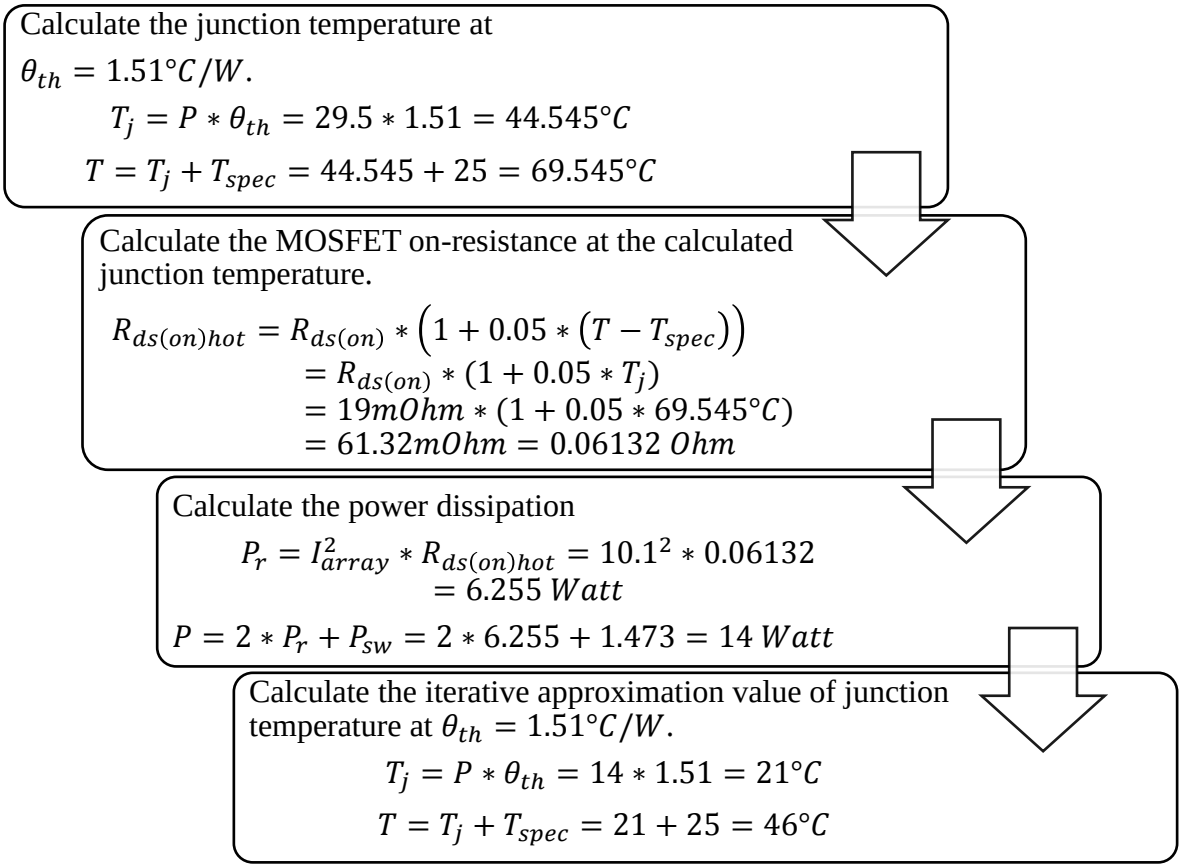

4.2.2 DC Filter

To get the maximum power from the PV panels, it is important that a DC current is drawn from them. The current ripple from the switching circuit must be smothered by a filter. Then the low pass filter is needed for eliminating the higher harmonics in outputs [30]. The LC filter is shown in Figure 22 as the DC filter in this project. The function of the cut-off frequency (f) is

$$f = \frac{1}{2\pi\sqrt{L * C}}$$

Setting the inductance and conductance, $L = 15\mu H\ ,\ C = 35\mu F$, the frequency is calculated

$$f = \frac{1}{2\pi\sqrt{L * C}} = \frac{1}{2\pi\sqrt{15\mu H * 35\mu F}} = 6.95\ kHz$$

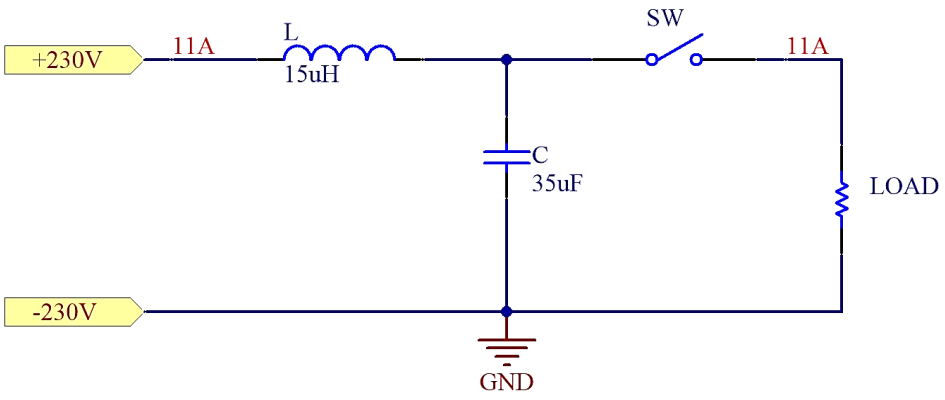

Figure 27: Low Pass DC Filter

In this project, the high switching frequency of H-bridge is 30 kHz, and the maximum current is 10.83 Amps (Appendix 1). A discontinuous current flows at the input of the H-bridge; this current needs to be smoothed to close to DC to maintain steady PV panel current. This is done using an LC low pass filter – the capacitor provides a low impedance for the switching harmonics, and the inductor blocks high frequency currents from flowing in the panels. The cut-off frequency is 5 times lower than the switching frequency, to ensure good filtering. The inductor is rated for the panel current, and the capacitor is rated to carry a ripple current of 14 Amps.

4.2.3 Auxiliary Converter Circuits

4.2.3.1 Overvoltage snubber

As the MOSFET peak rated voltage V_{ds} is 300 Volts, which is not a lot greater than the solar panel peak voltage, it is important to limit switch voltages. A clamping RCD snubber is designed. The function of the snubber capacitor is to absorb energy in any stray inductance when each MOSFET turns off. The capacitor voltage rises on MOSFET switch-off, and then is returned to the PV rail voltage via the snubber resistors [31]. Figure 29 shows the expected snubber waveforms, and a diagram indicating the source of inductance between two parallel panels on a PCB.

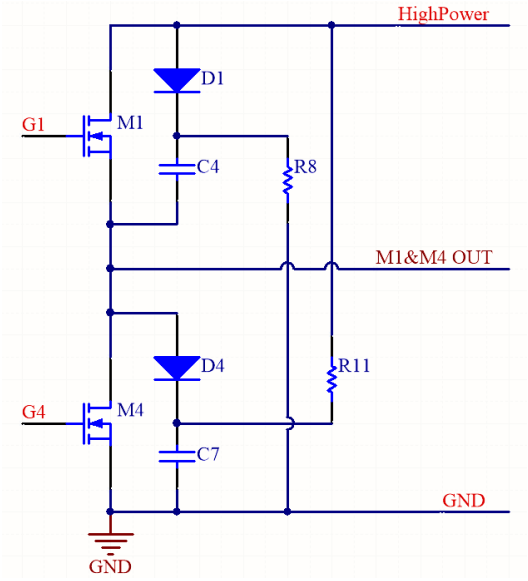

Figure 28: Schematic of the snubber circuit

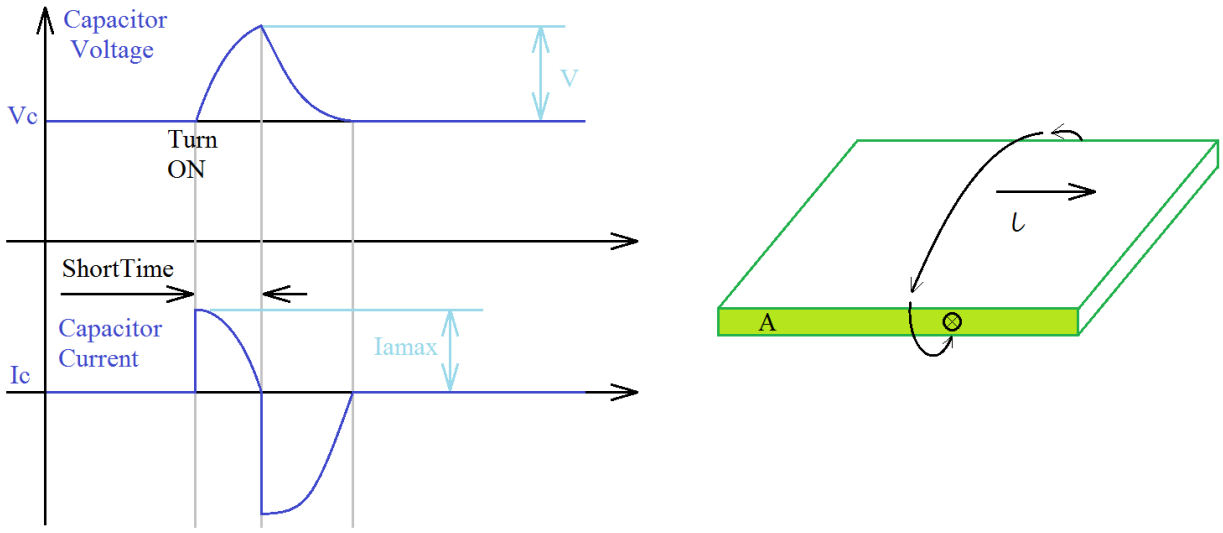

Figure 29: Waveform when switch off and the magnetic circuit through PCB

The magnetic reluctance of the circuit board is $R = \frac{l}{\mu_0 A}$. The inductance is the inverse of magnetic reluctance,

$$L = \frac{1}{R} = \frac{\mu_0 A}{l}$$

where μ_0 is the permeability of vacuum ($4\pi * 10^{-7} H/m$); setting the length of the magnetic circuit is $l = 10mm = 10 * 10^{-3} m$, the cross-sectional area (green area in Figure 29) of the magnetic circuit is A = 2mm * 60mm = $1.2 * 10^{-4} m^2$ (Figure A8-2 in Appendix 8).

$$L = \frac{4\pi * 10^{-7} * 1.2 * 10^{-4}}{10 * 10^{-3}} = 15.08 * 10^{-9} H$$

Setting the maximum current I_{amax} of array output equal to twice of the short circuit current of PV panel DJ-195D/A, $I_{amax} = 2I_{sc} = 2 * 5.56A = 11.12A$.

$$W = \frac{1}{2} * L * I_{amax}^2 = \frac{1}{2} * 15.08 * 10^{-9} * 11.12^2 = 0.932 * 10^{-6} J$$

The snubber capacitance is calculated to equal to 6.8nF, and the snubber resistance is 1k Ohms, and then the calculation result will be verified. The voltage rise above the panel voltage is limited to 20 Volts, and the minimum time the capacitor has to return to the panel voltage is $3 * 10^{-5}\ seconds$.

$$t_{on,min} \approx 3RC$$

$$R < \frac{t_{on,min}}{3C} = \frac{1/30kHz}{3 * 6.8nF} = 1.633\ kOhms$$

The better buffer of the snubber circuit is with the lower snubber resistance and the higher snubber capacitance, the resistance value is setting to be 1k Ohms, $R = 1kOhms < 1.633\ kOhms$.

$$W = \frac{1}{2} C V^2$$

$$V = \sqrt{\frac{2W}{C}} = \sqrt{\frac{2 * 0.932 * 10^{-6}}{6.8 * 10^{-9}}} = 16.556\ Volt < 20\ Volt$$

$$\omega = \frac{1}{\sqrt{L * C}} = {}^{1}/_{\sqrt{15.08 * 10^{-9} * 6.8 * 10^{-9}}} = 9.875 * 10^{7}$$

$$f = \frac{\omega}{2\pi} = \frac{9.875}{2\pi} * 10^{7} = 15.717MHz$$

The charge time of the snubber capacitor is t,

$$t = \frac{T}{4} = \frac{1}{4f} = \frac{2\pi}{4\omega} = 15.907 * 10^{-9}s = 15.907ns$$

The switching frequency of MOSFETs is 30 kHz, the switching period is 33.3µs. The capacitor charge time is extremely short compared to the switching period. The 6.8nF inductance and the 1k Ohms resistance will be used in this project.

4.2.3.2 Gate Driver Circuit

The connection schematic for the Driver IC [32] is shown in Figure 30. M1 is the high frequency switched MOSFET and M4 is MOSFET low frequency switched, R_{24}&R_{27} are the internal gate resistors, D_7 is the bootstrap diode, and C_{12} is the bootstrap capacitor ($C_{boot} = C_{12}$). The driver current flows in the series gate resistor ($R_{24} = R_{27} = 3.4\ Ohms$) to supply the MOSFET gate [33].

The Driver IC supplies the peak charging current to gate, and then the MOSFET turns on. As shown in Figure 30, three power supplies drive the typical inverter, a logic supply, an isolated low and high side driver supply and a high-voltage supply. The logic supply is the PWM signal with +3.5 Volt peak value, the isolated low & high side driver supply is VSS & VCC on pins 8 & 12, and the high-voltage supply is the positive power of the PV array output [34].

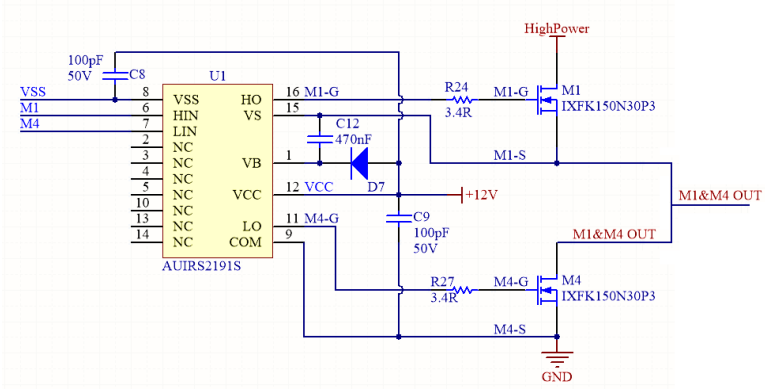

Figure 30: Schematic of MOSFETs & Driver IC

When the driver of low side runs on, C_{boot} (the bootstrap capacitor) is charged, and there is output pin below V_{DD} (supply voltage of the gate driver). Only at the turn-on time of the high side switch, C_{boot} is discharged. C_{boot} is the voltage for supplying the high-side circuit [35]. The bootstrap capacitor C_{boot} is equal to

$$C_{boot} = \frac{Q_{total}}{\Delta V_{boot}}$$

Where Q_{total} is the total amount of the C_{boot} charge;

ΔV_{boot} is the voltage drop of C_{boot}.

$$Q_{total} = Q_{gate} + \left(I_{lkcap} + I_{lkgs} + I_{qbs} + I_{lk} + I_{lkdiode}\right) * t_{on} + Q_{ls}$$

$$\Delta V_{boot} = V_{DD} - V_F - V_{gsmin}$$

Where Q_{gate} is the total charge of MOSFET gate;

I_{lkcap} is the leakage current of C_{boot};

I_{lkgs} is the leakage current of gate-source switch;

I_{qbs} is the quiescent current of the bootstrap circuit;

I_{lk} is the leakage current of the bootstrap circuit;

$I_{lkdiode}$ is leakage current of the bootstrap diode;

t_{on} is the turn-on time of MOSFET on high-side;

Q_{ls} is the required charge of the internal level shifter,

for all high-voltage gate drivers, $Q_{ls} = 3nC$;

V_{DD} is supplied voltage by the driver gate;

V_F is the forward voltage of the bootstrap diode;

V_{gsmin} is the minimum voltage of gate-source MOSFET.

4.3 System Control

Arduino is an easy tool in electronics and programming, its offerings range from simple 8-bit boards to products for IoT applications, 3D printing, and wearable electronic, and embedded environments. Arduino has open-source software, and Arduino boards are also completely open-source, the code is easily written and simply uploaded to the board. It can run on most computer environments; Windows, Mac OS X, and Linux. Any kind of Arduino board uses the same software. As it offers an accessible and simple user experience, thousands of different projects and applications use Arduinos. Arduino is not only easily to use for beginners, but also very flexible for advanced users [36]. Arduino offers several advantages:

- Compare with other microcontroller platforms, Arduino boards are relatively cheap.
- Arduino software can operate in Windows, Macintosh OSX, and Linux environments.
- The program code of Arduino is written simply and clearly.
- Both Arduino software and Arduino hardware are Open source and extensible.

4.3.1 MPPT Control

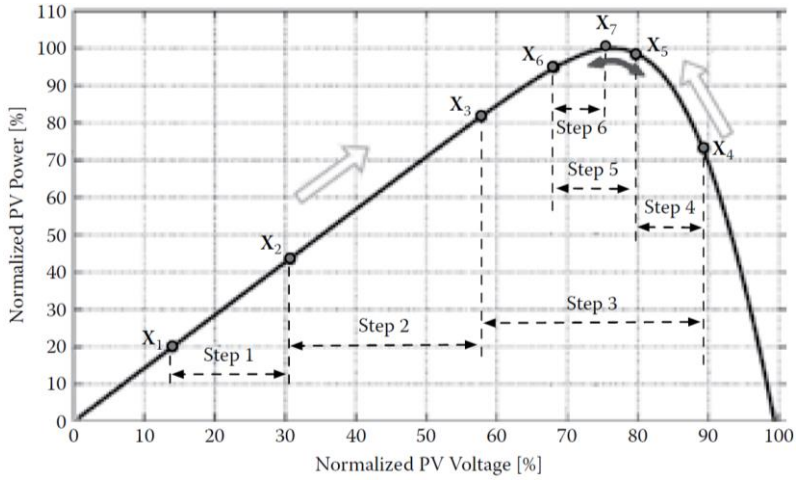

Figure 31: Variable step MPPT of the ImP&O method

The ImP&O method is the chosen algorithm to be used for this MPPT. The most significant part is the duty cycle D which is calculated from the changes of output PV power and voltage (dP and dV). The changed step size ΔD represents the next perturbation.

$$dP > 0 \begin{cases} dV > 0 \rightarrow \Delta D > 0 \\ dV < 0 \rightarrow \Delta D < 0 \end{cases}$$

$$\mathrm{dP} < 0 \begin{cases} \mathrm{dV} > 0 \rightarrow \Delta \mathrm{D} < 0 \\ \mathrm{dV} < 0 \rightarrow \Delta \mathrm{D} > 0 \end{cases}$$

Referring to the above Figure 31, when the operating point moves from x_1 to x_2, there is

$dP = P_2 - P_1 > 0$, and $dV = V_2 - V_1 > 0$, so the step size $\Delta D > 0$, the perturbation direction is the positive which is the increased voltage. When the operating point moves from x_4 to x_5, $dP = P_5 - P_4 > 0$, and $dV = V_5 - V_4 < 0$, so the step size $\Delta D < 0$, the perturbation towards to the negative direction which results in decreased voltage.

Multiply the changes of the power and voltage ($dP * dV$) to simply the above equations,

$$\begin{cases} dP * dV > 0 \rightarrow \Delta D > 0 \\ dP * dV < 0 \rightarrow \Delta D < 0 \end{cases}$$

For A high efficiency of MPPT, the following is the calculation function of the variable step size ΔD.

$$|\Delta D| = N\frac{|P_{new} - P_{old}|}{|V_{new} - V_{old}|} = N\frac{|dP|}{|dV|}$$

Based on these two equations above,

$$\Delta D = N\frac{dP}{dV}$$

where N is the scaling factor, setting N=0.06. The extreme of the change of duty cycle is setting $|\Delta D| < \Delta D_{max} = 0.3$.

The permissible error Err is used in this system to avoid unnecessary perturbations near the MPP, to optimize the MPPT performance. The permissible error (Err) is used for comparing with the change of the power (dP) before the multiplication and its sign judgment (dP/dV).

$$\begin{cases} |dP| < Err \rightarrow \Delta D = 0 \\ |dP| > Err \rightarrow \Delta D = N\dfrac{dP}{dV} \end{cases}$$

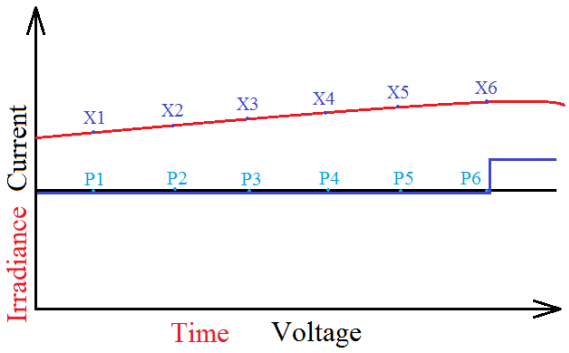

Figure 32: Diagram of MPPT control with slowly changed curve

In this operation, locking variables V_{block}, I_{block} and P_{block} are used in this ImP&O control system. When the curve moves very slowly (red line), as shown in Figure 32, the change between point x_1 and x_2 is very small ($|dP| < Err$), the duty cycle will not change, ΔD=0. At this time, the values of voltage, current and power at the point x_1 will be saved as V_{block}, I_{block} and P_{block}. When the locking values is not equal to zero, the old value (V_{old}, I_{old} and P_{old}) will be equal to the locking values. At the last, the compared points will become to the point x_1 and x_6, $|dP| > Err$, then the duty cycle changes with the irradiance, the operation point is close to the MPP (blue curve). The flow chart of the ImP&O algorithm is shown in Figure 33.

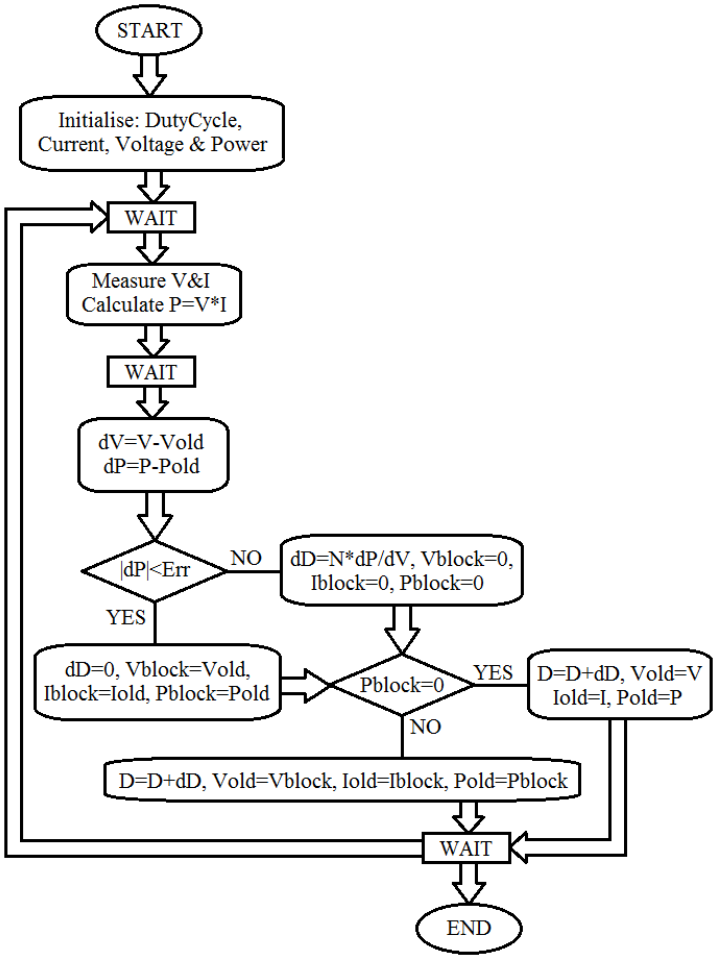

Figure 33; Logic block diagram of MPPT control

4.3.2 Relay Control

After the DC/AC inverter conversion from the DC PV power to AC power, the AC power will supply the household water heater. When the generation energy in PV is not enough for heating water, for instance at night time, the water heater will be connected with the main grid. This is the operation function of the control system.

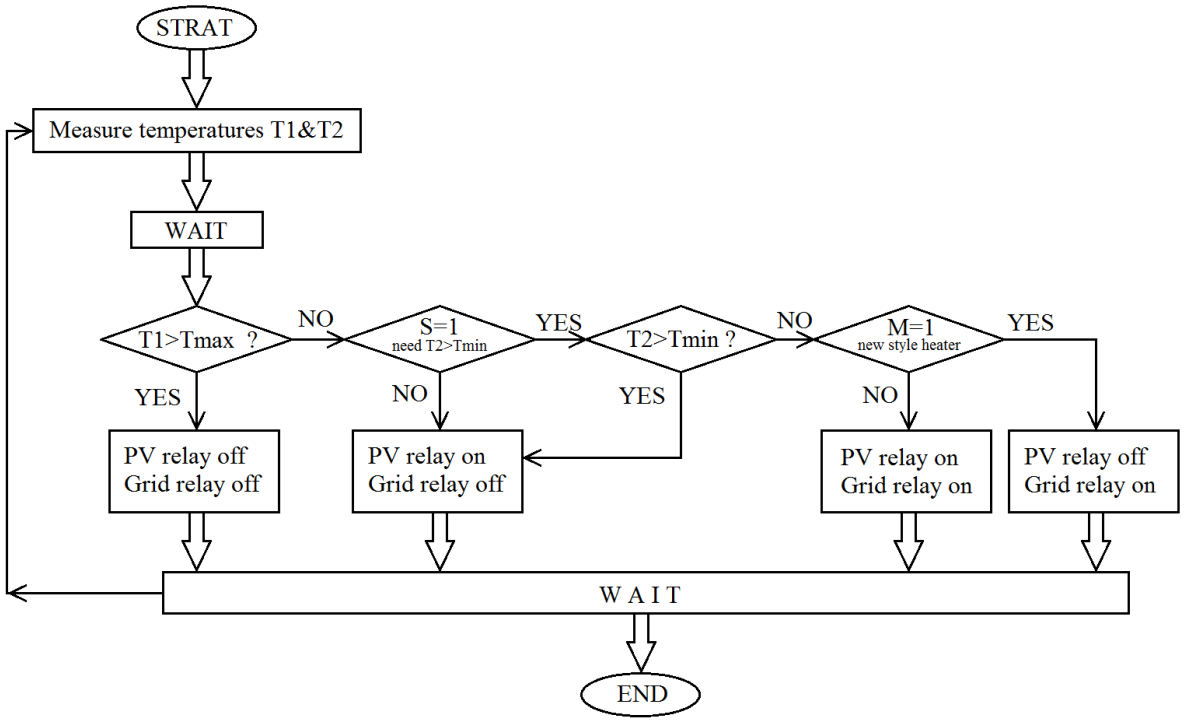

Figure 34: Logic block diagram of the control system.

In a hot water cylinder, the hotter water is mostly located at the top of tank, and the colder water is at the bottom. As shown in Figure 34, there are two temperature sensors in the household water heater tank. These two temperatures (T_1 & T_2) are tested by two sensors located on the top and bottom of the tank. The top sensor is used to test the higher temperature of the tank water (T_1), when the top tested temperature reaches maximum water temperature, $T_1 \geq T_{max}$, both of the supplies will be disconnected. The bottom sensor is for testing the lower water temperature in the tank (T_2), the bottom temperature compares with the minimum value T_{min} to switch relays of supply source.

Switch M controls the style of water heater, new & old. The new style heater can be supplied by PV panels and grid at the same time (M=1), only one energy source can be used by the old style heater (M=0). Heater style is needed to set only at the first use time. If the temperature is needed to be higher than T_{min}, setting S=1, the water heater will be supplied by the grid electricity when $T_2 \leq T_{min}$. If the lowest water temperature is unlimited, setting S=0, the relay of grid will be off.

4.3.3 User Interface

MPPT control uses the measured output current and voltage from the solar array to calculate the duty cycle, and 4 controlled PWM signals are output for MOSFET switching. By this way, PV panels operate on the maximum power point and generation max-power. Whether the generated power will be used or not is controlled by relay control. A LCD display will be used to show all of the important parameters (Figure 35).

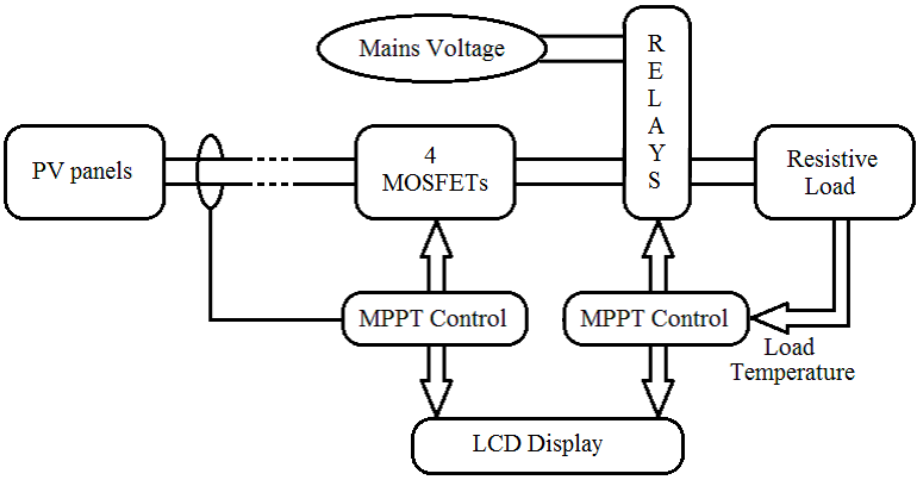

Figure 35: User Interface block diagram of PV conversion control system

Chapter 5

SIMULATION

5.0 Introduction

MATLAB is software for engineering and mathematical analysis and design. MATLAB solves and optimizes scientific and engineering problems by its matrix-based MATLAB language. Data could be easily visualized by the built-in graphics to gain insights [37].

In this chapter, the PV conversion system will be simulated by MATLAB. The simulation of the household water heater system will be classed by different sub-system in MATLAB (Figure 36).

- The PV power sub-system will simulate the generation of the solar array. This sub-system will only be used in this simulation chapter, and the output energy will be generated by PV panel DJ-195D/A in the application.
- The power circuit sub-system is the most significant part in the project. Up to 2.4k Watts will flow in this circuit. The H-bridge converter is in this sub-system.
- The resistive load sub-system is the equivalent resistance of the water heater.
- The control sub-system is the central processing unit of the project. Arduino will be used to implement the control function in the actual PV conversion system.

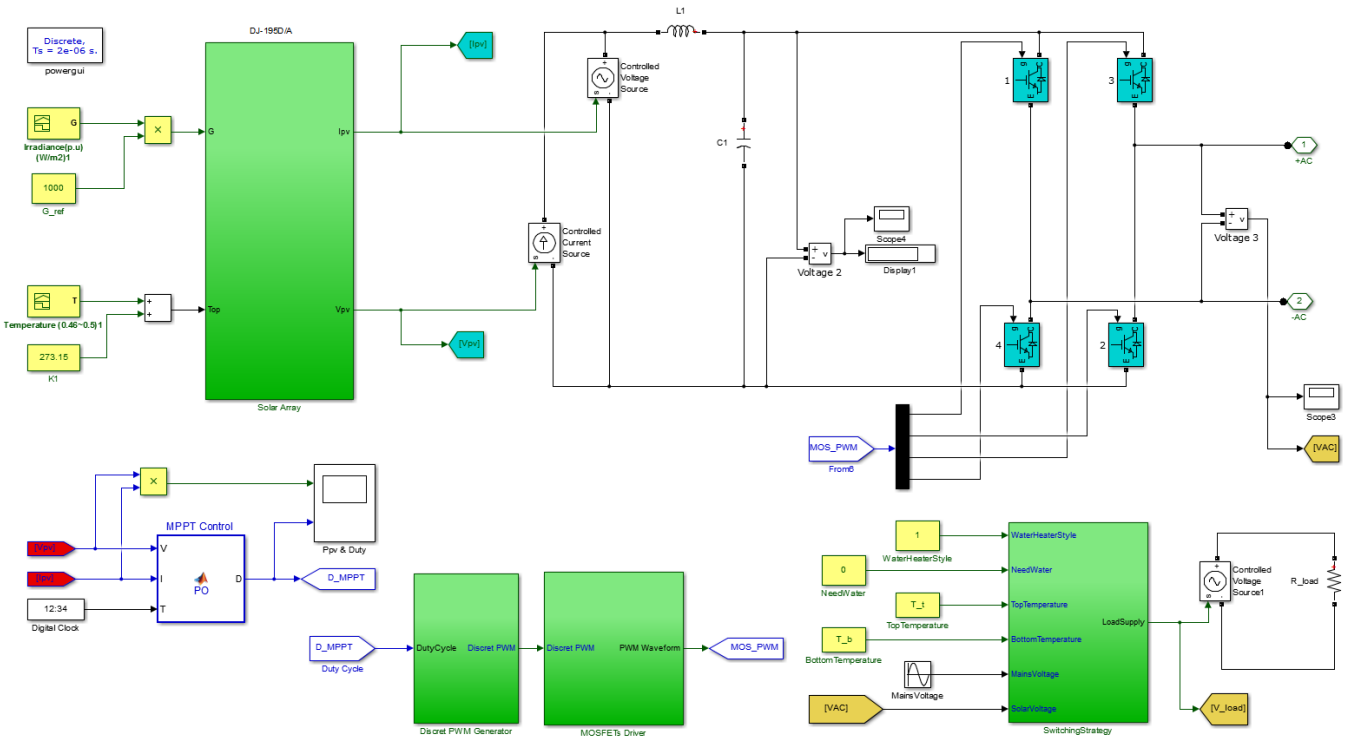

Figure 36: The simulation of PV conversion system in MATLAB

5.1 PV Power sub-system

In the PV power sub-system, the solar array with 12 PV panels is simulated. As shown in Figure 37, the current and voltage generated by one PV panel will be outputted firstly, and then modified according to the solar array connection, 2 strings parallel connected of 6 panels.

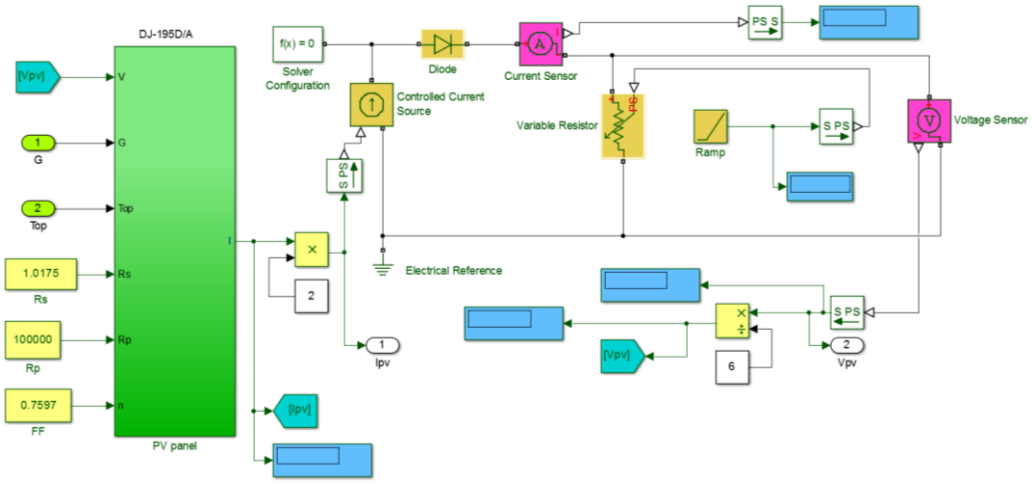

Figure 37: The sketch view of PV power sub-system in MATLAB

5.1.1 Parameter Calculation

Referring to the function of section 4.1, and according to Kirchhoff's laws, the output of PV panel [38-42] is

$$I = I_{ph} - I_{sat}\left(e^{\frac{V+IR_s}{AV_t}} - 1\right) - \frac{V + IR_s}{R_p}$$

These two resistors, parallel resistance R_p and serial resistance R_s, are the main parameters for the PV panel. The model can be simplified by ignoring $R_s + R_p$, resulting in

$$I = I_{ph} - I_{sat}\left(e^{\frac{V}{AV_t}} - 1\right)$$

$$I_{sat} = C * T^3 * e^{\frac{E_{gap}}{K*T}}$$

Where V_t, the thermal voltage, $V_t = kT/q$;

A, the ideality factor;

C, the temperature coefficient,

I_{sat}, the saturation current of the diode;

I, the PV current;

V, the PV voltage;

I_{ph}, the photo-induced current;

E_{gap}, the band gap of the semiconductor material, $E_{gap} = 1.124\ eV = 1.8e-19\ J$.

The series resistor R_s, the parallel resistor R_p and the thermal voltage V_t,

$$R_s \approx -\frac{dI}{dV}|_{V=V_{OC}}$$

$$R_p \approx -\frac{dV}{dI}|_{I=I_{SC}}$$

$$V_t = \frac{KT}{q} = \frac{(1.3806503e-23) * 298.15}{1.60217646e-19} = 0.0257\ V$$

Where K is the Boltzmann constant, K=1.3806503e-23 J/K, T is the absolute temperature of the p–n junction, and q is the magnitude of charge of an electron (the elementary charge) q=1.60217646e-19 C.

The derivative of the I-V characteristics is described by:

$$\frac{di}{dv} = -\frac{\frac{I_{sat}}{AV_t}e^{\frac{V+IR_s}{AV_t}} + \frac{1}{R_p}}{1 + \frac{I_sR_s}{AV_t}e^{e^{\frac{V+IR_s}{AV_t}}} + \frac{R_s}{R_p}}$$

The panel of DJ-195D/A is used for testing in this project. For Standard Test Conditions (STCs), the three points, ($V_{OC,STC}$, 0), (0, $I_{SC,STC}$) and ($V_{mpp,STC}$, $I_{mpp,STC}$), where $V_{OC,STC}$ is the open-circuit voltage, $I_{SC,STC}$ is the short-circuit current, $V_{mpp,STC}$ & $I_{mpp,STC}$ are the MPP

conditions (Appendix 1). The photo-induced current I_{ph} is calculated straightforwardly by the above equation, because it is significantly higher than the diode current, so that in STCs it is assumed to be equal to the short-circuit current I_{SC}, (0, $I_{SC,STC}$).

$$I_{SC} = I_{ph} - I_{sat}\left(e^{\frac{I_{SC}R_s}{An_sV_{t,STC}}} - 1\right)$$

$$I_{ph,STC} = I_{SC,STC} = 5.56\,A$$

In the open-circuit condition, (V_{oc}, 0),

$$0 = I_{ph,STC} - I_{sat,STC}\left(e^{\frac{V_{OC,STC}/n_s}{AV_{t,stc}}} - 1\right) \approx I_{ph,STC} - I_{sat,STC} * e^{\frac{V_{OC,STC}/n_s}{AV_{t,stc}}}$$

By neglecting the unitary term with respect to the exponential one, the equation can be approximated by

$$V_{OC,STC} \approx -An_sV_{t,STC}\ln\frac{I_{sat,STC}}{I_{ph,STC}}$$

Where: $\alpha_v = \frac{dV_{OC}}{dT}|_{STC}$, open-circuit voltage-temperature coefficient; $\alpha_i = \frac{dI_{SC}}{dT}|_{STC}$, short-circuit current/temperature coefficient;

Open-circuit voltage-temperature coefficient,

$$\alpha_v = \frac{dV_{OC}}{dT} = \frac{d}{dT}(n_sAV_{t,STC}\ln I_{ph,STC} - n_sAV_{t,STC}\ln I_{sat,STC})$$

Including for the temperature dependence of the thermal voltage,

$$\alpha_v = \frac{n_sAV_{t,STC}}{T_{STC}}\ln\frac{I_{ph,STC}}{I_{sat,STC}} + n_sAV_{t,STC}(\frac{1}{I_{ph,STC}}\frac{dI_{ph,STC}}{dT} - \frac{1}{I_{sat,STC}}\frac{dI_{sat,STC}}{dT})$$

$$\frac{1}{I_{sat,STC}}\frac{dI_{sat,STC}}{dT} = \frac{3}{T_{STC}} + \frac{E_{gap}}{KT_{STC}^2}$$

$$\frac{1}{I_{ph,STC}}\frac{dI_{ph,STC}}{dT} = \frac{\alpha_i}{I_{ph,STC}}$$

$$\alpha_v = \frac{n_s A V_{t,STC}}{T_{STC}} \ln\frac{I_{ph,STC}}{I_{sat,STC}} + n_s A V_{t,STC}\left(\frac{\alpha_i}{I_{ph,STC}} - \frac{3}{T_{STC}} - \frac{E_{gap}}{KT_{STC}^2}\right)$$

$$\alpha_v = \frac{V_{OC,STC}}{T_{STC}} + n_s A V_{t,STC}\left(\frac{\alpha_i}{I_{ph,STC}} - \frac{3}{T_{STC}} - \frac{E_{gap}}{KT_{STC}^2}\right)$$

Where α_v = -0.34%/°C = -0.0034, α_i = 0.037%°C = 0.00037.

$$A = \frac{\alpha_v - \frac{V_{OC,STC}}{T_{STC}}}{n_s V_{t,STC}\left(\frac{\alpha_i}{I_{ph,STC}} - \frac{3}{T_{STC}} - \frac{E_{gap}}{KT_{STC}^2}\right)}$$

$$\alpha_v = -0.34\% = -0.0034;\ V_{OC,STC} = 46.14\,V;\ T_{STC} = 298.15\,K;\ V_{t,STC} = 0.0257\,V;$$

$$\alpha_i = 0.037\% = 0.00037;\ I_{ph,STC} = 5.56\,A;\ E_{gap} = 1.124\,eV = 1.8e-19\,J;$$

$$K = 1.3806503e-23\,\frac{J}{K};$$

$$n_s A = \frac{\alpha_v - \frac{V_{OC,STC}}{T_{STC}}}{V_{t,STC}\left(\frac{\alpha_i}{I_{ph,STC}} - \frac{3}{T_{STC}} - \frac{E_{gap}}{KT_{STC}^2}\right)}$$

$$= \frac{-0.0034 - (46.14/298.15)}{0.0257 * \left(\left(\frac{0.00037}{5.56}\right) - \left(\frac{3}{298.15}\right) - \left(\frac{1.8e-19}{(1.3806503e-23) * 298.15 * 298.15}\right)\right)}$$

$$= 39.2822$$

$$n_s A V_{t,STC} = 39.2822 * 0.0257 = 1.0096$$

In order to calculate I_{sat}, the open-circuit conditions can be used as well, from

$$I_{sat,STC} \approx I_{ph,STC} e^{-\frac{V_{OC,STC}}{n_s A V_{t,stc}}} = 5.56 * \exp\left(-\frac{46.14}{36.2822 * 0.0257}\right) = 1.7994e-21\ A$$

The temperature coefficient C,

$$C = \frac{I_{sat,STC}}{T_{STC} 3 e^{\frac{E_{gap}}{K T_{STC}}}} = \frac{I_{sat,STC}}{3 T_{STC} e^{\frac{E_{gap}}{K T_{STC}}}} = \frac{1.7994e-21}{3 * 298.15 * \exp(\frac{1.8e-19}{(1.3806503e-23) * 298.15})}$$
$$= 2.0558e-43$$

MPP data ($V_{mpp,STC}$, $I_{mpp,STC}$),

$$I_{mpp,STC} = I_{ph,STC} - I_{sat,STC}\left(e^{\frac{V_{mpp,STC}+I_{mpp,STC}R_s}{A n_s V_{t,STC}}} - 1\right)$$
$$\approx I_{ph,STC} - I_{sat,STC} e^{\frac{V_{mpp,STC}+I_{mpp,STC}R_s}{A n_s V_{t,STC}}}$$
$$= I_{ph,STC} - I_{ph,STC} e^{\frac{-V_{OC,STC}+V_{mpp,STC}+I_{mpp,STC}R_s}{n_s A V_{t,stc}}}$$

The series resistor,

$$R_s = \frac{n_s A V_{t,STC} \ln\left(1 - \frac{I_{mpp,STC}}{I_{ph,STC}}\right) + V_{OC,STC} - V_{mpp,STC}}{I_{mpp,STC}}$$
$$= \frac{39.2822 * 0.0257 * \ln\left(1 - \frac{5.05}{5.56}\right) + 46.14 - 38.59}{5.05} = 1.0175\ Ohms$$

In conclusion, for Standard Test Conditions (STCs), I_{ph}, I_{sat}, R_s, are all constant. From the above equations,

$$I = 5.56 - 1.7994 * 10^{-21}\left(e^{\frac{V+1.0175I}{1.0096}} - 1\right)$$

And for the MPP, based on the equation,

$$\frac{di}{dv} = -\frac{I_{mpp,STC}}{V_{mpp,STC}}$$

$$\frac{di}{dv} = -\frac{\frac{1.6365 * 10^{-19}}{1.0096} e^{\frac{V+0.5559I}{1.0096}}}{1 + \frac{1.6365 * 10^{-19} * 0.5559}{1.0096} e^{\frac{V+0.5559I}{1.0096}}} = -\frac{1.9679 * 10^{-19} e^{\frac{V+0.5559I}{1.0096}}}{1 + 1.0940 * 10^{-19} e^{\frac{V+0.5559I}{1.0096}}}$$

Fill Factor (FF) expresses the productivity of the solar cell energy, it is effected by these two resistances R_s & R_p.

$$FF = \frac{V_{MPP} I_{MPP}}{V_{OC} I_{SC}}$$

$$FF = \frac{38.59 * 5.05}{46.14 * 5.56} = 0.7597$$

The fill factor of DJ-195D/A is 0.76. For a household application, the panel DJ-195D/A is suitable. As shown in Figure 37, the series resistance R_s is 1.0175 Ohms, the parallel resistance R_p had been assumed to be infinity, so in the simulation system it is set to 100,000 Ohms.

5.1.2 Simulation Results and Sensitivities

In this PV power sub-system, the main affecting factors of PV penal generation must be considered which are irradiance and temperature. The simulation output of PV power system will follow these factors, it is similar with the actual situation.

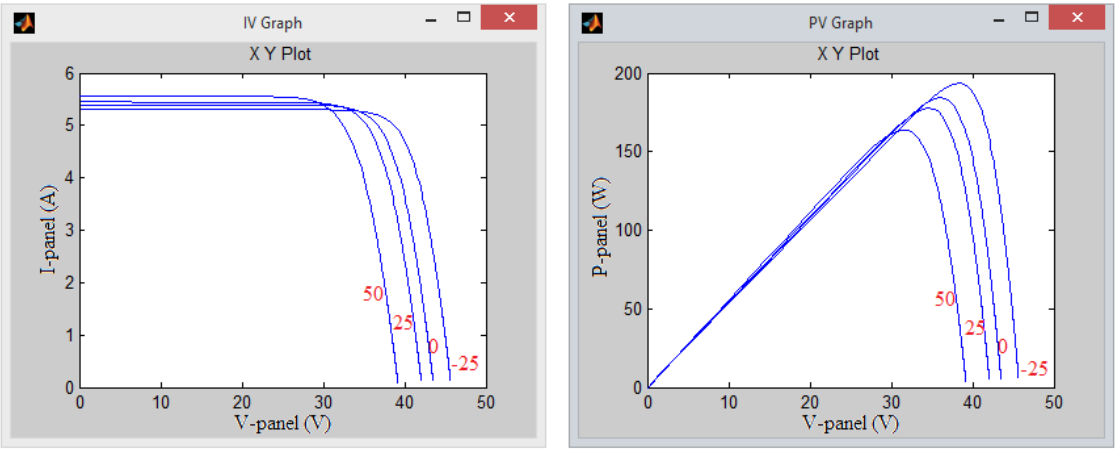

Figure 38: Simulation outputs of one PV panel with fixed irradiance ($G = 1000W/m^2$), temperature factors increases from -25°C to 50°C

In view of Figure 38, both of the open circuit voltage V_{oc} and the short circuit current I_{sc} of PV panel output are declined with the increasing temperature. This matches the Current-Voltage characteristics of DJ-195D/A datasheet (Appendix 1). Table 8 shows the R-I-V internship when the temperature is -25°C and the irradiance is $1000W/m^2$ (P_{mpp}=195.3Watts, $I_{sc} = 5.291\ Amps$, $V_{oc} = 46\ Volts$).

Table 8: The R-I-V characteristics when $T = -25°C$ and $G = 1000W/m^2$

Resistance (Ohms)	0.1	1	10	20	23	30	50	100	1000
Current (Amp)	5.291	5.291	5.289	5.258	5.047	4.169	2.629	1.351	0.138
Voltage (Volt)	0.1764	1.764	17.63	35.05	38.69	41.69	43.82	45.03	46

According to Figure 39 & Figure 40, the short circuit current I_{sc} of PV panel output drops with the decreasing irradiance, but the open circuit voltage V_{oc} is not changed with the fixed temperature T=25°C. The trend of I-V characteristics with irradiance (Figure 39) is same with the simulation result of software PVsyst (Figure 41)

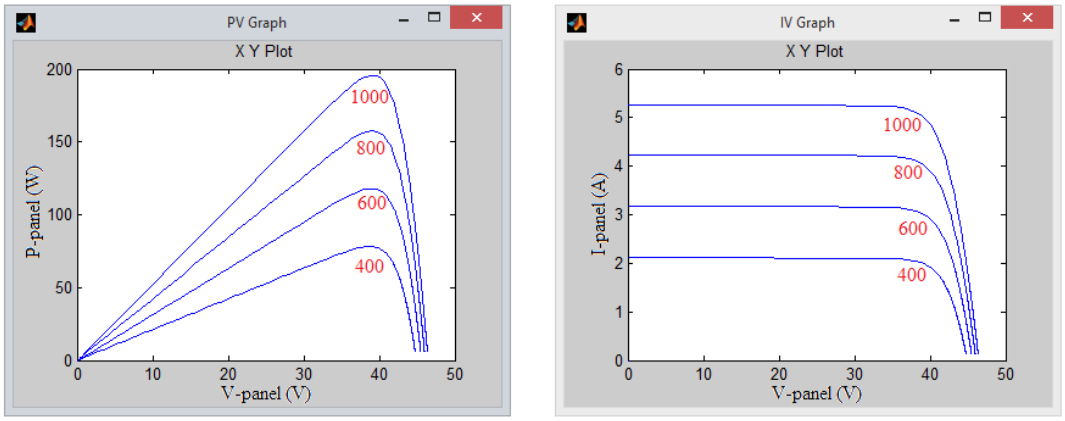

Figure 39: Simulation outputs of PV panel with fixed temperature T=25°C, irradiance factors decreases from $G = 1000W/m^2$ to $G = 400W/m^2$

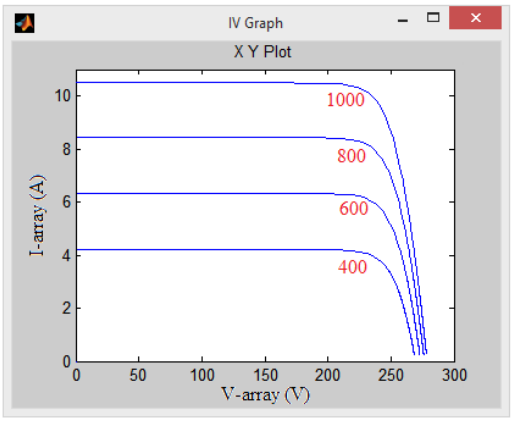

Figure 40: Simulation I-V characteristics of solar array with fixed temperature T=25°C, irradiance factors decreases from $G = 1000W/m^2$ to $G = 400W/m^2$

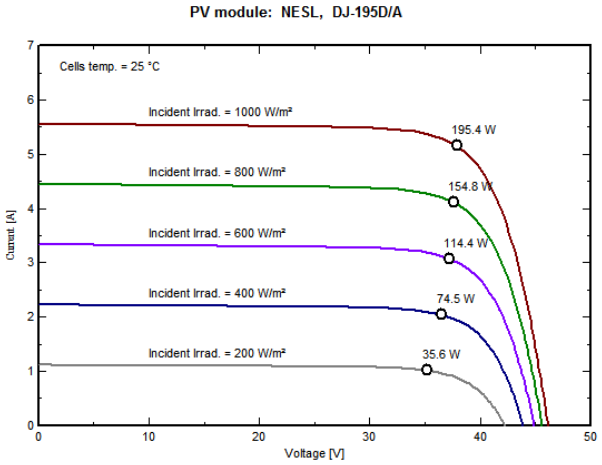

Figure 41; I-V characteristics trend with irradiance in PVsyst

5.2 Power Circuit sub-system

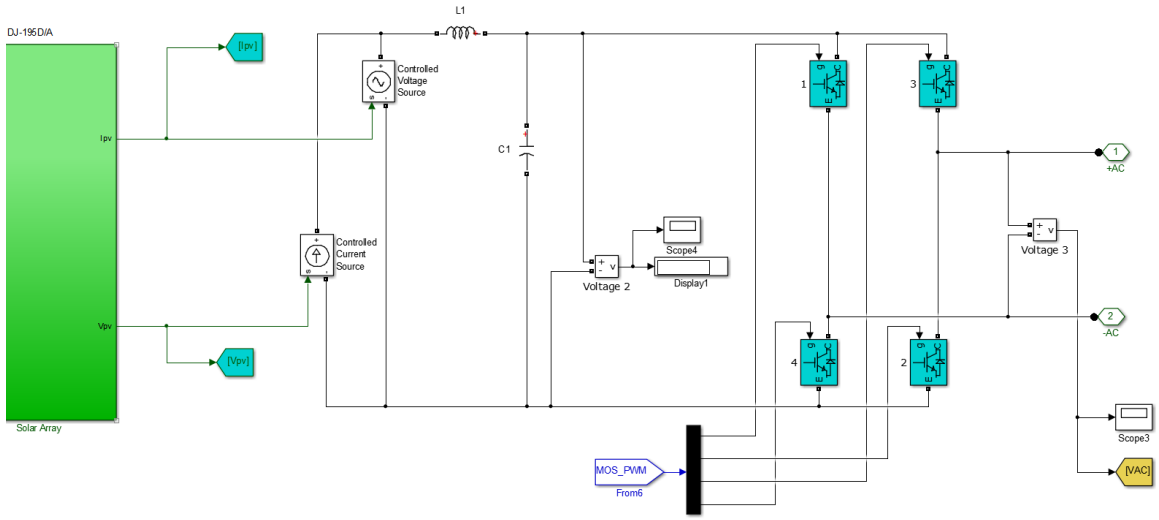

Figure 42: Power Circuit sub-system schematic in MATLAB

5.2.1 H-Bridge

As shown in Figure 42, IGBT/Diode elements are used instead of MOSFETs of the H-bridge for simulation, the parameters are also setting the same with MOSFET IXFK150N30P3 (Appendix 3). As shown in Figure 43, the H-bridge converts the PV DC energy to an AC energy with 50 Hz switching frequency, each positive/negative output switches with 30 kHz high frequency. This AC output energy could directly supply the household water heater without any more transformation.

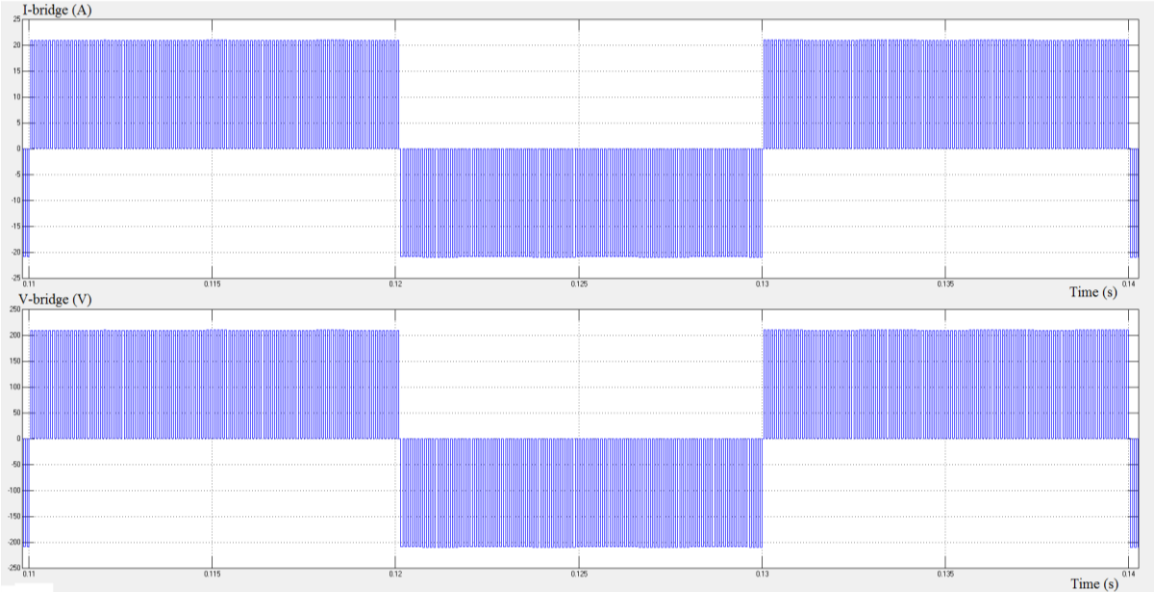

Figure 43: Output of H-bridge, output current with 20.9Amps peak value (the first waveform) and output voltage with 209.4Volts peak value (the second waveform).

5.2.2 DC Filter

In accordance with section 4.2.2, a LC low pass filter is used to block the high frequency currents from flowing in the PV panels. Inductance and capacitance of this DC filter are respectively $L = 15\mu H$, $C = 35\mu F$, and the cut off frequency is $f = 6.95\ kHz$ (Figure 44). The rated maximum ripple current of the filter capacitor is 31.5 Amps.

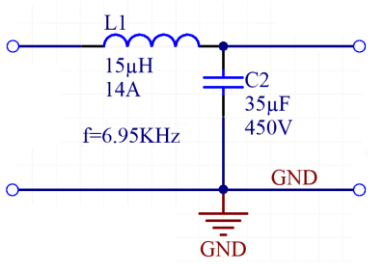

Figure 44: Low Pass LC Filter

5.2.3 Gate Driver

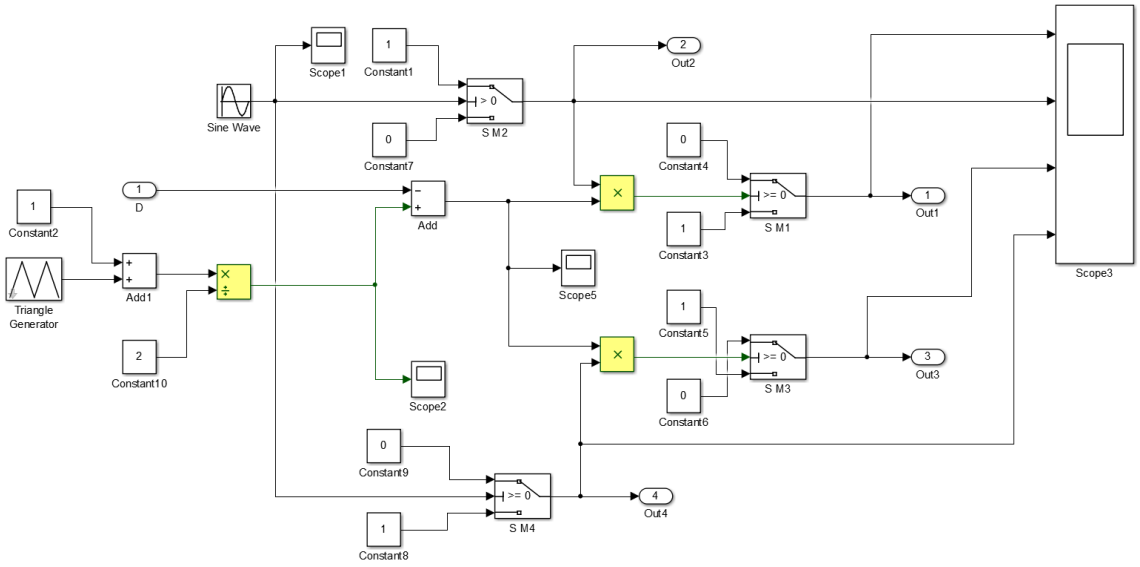

Figure 45: Gate driver circuit schematic

The gate driver circuit outputs PWM control signals for the 4 H-bridge MOSFETs based on the duty cycle of MPPT control. The switching frequency is decided by the gate driver circuit in MATLAB. As shown in Figure 45, the frequency of the triangle generator controls the switching of switches 1&3, the sine wave frequency is the low switching frequency of switches 2&4. The low frequency switching signal directly controls the bottom two switches (2&4) and steers the high frequency switching signal to the top two switches (3&1). The resultant MOSFET switching signal are shown in Figure 46 & Figure 47.

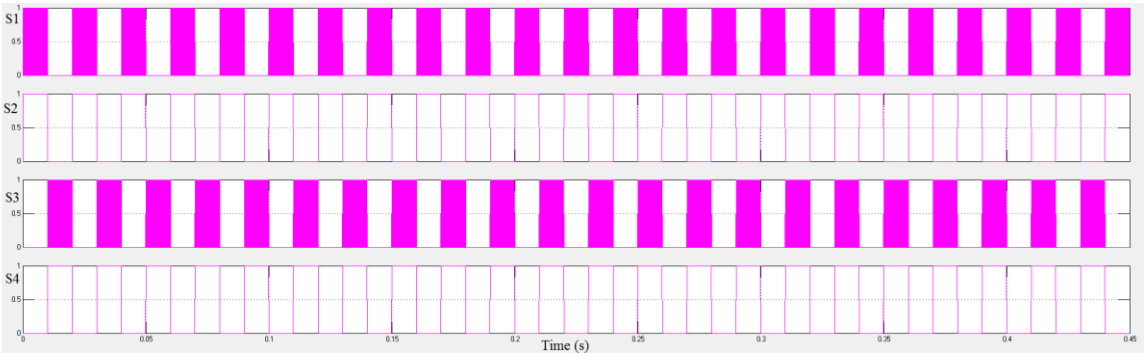

Figure 46: Four PWM control signals output of the gate driver circuit

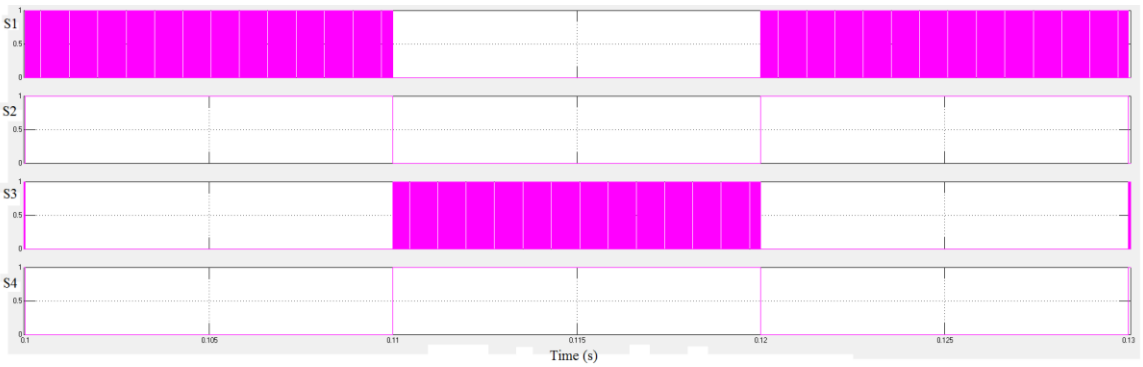

Figure 47: Enlarged views of 4 PWM control signals output (Figure 46)

5.3 Resistance Load sub-system

In this simulation sub-system, the load is modelled by an equivalent resistance (Figure 48). In according with the maximum power output of the solar array (231.54 Volts, 3k Watts), the equivalent resistor could be calculated.

$$R_{load} < \frac{V_{array}^2}{P_{array}} = \frac{231.54^2}{3000} = 17.9\ Ohms$$

At this resistance load sub-system, the equivalent resistance is setting to equal to 10 Ohms.

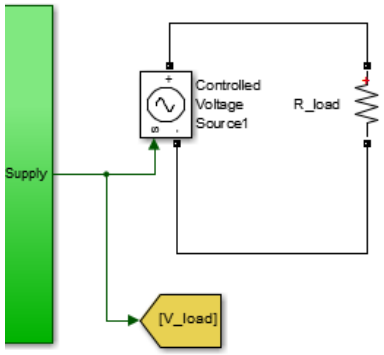

Figure 48: Resistance load schematic

5.4 Control sub-system

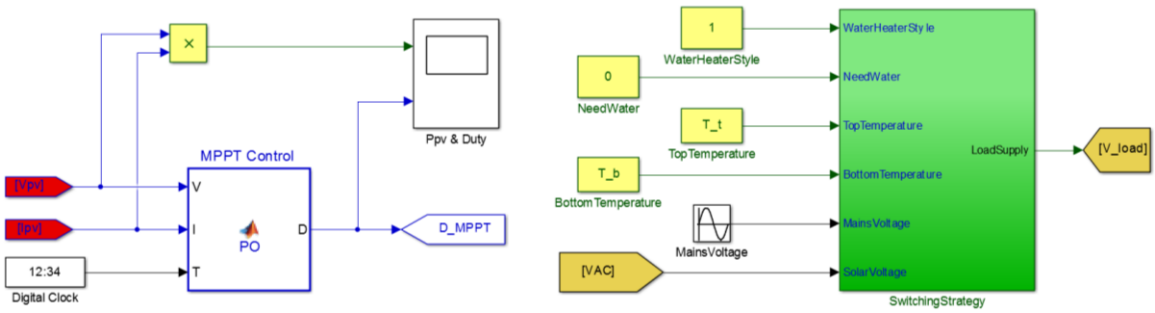

Figure 49: Control system schematic

5.4.1 MPPT Control

MPPT control tracks the MPP of the solar array in this project. MPPT determines the efficiency of PV power system, so it is one of the most important controller for the project. For the simulation in MATLAB, the MPPT function is achieved by a MPPT program. The MPPT control program calculates the duty cycle in according with the current and voltage of the solar array, the block flow chart is referred to Figure 33 in chapter 4. The output duty cycle of MPPT operation is shown in Figure 50.

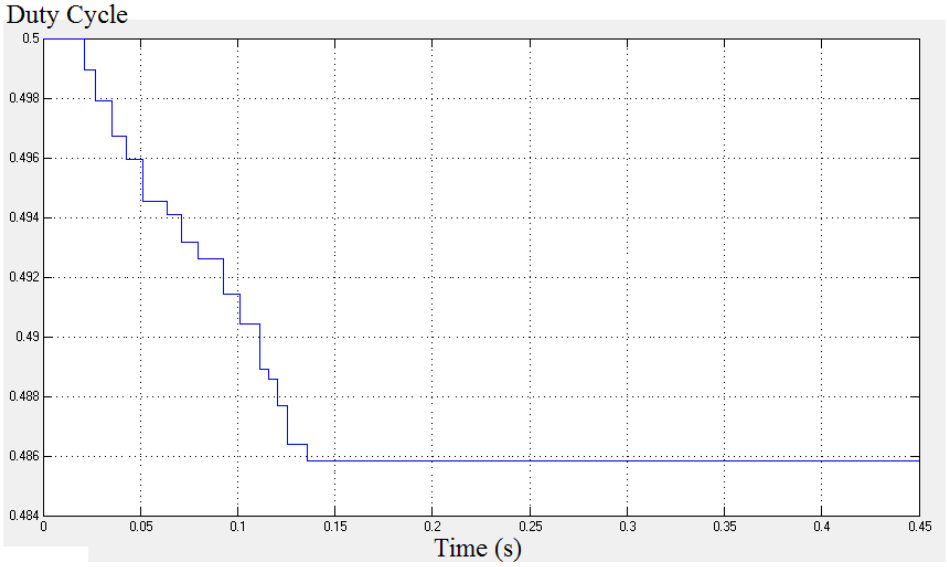

Figure 50: Calculation output of duty cycle by MPPT controller in MATLAB

5.4.2 Relay Control

The relay control switches the supply source of the household water heater between PV panels or main grid. When hot water is needed, the input water temperatures at top and bottom of the water heater tank decide the source of power to supply the load. The water heater mode style is the decisive factor which is either the single source from PV panels or main grid or the source from both of PV panels and main grid (Figure 34 in Chapter 4). In this project, the heater is operated by PV panels supply most of the time. When the solar array generation is not enough to heat water, the heater will be supplied by main grid. Figure 51 shows the input and output of the relay controller.

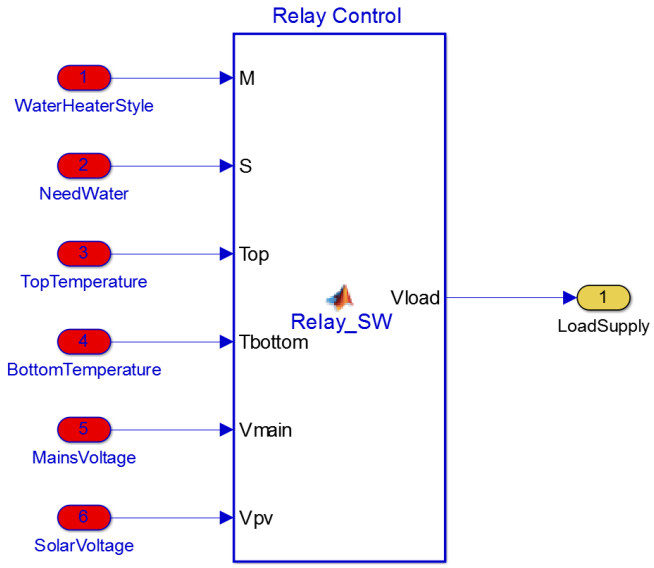

Figure 51: Relay controller in MATLAB

5.5 Simulation Results

In this section, a simulation of the PV conversion system is conducted to demonstrate and analyse the PV conversion system. The PV conversion system under STC (the Standard Test Condition, T=25°C, $G = 1000W/m^2$). Figure 52 and Figure 53 show the simulated generation electricity of one PV panel and the solar array. Both of these two characteristic curves are on the maximum power point, showing that the MPPT control is implemented and operates well. After about 0.15 seconds, the generation power of solar array outputs is

stable and holds at the maximum value. Comparing Figure 55 with Figure 46, the AC output matches the 4 PWM control signals output of the gate driver. The time from start to 0.05 seconds shows the details of MPPT operation in Figure 55.

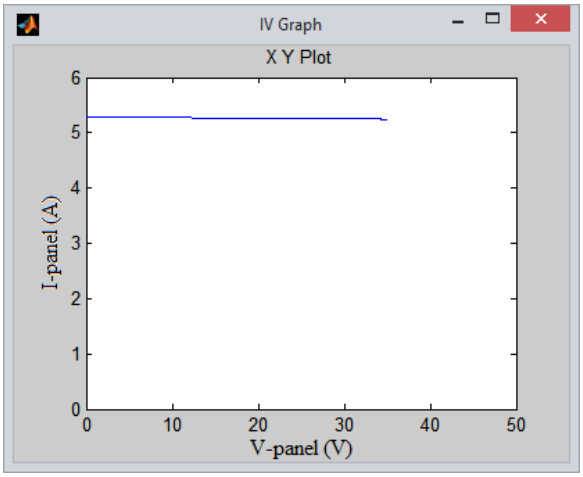

Figure 52: Simulation output I-V characteristics of one PV panel in the PV conversion system

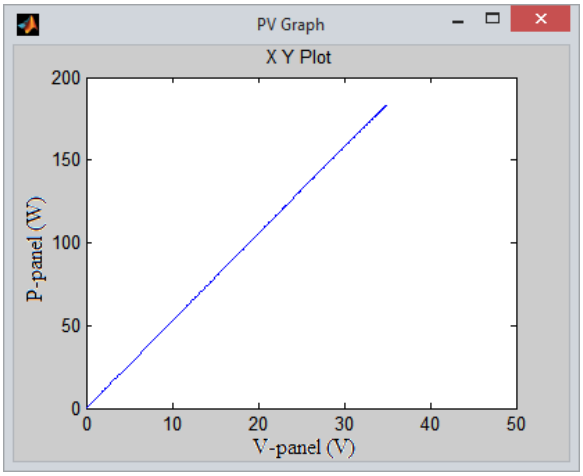

Figure 53: Simulation output P-V characteristics of the solar array in the PV conversion system

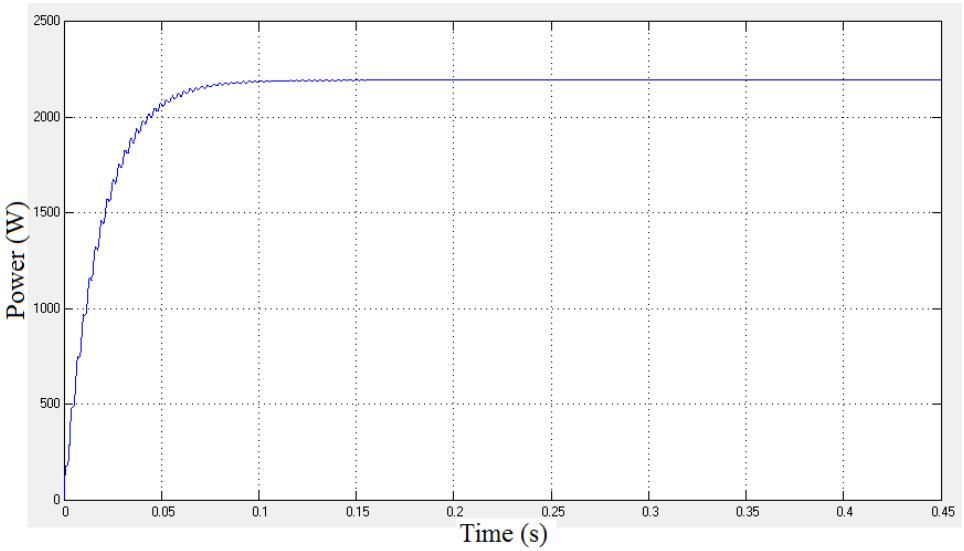

Figure 54: Simulation generated power of the solar array with MPPT control in the PV conversion system

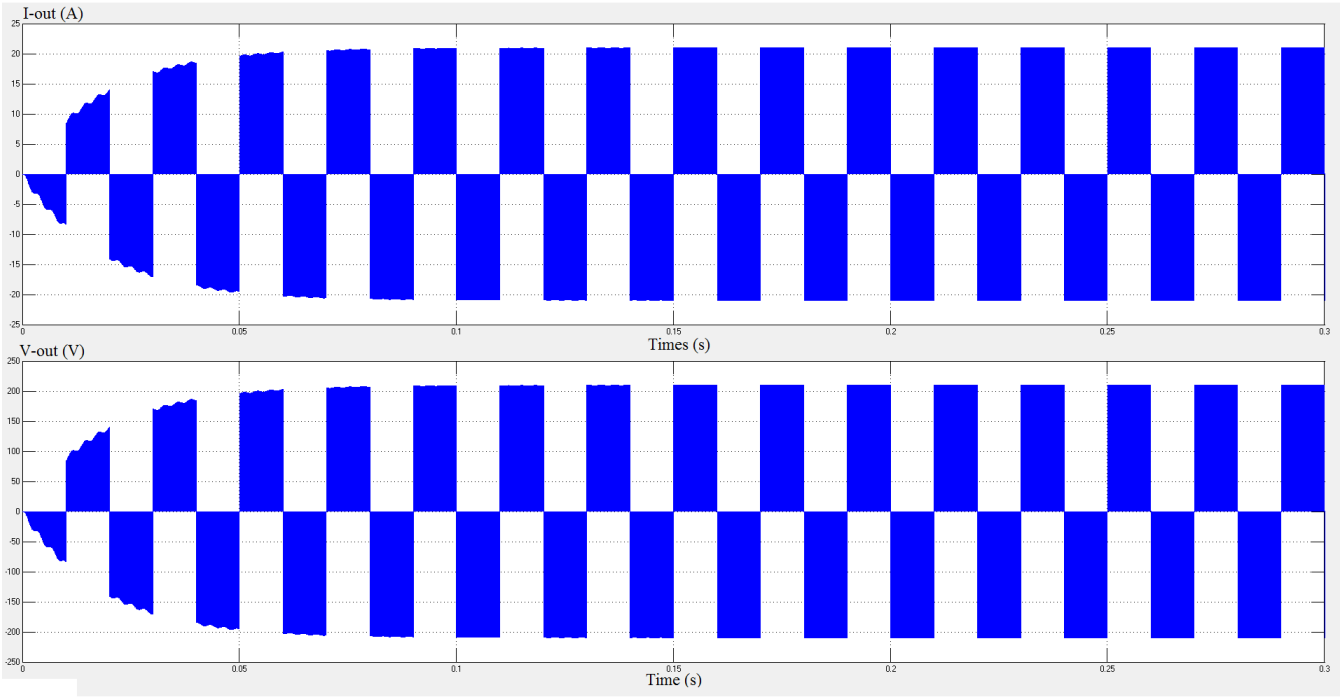

Figure 55: AC output of the H-bridge conversion in MATLAB

Chapter 6

SCHEMATIC & CIRCUIT BOARD DEVELOPMENT

6.0 Introduction

In this chapter, the circuit schematic and circuit board of the project is presented. At the centre of the circuit, this chapter will focus on the PCB. The tool of choice for the project is Altium Designer. Altium is very easy to use and up to date component database. As a tool for PCB design, its odds of production success are high. Altium has a centralized platform for management and design, almost all of the small and key details are automatically set, the designs can be protected efficiently and the integrity of ECAD data and the workflow can also be managed. The latest technology is constantly being updated in Altium, for instance new products or new processor architectures [43].

6.1 Schematic

6.1.1 Main Board

The main board and the PCB layout in Altium Designer is shown in this section. There are four sections of the main board; current and voltage sensor circuit, DC filter circuit, H-bridge conversion and MOSFET snubber circuit and gate driver circuit.

6.1.1.1 Sensor Circuit & Filter

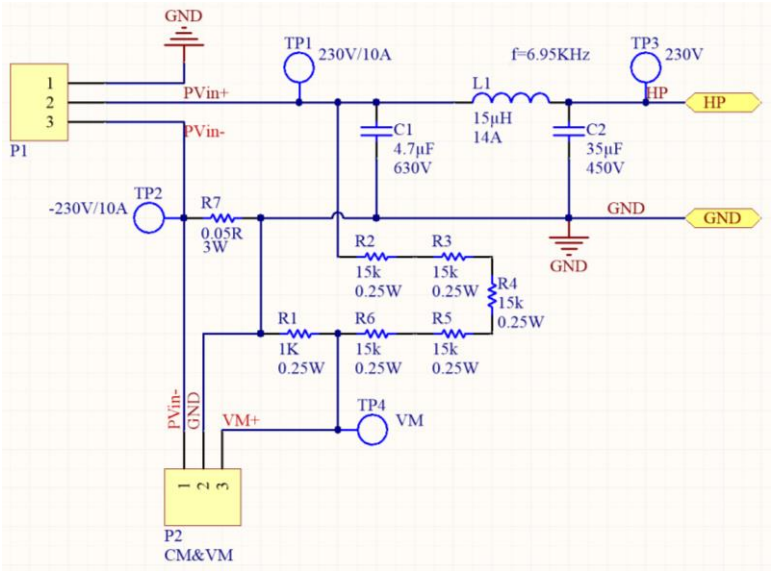

Figure 56: Schematic of current and voltage sensor circuit and DC filter circuit with PV power input.

The DC low pass filter with a 6.95 kHz cutoff frequency has been described in section 4.2.2. The sensor circuits will be analysed here. In according with the peak current and peak voltage supplied by solar array (Appendix 1),

$$I_{array,peak} = 2 * I_{sc} = 2 * 5.56\ Amps = 11.12\ Amps$$

$$V_{array,peak} = 6 * V_{oc} = 6 * 46.14\ Volts = 276.84\ Volts$$

the peak values of sensor circuit from P_2 are

$$V_{cm,peak} = -I_{array,peak} * R_{sensor} = -I_{array,peak} * R_7$$

$$V_{cm,peak} = -11.12\ Amps * 0.05\ Ohms = -0.556\ Volts$$

$$V_{vm,peak} = V_{array,peak} * \frac{R_1}{R_1 + R_2 + R_3 + R_4 + R_5 + R_6}$$

$$V_{vm,peak} = 276.84 * \frac{1\ kOhms}{1 + 15 + 15 + 15 + 15 + 15\ kOhms} = 3.64\ Volts$$

Because of the negative output voltage of current sensor, there will be one more operational amplifier circuit than the voltage sensor. The output sensor voltages from the signal input to the Arduino board; its input voltage is kept lower than 6 Volts for safety reasons (Appendix 5). This is the reference rule for setting the sensor resistances.

6.1.1.2 H-Bridge & Snubber

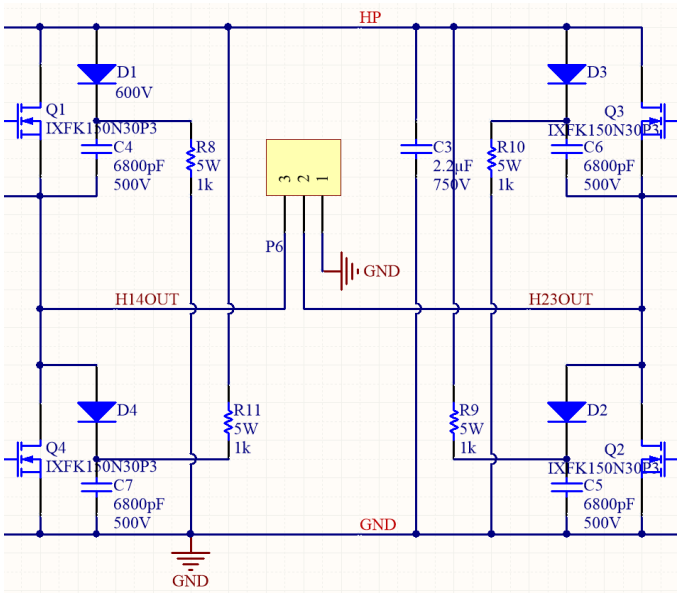

Figure 57: Schematic of H-bridge conversion with MOSFET snubber circuit

The 4 MOSFET H-bridge conversion circuit and the snubber circuit have been discussed in chapter 4, and the snubber capacitance ($C_{snubber} = 6.8\ nF$) and resistance ($R_{snubber} = 1\ kOhms$) have been discussed and calculated in section 4.2.3.1. Figure 57 shows the connection of the 4 MOSFETs and snubber. The output of P6 is the switched AC power which is used to supply the household water heater in this PV conversion system.

6.1.1.3 Gate Driver Circuit

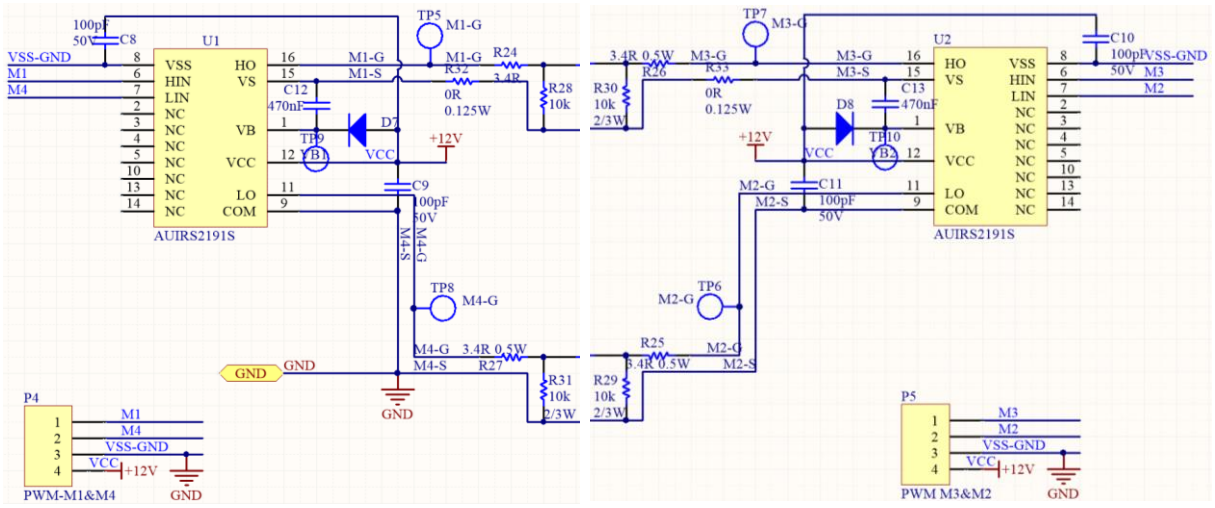

58-a) Left side gate driver with the PWM control signals of MOSFET 1&4

58-b) Right side gate driver with the PWM control signals of MOSFET 2&3

Figure 58: Left and right schematics of gate driver circuits

Based on the equation in section 4.2.3.2,

$$C_{boot} = \frac{Q_{total}}{\Delta V_{boot}}$$

the voltage drop and the total amount of the C_{boot} charge are

$$\Delta V_{boot} = V_{DD} - V_F - V_{gsmin}$$

$$Q_{total} = Q_{gate} + \left(I_{lkcap} + I_{lkgs} + I_{qbs} + I_{lk} + I_{lkdiode}\right) * t_{on} + Q_{ls}$$

Refer to the database of Driver IC AUIRS2191S (Appendix 7),

$$Q_{gate} = 197\ nC, \qquad I_{lkcap} = 0, \qquad I_{lkgs} = \pm 200\ nA, \qquad I_{qbs} = 200\ uA,$$

$$I_{lk} = 50\ uA, \qquad I_{lkdiode} = 10\ nA, \qquad t_{on} = \frac{1}{2} * \frac{1}{f_{sw}} = \frac{1}{2} * \frac{1}{30\ kHz} = 16.7\ us,$$

$$Q_{ls} = 3nC, \qquad V_{DD} = 12\ Volts, \qquad V_F = 1.25\ Volts, \qquad V_{gsmin} = 3\ Volts$$

$$Q_{total} = 197\ nC + (0 + 200nA + 200\ uA + 50\ uA + 10\ nA) * 16.7\ us + 3\ nC$$

$$Q_{total} = 200.418\ nC = 200\ nC$$

$$\Delta V_{boot} = 12 - 1.25 - 3 = 7.75\ Volts$$

To verify the boot capacitance,

$$C_{boot} = 470\ nF > \frac{200\ nC}{7.75\ Volts} = 25.8\ nF$$

the gate driver circuit could run on the boot capacitance $C_{boot} = 470\ nF$.

6.1.2 Control Board

6.1.2.1 OpAmp for Current Sensor

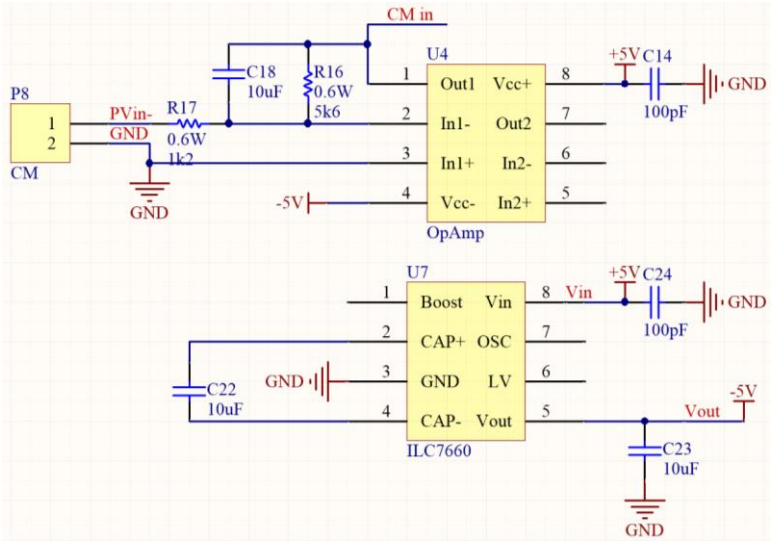

Figure 59: Schematic of Operational Amplifier Circuit for Current Sensing

According to the calculated output signal of current sensor circuit, $V_{cm,peak} \in (-0.556,0)\ Volts$, because the negative voltage cannot be readed by the analog pins of Arduino, the inverting operational amplifier circuit is necessary for testing the generation current of solar array. As shown in Figure 59, a negative source is required for

the OpAmp chip (-Vss=-5V), and there is an extra simple voltage conversion circuit to provide this.

The gain of OpAmp is

$$G = \frac{V_{out}}{V_{in}} = \frac{R_{16}}{R_{17}} = \frac{5.6\ kOhm}{1.2\ kOhm} = 4.67$$

$$V_{out,peak} = G * V_{in,peak} = G * V_{cm,peak} = 4.67 * 0.556 = 2.6\ Volts < 6\ Volts$$

For the stable output of OpAmp, one capacitor is paralleled with the resistor R_{16} to be a low pass DC filter. The cut off frequency of the RC low pass filter is

$$f = \frac{1}{2\pi * R * C} = \frac{1}{2\pi * 5.6\ kOhms * 10\ uF} = 2.84\ Hz$$

6.1.2.2 Temperature Sensors

As shown in Figure 60, there are two temperature sensors U_5&U_6 to measure the top and bottom temperatures of heater tank water. The chip TM-DS18S20 is a digital output temperature sensor, the output signal from pin 2 can directly connect with a digital pin of Arduino board. The characteristics are shown in Table 9.

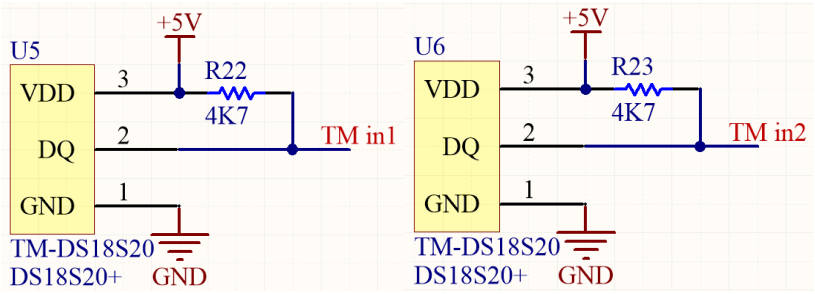

Figure 60: Schematic of 2 temperature sensor circuits

Table 9: DC electrical characteristics of temperature sensor TM-DS18S20

($V_{DD} = 3.0{\sim}5\ Volts,\ T_A = -55°C{\sim}+125°C$, unless otherwise noted.)		
Supply voltage	V_{DD}	+3.0 Volts ~ +5.5 Volts

DQ input current	I_{DQ}	5 uA
Temperature error	T_{err}	±2°C (-55°C to +125°C)
Drift		±0.2°C

6.1.2.3 Relay Control Circuit

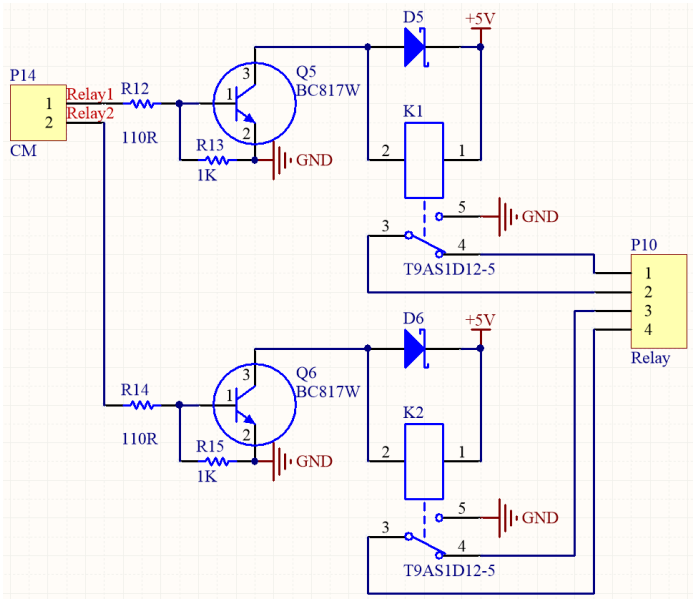

Figure 61: Schematic of relay control circuit to switch the main grid and solar array

The household water heater can be supplied by two sources, the main grid and the designed solar array. In this control system, two relays are used to switch these two power sources. When there is a 'HIGH' control signal from Arduino to the relays control circuit, the corresponding relay (K1/K2) will be energised, and the water heater will be supplied by the corresponding power source (Figure 61).

6.1.2.4 Supply Transformation

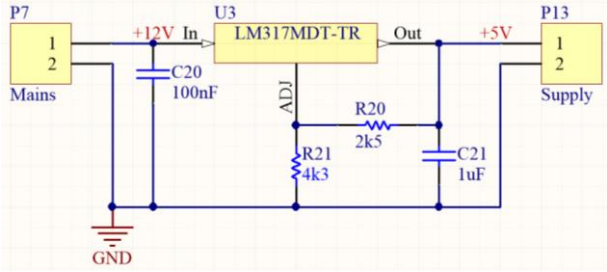

Figure 62: Schematic of power supply transformation circuit

There are two voltage levels in the low power control system, this is the reason why a power supply transformation circuit is required here to transform the power between +12V and +5V. These two resistors are the decisive factors of proportional relation between the input voltage value and the output.

$$\frac{V_{out}}{V_{in}} = \frac{R_{21} - R_{20}}{R_{21}} = \frac{5\ Volts}{12\ Volts}$$

Then the resistances could be calculated, $R_{21} = 4.3\ kOhms$, $R_{20} = 2.5\ kOhms$.

6.2 Printed Circuit Board (PCB)

6.2.1 Main Board

The board design of PCB is dominated by avoiding EMI and minimising stray inductance. The PCB design needs to comply with the following design principles [44]. The design principles could be classed to two main parts, layout principles and routing principles.

- Layout principles
  - The significant components should be placed first of all, and then in according to the tracks alignment, place the other components;
  - The tracks should be as short as possible which transmit the high frequency signals;
  - The analog circuit and the digital circuit should be separated;

- The high power circuit and the low power circuit should be some distance apart;
- For the heavy components, an extra fixing device is needed;
- The heat sink is required for the heat generating components;
- Switching components should be placed where they can be controlled easily.

- Routing principles
  - The input track and the output cannot be paralleled;
  - The width of tracks should not be too narrow;
  - The gap between two tracks should not be too small;
  - The corner degree of turning track must be bigger than 90°, and the number of corners of each track should be minimised;
  - The width of source tracks and address tracks should be bigger than signal tracks.

Based on these rules, the PCB size is matched with the size of the heat sink. For fixed with the heat sink, the size and place of fixed holes are same with the heat sink too. The photograph of the final board is shown in Figure 63, the layout schematics of PCB had been shown in the figures of Appendix 5. The length of PCB is 139.7mm (including 4 MOSFETs), and the width of PCB is 127mm (Appendix 4).

Figure 63: Top view photograph of Main board

Chapter 7

CONTROL PROGRAM

7.0 Introduction

The Arduino board offers easy to use hardware with widely available software tools. Working processes of all the microcontrollers of Arduino boards have been simplified, the easy-to-use system has simplified the tedious programming details of microcontroller. This open source prototyping platform has been the processing unit for thousands projects in the last several years. Most computers can run the software, like Mac, Windows, and Linux. From complex scientific instruments to everyday applications, both beginners and experts use the Arduino system [36].

In this chapter, the control program is compiled in the Arduino platform and runs in Arduino boards. The program is classed into six sub-programs, voltage & current reading and MPPT, PWM, temperature reading, switching reading, relay control and LCD display. PWM sub-program runs on an Arduino UNO board, the other five sub-programs operate on an Arduino Mega2560 board.

7.1 Voltage & Current Reading and MPPT

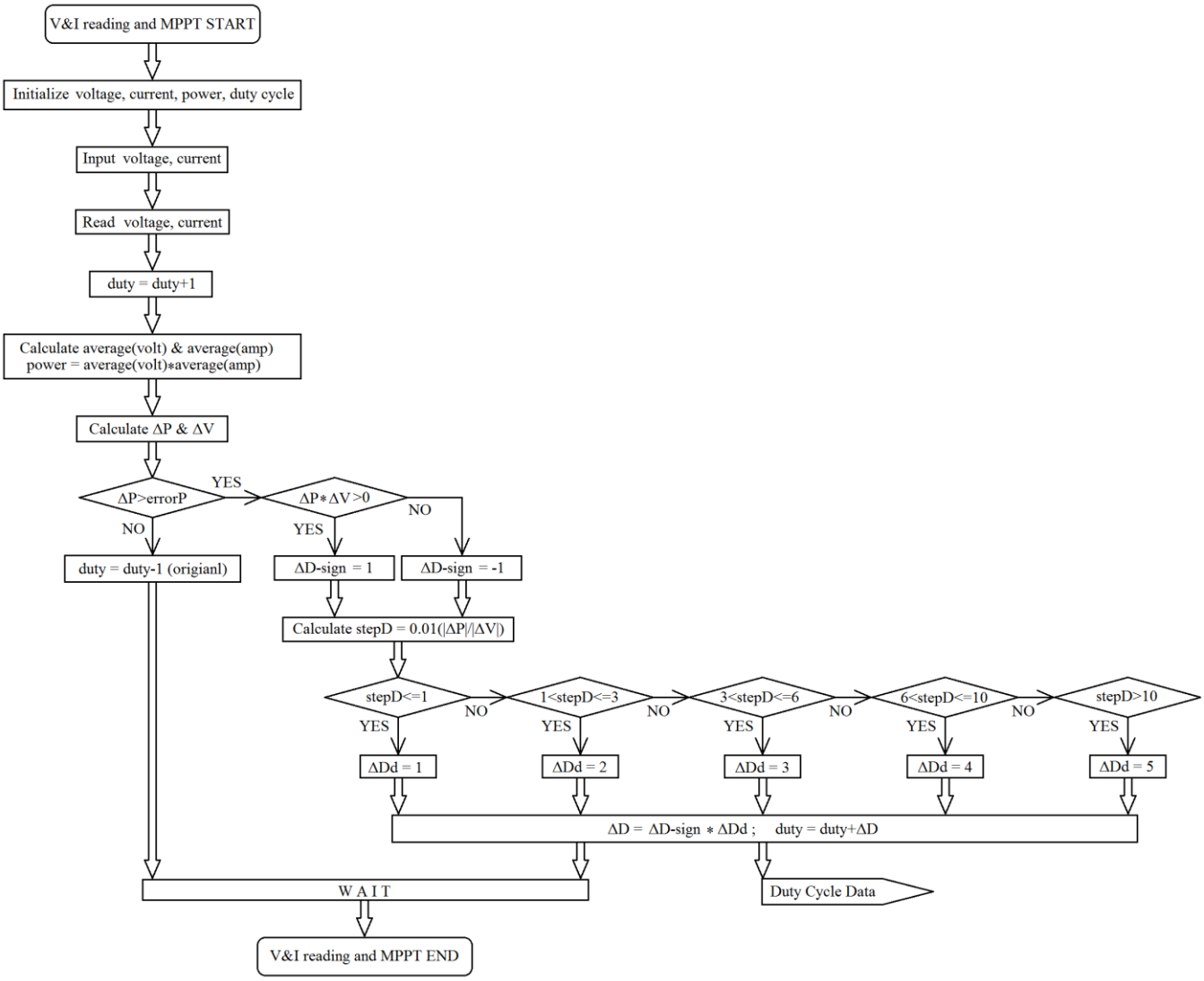

Figure 64: Flow chart of voltage & current reading and MPPT

Measured voltage and current by sensors is transferred into the analog-pin of Arduino Mega2560 board to read the values of PV voltage and current. The reading results are the averages for filtering the noise of PV outputs. In this sub-program, the instruction millis() is used to calculate the averages. Allowed error of power is also used for reducing sensitivity to noise, it is set to $error_P$=0.1. ΔD_d is the absolute value of ΔD, it is used to reduce the change rate of duty cycle. The sign of ΔD (ΔD-sign) and ΔD_d will be transferred to PWM

sub-program to generate the PWM waveform with a changed duty cycle. This flow diagram implements the MPPT tracking system described in section 4.3.1.

7.2 PWM Generation

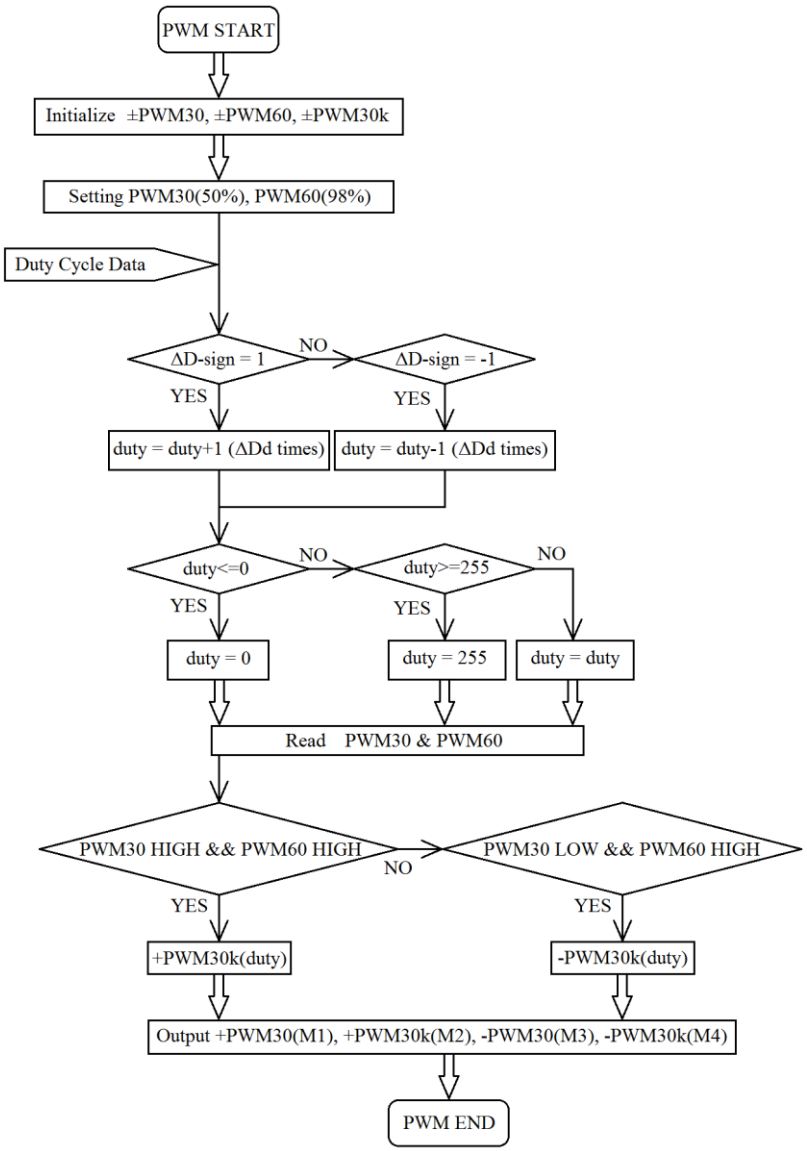

Figure 65: Flow chart of PWM sub-program, low frequency switching and high frequency PWM

ΔDd and ΔD-sign is the calculation result of section 7.1, when ΔD-sign=1, ΔD>0, duty cycle increases, the ΔDd is the increasing value.

$$duty = duty + \Delta\mathrm{Dd}$$

$$\Longrightarrow \Delta\mathrm{Dd}\ \text{times} \quad \begin{cases} \mathrm{duty} = \mathrm{duty} + 1 \\ \cdots \\ \mathrm{duty} = \mathrm{duty} + 1 \end{cases}$$

$$\Longrightarrow \begin{matrix} \mathrm{duty} = \mathrm{duty} + 1 \\ keep\ \Delta\mathrm{Dd}\ \text{interval time (delay}(\Delta\mathrm{Dd}))\end{matrix}$$

The additional 60 Hz signal is used to avoid that two MOSFETs on the same side turn on simultaneously. The 2% of 60 Hz PWM is the off period of the MOSFETs in one side of the converter.

$$t_{interval} = 2\% * \frac{1}{60} = 0.0033\ s = 3.3\ ms$$

In this sub-program, analogWrite() is the instruction to output the high frequency PWM in digital pins of Arduino UNO board [45]. Because the PWM program runs mistakes when the delay() instruction runs also in the program, this sub-program is moved to operate on another board, Arduino UNO. There are four PWM outputs from the UNO to control the four MOSFETs.

7.3 Temperature Reading

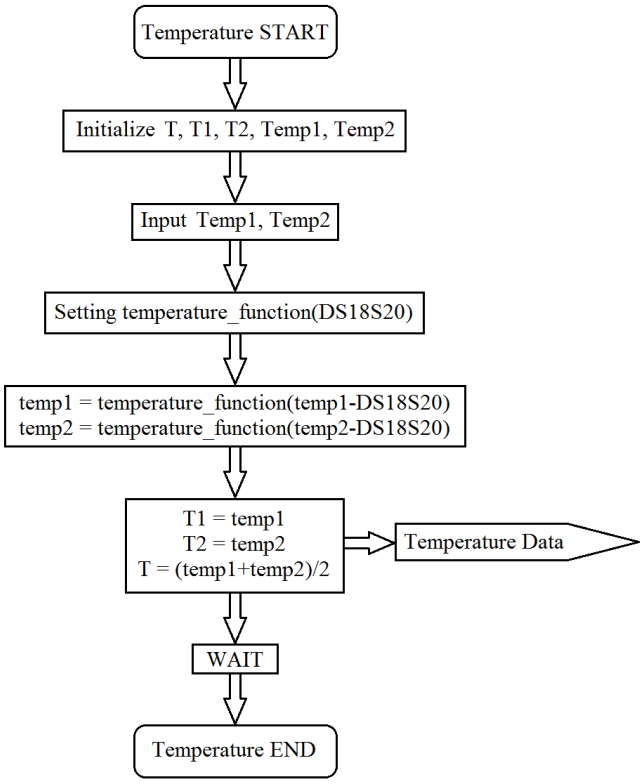

Figure 66: Flow chart of temperature reading sub-program

Temperature_1 is the water temperature of the top area in the heater tank, Temperature_2 is the water temperature of the bottom area. Generally in a water tank, the highest water temperature is at top area and the lowest is at bottom. The setting extremes of water heating should compare with these two temperatures. The water temperature of whole tank is approximated by the average of top and bottom temperatures. In this project, the temperature sensors are the chip DS18S20, the temperature_function() is the sensor function of DS18S20 in Arduino.

7.4 Switch Reading

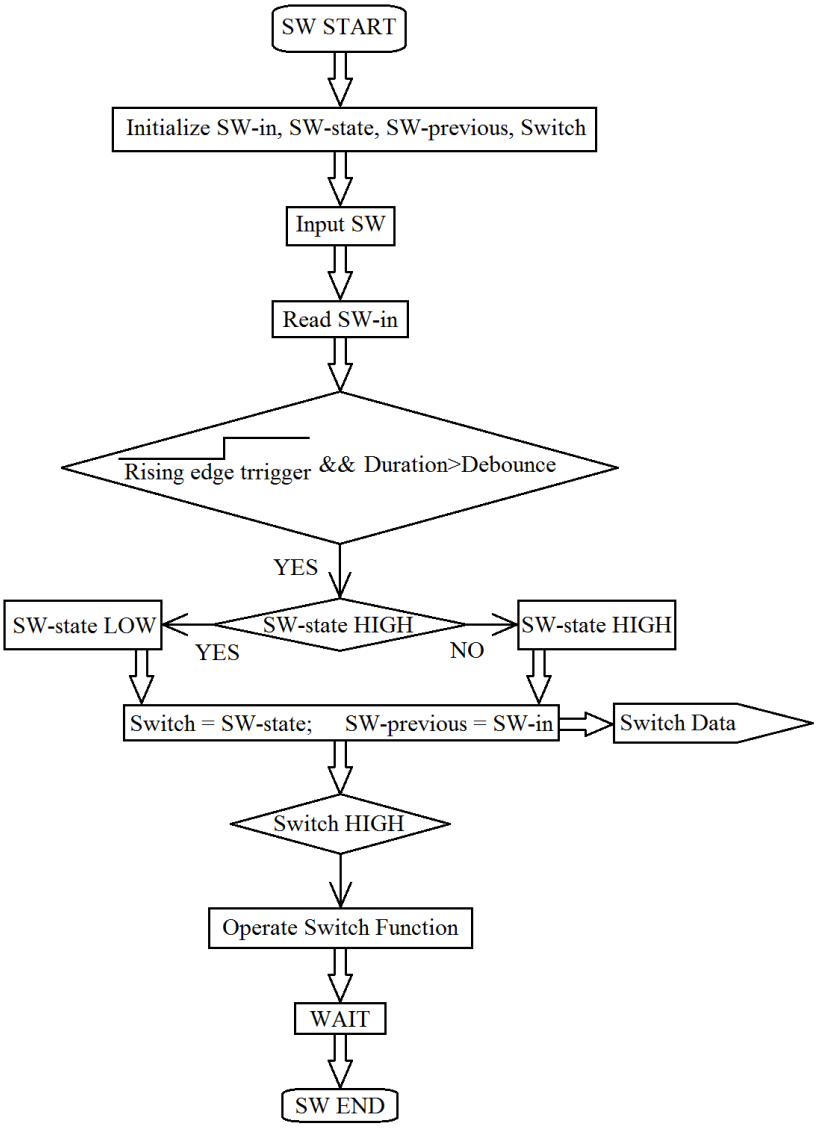

Figure 67: Flow chart of switch reading sub-program with debounce function.

There are six switches in this control system to set parameters T_{max} (T_{maxup} & T_{maxdn}), T_{min} (T_{minup} & T_{mindn}), water heater style M (new style heater with two power sources & old style with only one source) and hot water demand S (NEED – keep $T_2 \leq T_{min}$ & NEEDNOT – unlimited the lowest water temperature). If the extremes of water temperature need to be reset, press the corresponding switch and hold on a short time. The short time is setting by the debounce value,

$$t_{hold} = debounce * 20\ us$$

The switching reading of temperature setting is set to rising edge trigger. When the button is pressed at the first time, the corresponding parameter will change, if the number is the needed value, press the button again, the parameter changing will stop. The function debounce() is used in the switch program, is derived from the Arduino library [45]

7.5 Relay Control

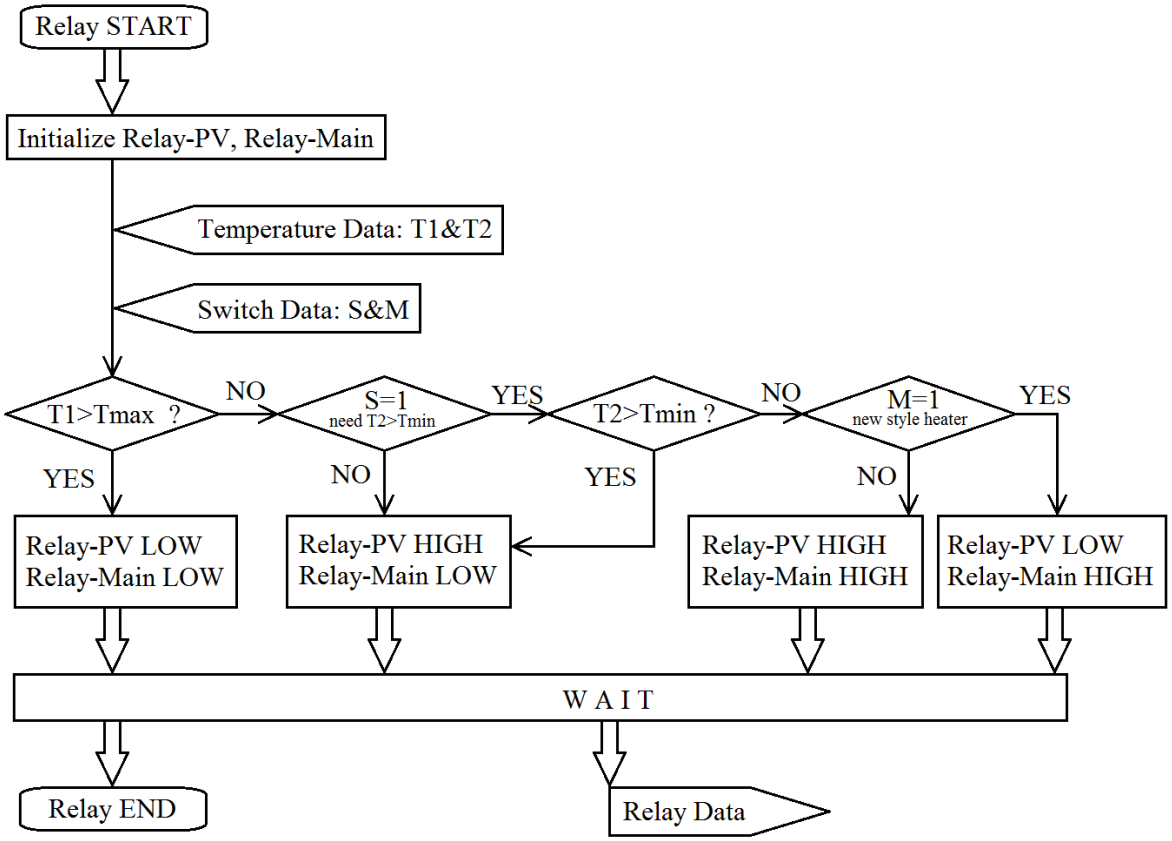

Figure 68: Flow chart of relay control sub-program

In this sub-program, the tested temperatures from 7.3 and the switches state (S & M) from 7.4 are the factors to switch the power sources, PV energy and main energy. The details of relay control is shown in section 4.3.2. The outputs are directly transferred to two relays, relay-PV and relay-main, these signals control that the water heater is supplied by PV panels

or main grid. The extreme temperatures control the water temperature in the heater tank, in this project, setting

$$T_{max} = 90°C \qquad T_{min} = 55°C$$

7.6 LCD

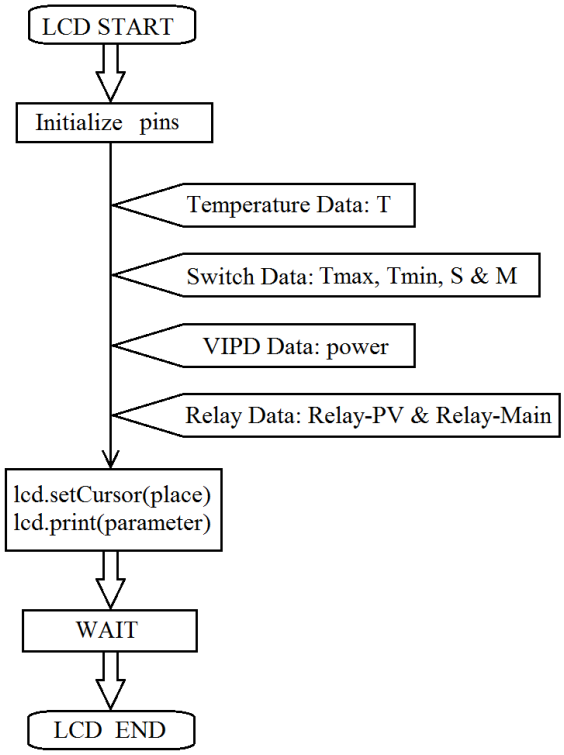

Figure 69: Flow chart of LCD sub-program

LCD sub-program, LiquidCrystal lcd(), is the Library program of Arduino [45]. It only needs to set the pin connection with LCD, the parameters can be shown on the display screen, and the place can be changed by the instruction lcd.setCursor(). The screen layout of parameter places has been shown in Figure 70 and Figure 71. The 16*2 screen shows extreme temperatures & tank water temperature, heater style, hot water demand, supply source and generated power of PV panels.

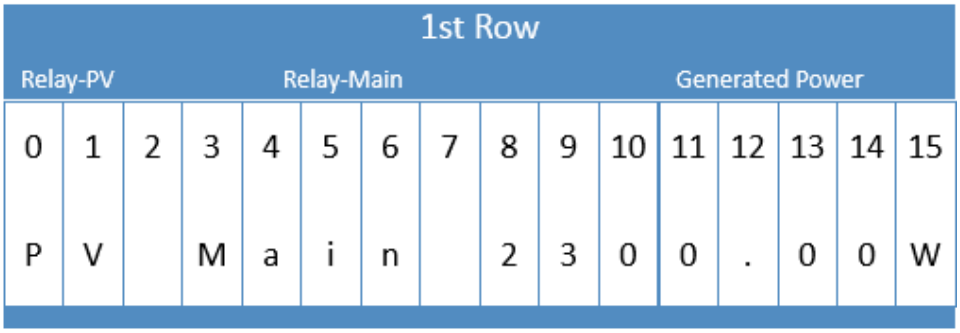

Figure 70: Parameters layout of first row on display screen

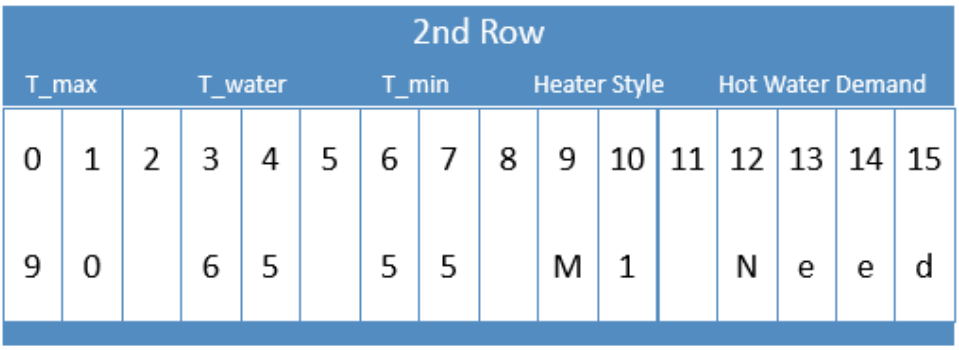

Figure 71: Parameters layout of second row on display screen

Chapter 8

RESULTS AND ANALYSIS

8.1 PWM Control Signals from Arduino UNO

The Arduino program was presented in Chapter seven. The Arduino UNO board outputs the 5 Volt PWM signals with 31 Hz and 31 kHz frequency. The PWM signals to control M1 & M2 and M3 & M4 are respectively shown in Figure 72 and Figure 73; enlarged views are also shown at the turn-on and turn-off moments. As designed in section 7.2, there is a short time interval between two PWM of the MOSFET pairs between M2 and M3 (green line and purple line in Figure 72) and between M1 and M4 (red line and green line in Figure 73). These four 5 Volt signals are transferred into two gate drivers, and four 12 Volt PWM signals are used to switch the four MOSFETs (Figure 74).

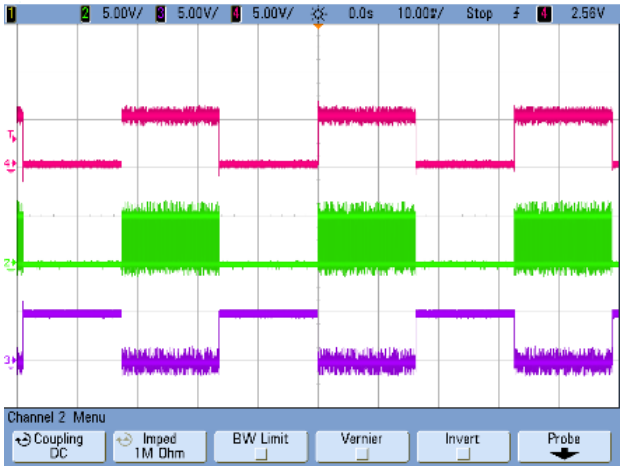

72-a) Δy = 5V/div, Δx = 10ms/div (red – M1, green – M2, purple – M3)

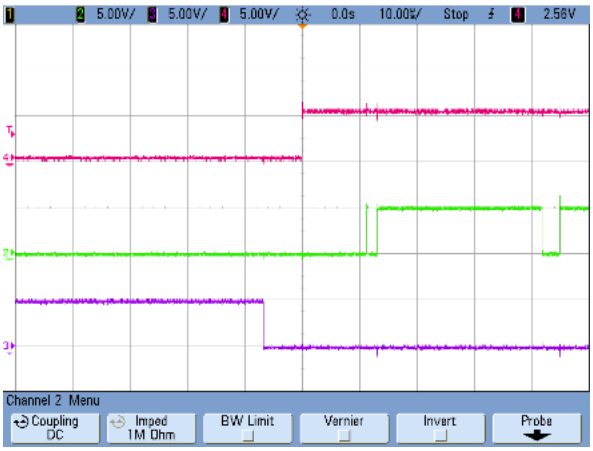

72-b) enlarged views at turn-on moment,Δy = 5V/div, Δx = 10us/div

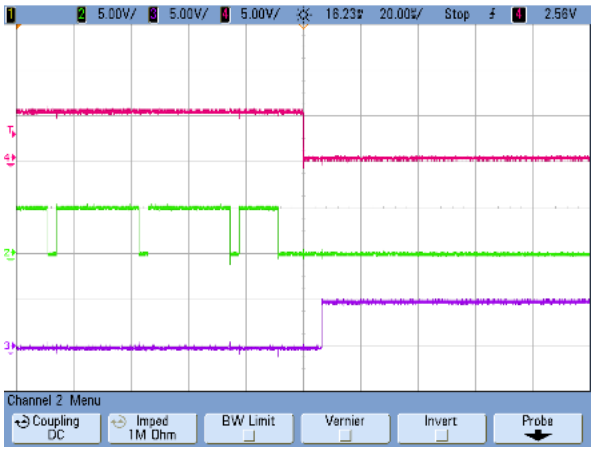

72-c) enlarged views at turn-off moment,Δy = 5V/div, Δx = 20us/div

Figure 72: Output PWM of M1 & M2 & M3 from Arduino UNO

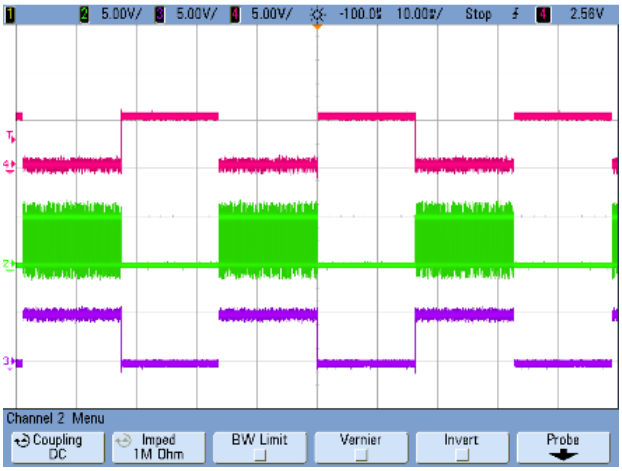

73-a) Δy = 5V/div, Δx = 10ms/div (red – M1, purple – M3, green – M4)

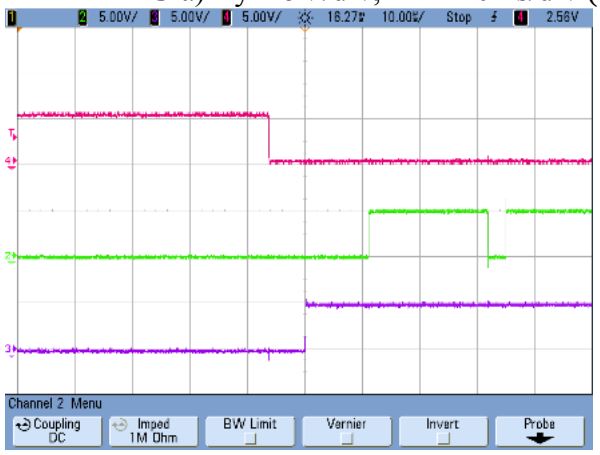

73-b) enlarged views at turn-on moment, Δy = 5V/div, Δx = 10us/div

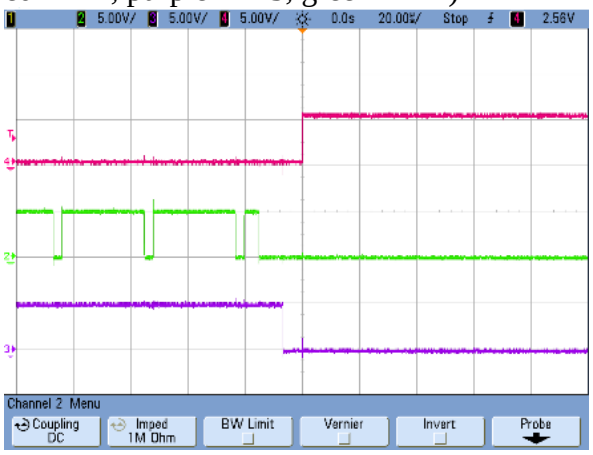

73-c) enlarged views at turn-off moment, Δy = 5V/div, Δx = 10us/div

Figure 73: Output PWM of M1 & M3 & M4 from Arduino UNO

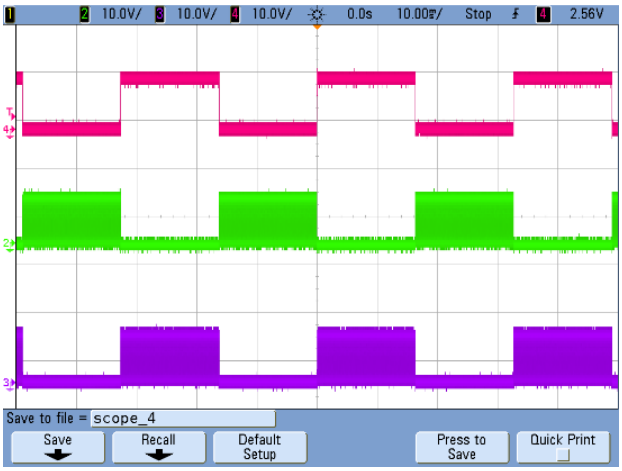

Figure 74: Gate driver outputs

(red – M1, green – M2, purple – M3, Δx = 10V/div, Δy = 10ms/div)

8.2 AC Output

In this project, switching control signals from the gate drivers are connected to the gate pins of the four MOSFETs. AC power is generated by the H-bridge with MOSFETs turn-on & turn-off, and household water heater runs on this AC power. H-bridge AC waveforms are shown in Figure 75, from the enlarged views, there is a short time interval (about 26us) between the positive and negative outputs. This interval is used to avoid circuit short (as designed in section 7.2). As shown in Figure 76, the time from M1 & M2 turn-on to be stable is about 500ns, the fluctuation is only 10% of output amplitude. It is the same with the output wave at M3 & M4 turn-on moment (Figure 77-a)). The fluctuation at M3 & M4 turn-off moment is more stable than the turn-on moment, the rate of over range is only 5.7% (Figure 77-b)). These waveforms are captured at 170 Volts with a duty cycle of 89.5%, resulting in a load current of 1.3 Amps. At this power level the converter is 99% efficient.

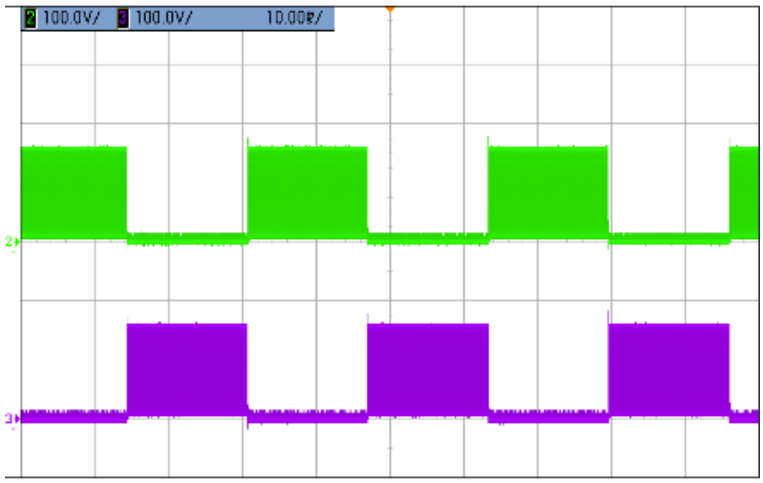

75-a) Δy = 100V/div, Δx = 10ms/div (green – M1 & M2, purple – M3 & M4)

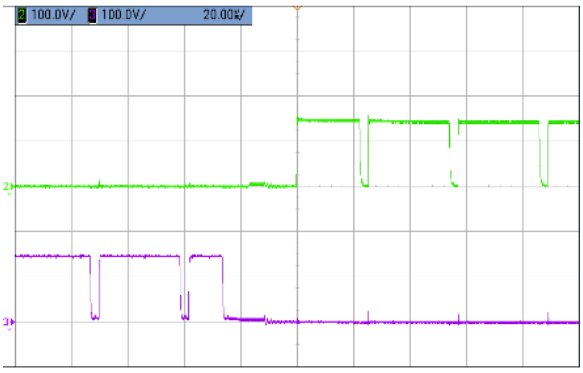

75-b) enlarged views at the moment of M3 & M4 turn off and M1 & M2 turn on (Δy = 100V/div, Δx = 20us/div)

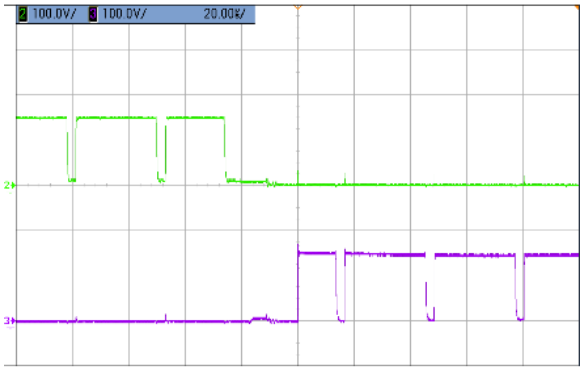

75-c) enlarged views at the moment of M1 & M2 turn off and M3 & M4 turn on (Δy = 100V/div, Δx = 20us/div)

Figure 75: H-bridge AC output

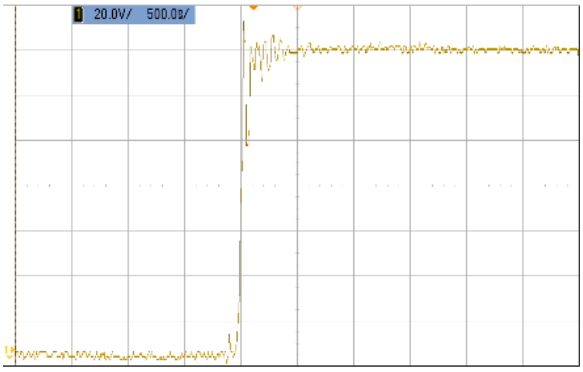

76-a) Δy = 20V/div, Δx = 500ns/div

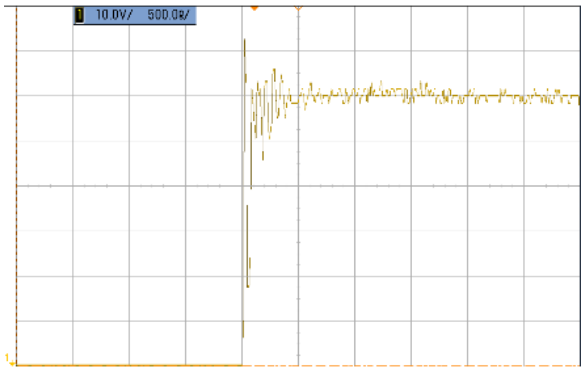

76-b) Δy = 10V/div, Δx = 500ns/div

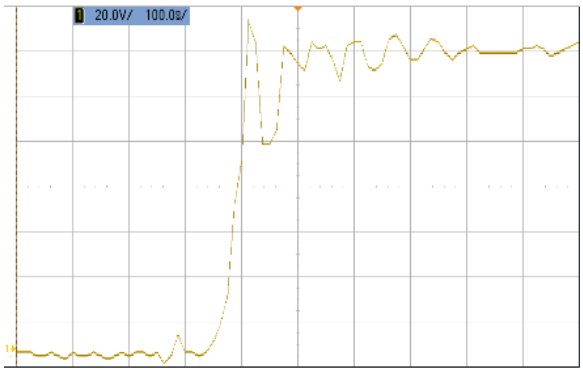

76-c) Δy = 20V/div, Δx = 100ns/div

Figure 76: Enlarged views of Figure 74 at M1 & M2 turn on moment

77-a) M3 & M4 turn on moment
Δy = 20V/div, Δx = 200ns/div

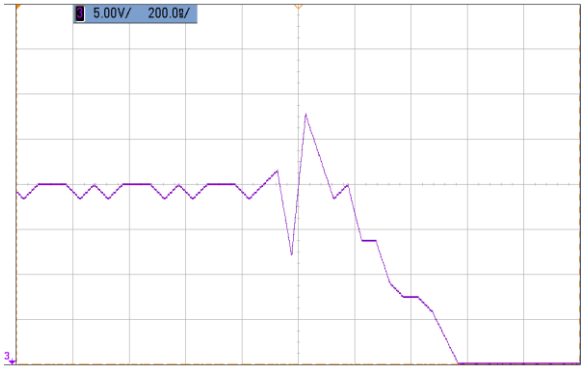

77-b) M3 & M4 turn off moment
Δy = 5V/div, Δx = 200ns/div

Figure 77: Enlarged views of Figure 74 at moments of M3 & M4 turn on and turn off.

In another test at a similar voltage, the same waveforms are shown in Figure 78 and Figure 79. These show acceptable voltage 'rise' and fall times. The shown enlarged waveforms of Figure 79 are processed to reduce noises automatically by oscilloscope. These waveforms are captured at 230 Volts with a duty cycle of 48.6%, resulting in a load current of 10 Amps. The measured efficiency at this power (2.3k Watts) is 98%.

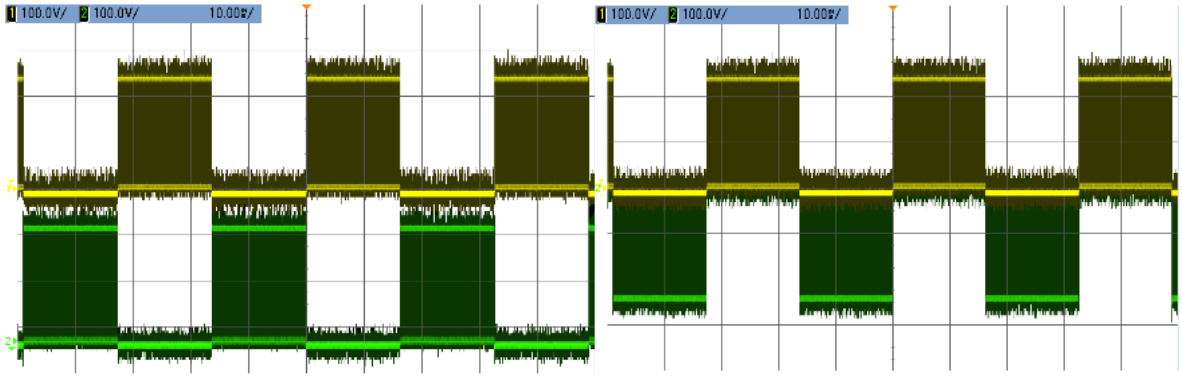

Figure 78: System output voltage between load and ground

(yellow – M1/M2 side of load, green – M3/M4 side of load, Δy = 100V/div, Δx = 10ms/div)

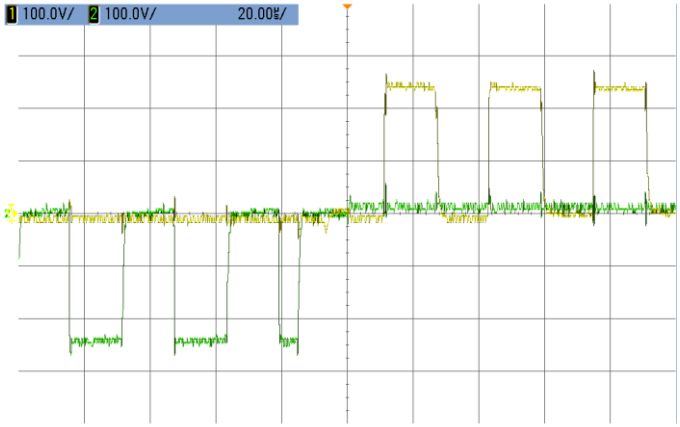

79-a) enlarged views at the moment of M3/M4 side (yellow) turn off and M1/M2 side (green) turn on (Δy = 100V/div, Δx = 20us/div)

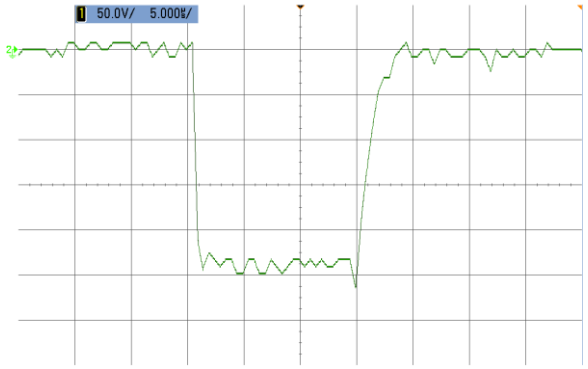

79-b) enlarged output views of M1/M2 side of load (Δy = 50V/div, Δx = 5us/div)

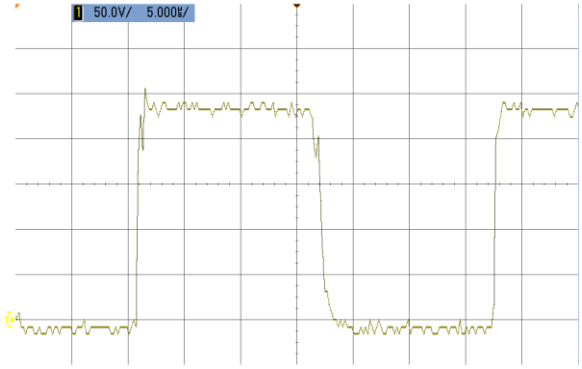

79-c) enlarged output views of M3/M4side of load (Δy = 50V/div, Δx = 5us/div)

Figure 79: Enlarged views of outputs in Figure 78

Chapter 9

CONCLUSION

Compared with other general PV systems, there are several features of this PV conversion system.

- The output is not sinusoidal. In this project, the output waveform reverses polarity following a square wave, the duty cycle at high frequency switching is controlled by the MPPT.
- The output frequency is not equal to the grid frequency. As the PV conversion system only supplies the resistive load, household water heater, the AC output power with lower frequency 31 Hz can drive the heater to heat water.
- This PV system is designed for most kinds of water heaters in the market; both one and two element water tanks. It means that a new water cylinder is not needed to match with this PV system.

For a household hot water heating system, compared with the traditional energy sources of fossil fuel, about 75% greenhouse gases can be saved by using a solar energy application system. The operating costs for PV systems are very low [46]. As an environment friendly energy source, solar energy is a free gift.

Hot water heating consumes nearly a third of electricity power of one house [47-48]. As shown in Table 5, for a typical household, $650 will be saved per year if the PV conversion system supplies the required energy for heating water. But actually, tank water can save some energy to use at next day. For example in a single day, the PV generation may not be enough to heat the amount of shower hot water. But because of the last sunny day, high temperature hot water may be saved in heater tank, and grid power is not needed to heat

water, and then no money is needed to pay for electricity. More than $650 can be saved by this PV conversion system in one year.

This PV conversion system can also be used for other domestic requirements. For instance, heat is transferred by water in the mostly heating system in the northern area of China. This PV system can also be used to supply the heating system to heat whole house, not only to heat the shower water.

REFERENCE

[1] E. E. Michaelides, Alternative energy sources. Berlin: Springer-Verlag Berlin and Heidelberg GmbH & Co. K, 2012, ch. 7

[2] S. Sreekanth, "A COMPARITIVE AND ANALYTICAL STUDY OF VARIOUSINCREMENTAL ALGORITHMS APPLIED IN SOLAR CELL," in *Computing, Electronics and Electrical Technologies (ICCEET), 2012 International Conference*, Kumaracoil: IEEE, 2012, pp. 452–456

[3] J. Ruggiero, "Department of Energy Commits to Energy Efficiency in U.S. Data Centers", *United States Department of Energy*, 2007. [Online]. Available: http://www.energy.gov/news/5504.htm. [Accessed: 21- Sept- 2015].

[4] C. Grieve, R. Lawson, and J. Henry, "Understanding the non-adoption of energy efficient hot water systems in New Zealand," *Energy Policy*, vol. 48, pp. 369–373, Sep. 2012

[5] N, Isaacs, L, Amitrano . Energy Use in New Zealand Households: Report on the Year 9 Analysis for the Household Energy End-Use Project HEEP), Judgeford, BRANZ, 2002

[6] EECA, *Making it Happen*. New Zealand Energy Efficiency and Conservation Strategy. New Zealand Government, Wellington, 2007

[7] Mark Z. Jacobson (2009). "*Review of Solutions to Global Warming*", Air Pollution, and Energy Securit*y* p. 4

[8] J. R. B. del Rosario and E. Dadios, "Development of a fuzzy logic-based PV solar tracking system simulated using QT fuzzy engine," in *Humanoid, Nanotechnology,*

Information Technology, Communication and Control, Environment and Management (HNICEM), 2014 International Conference, Palawan: IEEE, 2014, pp. 1–8

[9] "Trends 2014 in Photovoltaic Applications - IEA-PVPS," International Energy Agency Photovotaic Power Systems Programme, Sweden, 2015. [Online]. Available: http://www.iea-pvps.org/index.php?id=3&eID=dam_frontend_push&docID=2150. Accessed: Oct. 02, 2015

[10] R.A. Messenger and J. Ventre, "Photovoltaic, Systems Engineering*",* 2nd Edition Wiley Interscience , 2003

[11] V. Salas, E. Olias, A. Barrado and A. Lazaro, "Review of the maximum power point tracking algorithms for stand-alone photovoltaic systems", *Solar Energy Materials & Solar Cells*, vol.90, pp. 1555-1578, 2006

[12] Z. Jiang, "Design, Modeling and Simulation of a Green Building Energy System", 2016, pp. 1-7.

[13] A. Ahmad and L. Rajaji, "Modeling and Design of a Novel Control Algorithm for Grid Connected Photovoltaic (PV) Inverter System," in *Advances in Computing and Communications (ICACC), 2013 Third International Conference*, Cochin: IEEE, 2013, pp. 359–362

[14] N. Karami and N. Moubayed, "Optimized Heater Control For Low Current Consumption," in *2nd Renewable Energy for Developing Countries*, Beirut Lebanon: International Conference on Renewable Energies for Developing countries, 2014, pp. 12–16

[15] B. Lloyd, L. Wilson, and A. Adams, "Hot water use and water heating systems in remote indigenous communities," *Centre for Appropriate Technology Inc.*, 2000.

[16] J. Doucet, D. Eggleston, and j Shaw, "DC/AC Pure Sine Wave Inverter," Worcester polytechnic institute, Worcester, MA, 2007. [Online]. Available: https://www.wpi.edu/Pubs/E-project/Available/E-project-042507-092653/unrestricted/MQP_D_1_2.pdf. Accessed: Jun. 20, 2015

[17] R. E. Tarter, Solid-state power conversion handbook. United States: Wiley, John & Sons, 1993, ch. 2

[18] J.H. Suh, Y.H. Lee, B.S. Suh and D.S. Hyun, "A new snubber circuit for high efficiency and overvoltage limitation in three-level GTO inverters," *Industrial Electronics, Control, and Instrumentation, 1995., Proceedings of the 1995 IEEE IECON 21st International Conference on*, Orlando, FL, 1995, pp. 290-295 vol.1

[19] "Buyback rates when you export your excess energy," in Meridian Energy, 2015. [Online]. Available: https://www.meridianenergy.co.nz/your-home/tips-guides/generating-solar-energy/buyback-rates-when-you-export-your-excess-energy. Accessed: Dec. 19, 2015

[20] "What will power companies pay us for our solar power?," in SolarKing, 2015. [Online]. Available: http://solarking.co.nz/what-will-power-companies-pay-us-for-our-solar-power/. Accessed: Oct. 25, 2015

[21] "A powerful software for your photovoltaic systems," in *PVsyst*, 2012. [Online]. Available: http://www.pvsyst.com/en/. Accessed: Sep. 18, 2015

[22] "Mono Crystalline Solar Panel 185-200W," in NESL, 2014. [Online]. Available: http://www.nesl.cn/product/2014121212120.html. Accessed: Oct. 12, 2015

[23] Department of Building and Housing New Zealand Government, "Compliance Document for New Zealand Building Code Clause G12 Water Supplies – Third Edition," in Department of Building and Housing, New Zealand Government, 2007. [Online]. Available: http://www.building.govt.nz/assets/Uploads/building-code-

compliance/g-services-and-facilities/g12-water-supplies/asvm/g12-water-supplies-3rd-edition-amendment-7.pdf. Accessed: Nov. 01, 2015

[24] Standards New Zealand, "AS/NZS 4234:2008- Heated water systems - Calculation of energy consumption," in *Standards New Zealand*, 2008. [Online]. Available: https://shop-standards-govt-nz.ezproxy.canterbury.ac.nz/catalog/4234%3A2008%28AS%7CNZS%29/view. Accessed: Jul. 5, 2015

[25] P. Würfel, Physics of solar cells: From basic principles to advanced concepts, 2nd ed. Germany: Wiley-VCH Verlag GmbH, 2009, pp. 125–164

[26] P. J. Reddy, "Solar photovoltaic systems," in Science & technology of photovoltaic, Hyderabad, India: BS Publications, 2010, pp. 127–138

[27] P. J. Reddy, "Solar modules and arrays," in Science & technology of photovoltaic, Hyderabad, India: BS Publications, 2010, pp. 107-126

[28] J. Klein, "AN-6005: Synchronous buck MOSFET loss calculations with Excel model," in Fairchild semiconductor, 2014. [Online]. Available: https://www.fairchildsemi.com/application-notes/AN/AN-6005.pdf. Accessed: Jul. 12, 2015

[29] B. Edmunds, "AN1057:Heatsink Characteristics," in *International Rectifier*, 2002. [Online]. Available: http://www.infineon.com/dgdl/an-1057.pdf?fileId=5546d462533600a401535591d3170fbd. Accessed: Aug. 01, 2015

[30] K. H. Torvmark. "AN028: LC filter with improved high-frequency attenuation," in *Chipcon Products from Texas Instruments*, 1999. [Online]. Available: http://www.ti.com/lit/an/swra064/swra064.pdf. Accessed: Sep. 09, 2015

[31] "RC snubber circuit design for TRIACs," STMicroelectronics, NSW, Australia, Oct. 2007. [Online]. Available:

http://www.st.com/web/en/resource/technical/document/application_note/CD00004096.pdf. Accessed: Dec. 19, 2015

[32] "Application Note AN-978: HV Floating MOS-Gate Driver ICs," in International Rectifier, 2007. [Online]. Available: http://www.infineon.com/dgdl/an-978.pdf?fileId=5546d462533600a40153559f7cf21200. Accessed: Sep. 09, 2015

[33] "AN-6069: Application Review and Comparative Evaluation of Low-Side Gate Drivers," in Fairchild Semiconductor, 2007. [Online]. Available: https://www.fairchildsemi.com/application-notes/AN/AN-6069.pdf. Accessed: Aug. 24, 2015

[34] "AN-3009: Standard Gate-Driver Optocouplers," in Fairchild Semiconductor, 2013. [Online]. Available: https://www.fairchildsemi.com/application-notes/AN/AN-3009.pdf. Accessed: Sep. 09, 2015

[35] "AN6076: Design and Application Guide of Bootstrap Circuit for High-Voltage Gate-Drive IC," in Fairchild semiconductor, 2008. [Online]. Available: https://www.fairchildsemi.com/application-notes/AN/AN-6076.pdf. Accessed: Sep. 15, 2015

[36] "Arduino Products," in Arduino, 2015. [Online]. Available: https://www.arduino.cc/en/Main/Products/. Accessed: Oct. 10, 2015

[37] "MATLAB Features," in MathWorks, 2015. [Online]. Available: http://au.mathworks.com/products/matlab/features/. Accessed: Jul. 09, 2015

[38] N. Pandiarajan and R. Muthu, "Mathematical modeling of photovoltaic module with Simulink," *Electrical Energy Systems (ICEES), 2011 1st International Conference on*, Newport Beach, CA, 2011, pp. 258-263

[39] N. Belhaouas, M. S. Ait Cheikh, A. Malek, and C. Larbes, "Matlab-Simulink of photovoltaic system based on a two-diode model simulator with shaded solar cells,"

in Revue des Energies Renouvelables, Algeria: Renewable Energy Development Center Algeria, 2013, vol. 16, no. 1, pp. 65–73

[40] I. H. Altas and A. M. Sharaf, "A Photovoltaic Array Simulation Model for Matlab-Simulink GUI Environment," *Clean Electrical Power, 2007. ICCEP '07. International Conference on*, Capri, 2007, pp. 341-345

[41] H. Bellia, R. Youcef, and M. Fatima, "A detailed modeling of photovoltaic module using MATLAB," NRIAG Journal of Astronomy and Geophysics, vol. 3, no. 1, pp. 53–61, Jun. 2014

[42] A. Krismadinata, N. Rahim, H. W. Ping, and J. Selvaraj, "Photovoltaic module modeling using Simulink/Matlab," Procedia Environmental Sciences, vol. 17, pp. 537–546, 2013

[43] "Altium designer," in Altium, 2015. [Online]. Available: http://www.altium.com.au/. Accessed: Aug. 28, 2015

[44] "Getting Started with PCB Design," in Altium, 2008. [Online]. Available: http://www.altium.com.au/files/altiumdesigner/s08/learningguides/tu0117%20getting%20started%20with%20pcb%20design.pdf. Accessed: Jun. 12, 2015

[45] "Arduino Libraries," in Arduino, 2015. [Online]. Available: https://www.arduino.cc/en/Reference/Libraries/. Accessed: Oct. 10, 2015

[46] C. Aguilar, D. White and D. Ryan, "Domestic Water Heating and Water Heater Energy Consumption in Canada", *Canadian Building Energy End-Use Data and Analysis Centre*, 2005.

[47] A. Wood, A. Miller, and N. Claridge, "Moving to the sunny side of the street: Growing residential solar electricity in New Zealand," in EEA Conference & Exhibition 2013, Auckland: Electric Power Energy Centre, 2013, pp. 1–12

[48] M. Camilleri, L. Burrough, A. Pollard, and K. S. Smith, "Study report: energy use in New Zealand households," Branz, Porirua, 2010. [Online]. Available: http://www.branz.co.nz/cms_show_download.php?id=a9f5f2812c5d7d3d53fdaba15f2c14d591749353. Accessed: Jul. 31, 2015

Appendix 1: PV Panel

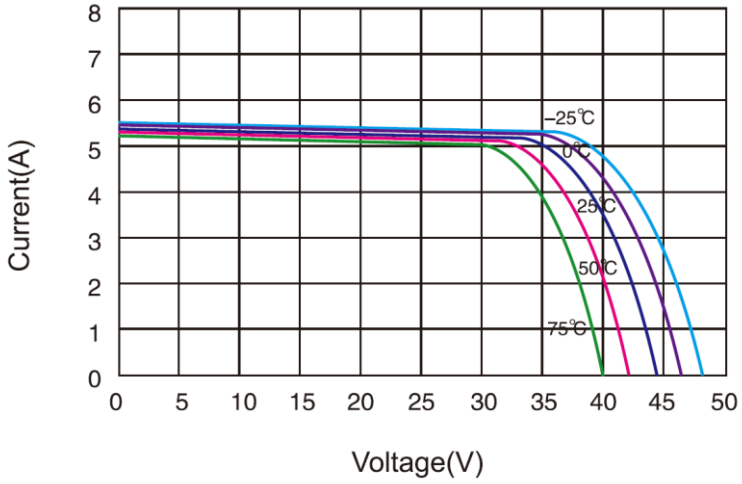

Figure A1-1: Current-Voltage characteristics (Irradiance: AM 1.5, 1000w/m^2)

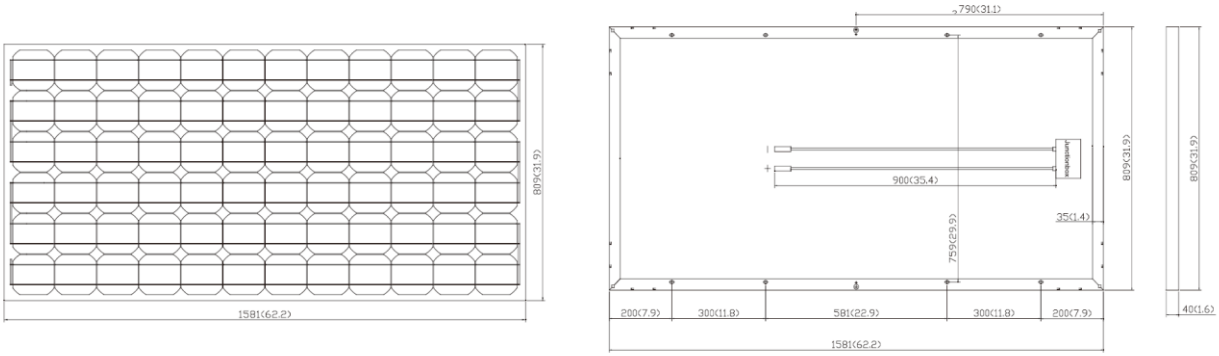

Figure A1-2: Dimensions mm(inch)

Table A1-1: Electrical Data of PV panels		
Model		DJ-195D/A
Peak power (±3%)	Pmax	195W
MPP (Maximum Power Point) voltage (rated voltage)	Vmp	38.59V
MPP (Maximum Power Point) current (rated current)	Imp	5.05A
Open circuit voltage	Voc	46.14V

Short circuit current	Isc	5.56A
Module efficiency		15.2%
Temperature coefficient	NOCT (Normal Operating Cell Temp) 48 ºC ± 2 ºC	
	Pmax	-0.48 %/ºC
	Voc	-0.34 %/ºC
	Isc	+0.037 %/ºC
STC (Standard Test Condition): Irradiance 1000W/m2, Module Temperature 25 ºC, AM (Air Mass)=1.5		

Table A1-2: Mechanical Data of PV panels	
Solar cell size	125mm*125mm
No of cells	6*12=72
Dimension (L*W*T)	1581mm*809mm*40mm
Weight	15.5kg

Table A1-3: Data of PV array			
Electrical data	Peak power	P_{array}	231.54 V
	MPP voltage (rated voltage)	V_{array}	10.1 A
	MPP current (rated current)	I_{array}	2.34 kW
Dimension	Length	L_{array}	3192 mm
	Width	W_{array}	5004 mm
	Thickness	T_{array}	40 mm
	Surface area	S_{array}	16 m^2

Appendix 2: Economic Analysis Tables

Table A2-1: Cost of panels and converter for grid connected solar system				
Panel No	Solar array output (kWatts)	DC/AC converter	Panels & converter costing price	
6	1.17	Three Phase 1.5kw 200V-240VDC	6*$293+$320	$2,078
12	2.34	Three Phase 3kw 200V-240VDC	12*$293+$694	$4,210
18	3.51	Three Phase 4kw 200V-240VDC	18*$293+$1001	$6,275
30	5.85	Three Phase 7kw 200V-240VDC	30*$293+$2059	$10,849
48	9.36	Three Phase 10kw 200V-240VDC	48*$293+$2348	$16,412

Note: All of the converter prices are found from websites, www.freeclansor.com and www.aliexpress.com

Table A2-1: Cost of panels and converter for grid connected solar system					
Panel No	Solar array output (kWatts)	Racking (0.5 $/W) & wiring (1 $/W) costing price ($)		Build costing price ($)	
6	1.17	1,170*(0.5+1)	1,755	2,078+1,755	3,853
12	2.34	2,340*(0.5+1)	3,510	4,210+3,510	7,720
18	3.51	3,510*(0.5+1)	5,265	6,275+5,265	11,540
30	5.85	5,850*(0.5+1)	8,775	10,849+8,775	19,624
48	9.36	9,360*(0.5+1)	14,040	16,412+14,040	30,452

Appendix 3: MOSFET

IXYS — Preliminary Technical Information

Polar3™ HiPerFET™ Power MOSFET

IXFK150N30P3
IXFX150N30P3

V_{DSS} = 300V
I_{D25} = 150A
$R_{DS(on)}$ ≤ 19mΩ
t_{rr} ≤ 250ns

N-Channel Enhancement Mode
Avalanche Rated
Fast Intrinsic Diode

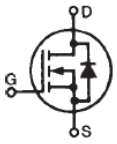

Symbol	Test Conditions	Maximum Ratings	
V_{DSS}	T_J = 25°C to 150°C	300	V
V_{DGR}	T_J = 25°C to 150°C, R_{GS} = 1MΩ	300	V
V_{GSS}	Continuous	± 20	V
V_{GSM}	Transient	± 30	V
I_{D25}	T_C = 25°C	150	A
I_{DM}	T_C = 25°C, Pulse Width Limited by T_{JM}	375	A
I_A	T_C = 25°C	75	A
E_{AS}	T_C = 25°C	4	J
P_D	T_C = 25°C	1300	W
dv/dt	$I_S \le I_{DM}$, $V_{DD} \le V_{DSS}$, $T_J \le 150°C$	35	V/ns
T_J		-55 ... +150	°C
T_{JM}		150	°C
T_{stg}		-55 ... +150	°C
T_L	Maximum Lead Temperature for Soldering	300	°C
T_{SOLD}	1.6 mm (0.062in.) from Case for 10s	260	°C
M_d	Mounting Torque (TO-264)	1.13/10	Nm/lb.in
F_C	Mounting Force (PLUS247)	20..120 /4.5..27	N/lb
Weight	TO-264	10	g
	PLUS247	6	g

TO-264 (IXFK)

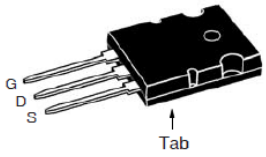

PLUS247 (IXFX)

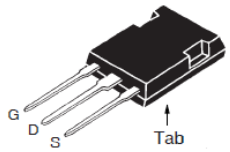

G = Gate D = Drain
S = Source Tab = Drain

Features

- Dynamic dv/dt Rating
- Avalanche Rated
- Fast Intrinsic Diode
- Low Q_G
- Low $R_{DS(on)}$
- Low Drain-to-Tab Capacitance
- Low Package Inductance

Symbol	Test Conditions (T_J = 25°C Unless Otherwise Specified)	Characteristic Values Min.	Typ.	Max.	
BV_{DSS}	V_{GS} = 0V, I_D = 3mA	300			V
$V_{GS(th)}$	$V_{DS} = V_{GS}$, I_D = 8mA	3.0		5.0	V
I_{GSS}	V_{GS} = ± 20V, V_{DS} = 0V			± 200	nA
I_{DSS}	$V_{DS} = V_{DSS}$, V_{GS} = 0V			25	µA
	T_J = 125°C			1	mA
$R_{DS(on)}$	V_{GS} = 10V, $I_D = 0.5 \bullet I_{D25}$, Note 1			19	mΩ

Symbol	Test Conditions (T_J = 25°C Unless Otherwise Specified)	Characteristic Values Min.	Typ.	Max.	
g_{fs}	V_{DS} = 10V, I_D = 60A, Note 1	65	110		S
C_{iss}	V_{GS} = 0V, V_{DS} = 25V, f = 1MHz		12.1		nF
C_{oss}			1910		pF
C_{rss}			40		pF
R_{Gi}	Gate Input Resistance		1.0		Ω
$t_{d(on)}$	**Resistive Switching Times**		44		ns
t_r	V_{GS} = 10V, $V_{DS} = 0.5 \bullet V_{DSS}$, $I_D = 0.5 \bullet I_{D25}$		30		ns
$t_{d(off)}$	R_G = 1Ω (External)		74		ns
t_f			12		ns
$Q_{g(on)}$	V_{GS} = 10V, $V_{DS} = 0.5 \bullet V_{DSS}$, $I_D = 0.5 \bullet I_{D25}$		197		nC
Q_{gs}			70		nC
Q_{gd}			65		nC
R_{thJC}				0.096	°C/W
R_{thCS}			0.15		°C/W

Source-Drain Diode

Symbol	Test Conditions (T_J = 25°C, Unless Otherwise Specified)	Characteristic Values Min.	Typ.	Max.	
I_S	V_{GS} = 0V			150	A
I_{SM}	Repetitive, Pulse Width Limited by T_{JM}			600	A
V_{SD}	I_F = 100A , V_{GS} = 0V, Note 1			1.5	V
t_{rr}	I_F = 75A, -di/dt = 100A/µs			250	ns
Q_{RM}	V_R = 100V, V_{GS} = 0V		2.9		µC
I_{RM}			23.0		A

Advantages

- Easy to Mount
- Space Savings

Applications

- DC-DC Converters
- Battery Chargers
- Switch-Mode and Resonant-Mode Power Supplies
- Uninterrupted Power Supplies
- AC Motor Drives
- High Speed Power Switching Applications

Appendix 4: HeatSink

Table A4-1: Database of HeatSink 394-2AB		
Standard P/N		394-2AB
Overall Dimensions	Length	5.5in (139.7mm)
	Height	1.5in (38.1mm)
	Width	5.0in (127.0mm)
Device Base Mounting Area		101mm*139mm
Base Mounting Holes		6
Thermal Resistance at Typical Load	Natural Convection	1.51°C/W
	Forced Convection	0.6°C/W

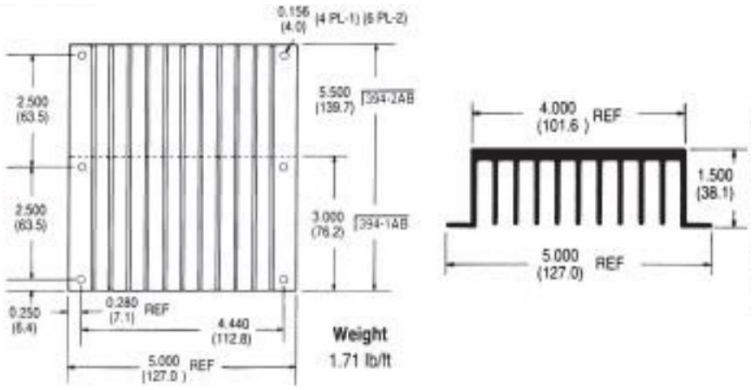

Figure A4-1: Mechanical Dimensions of HeatSink 394-2AB

Appendix 5: PCB

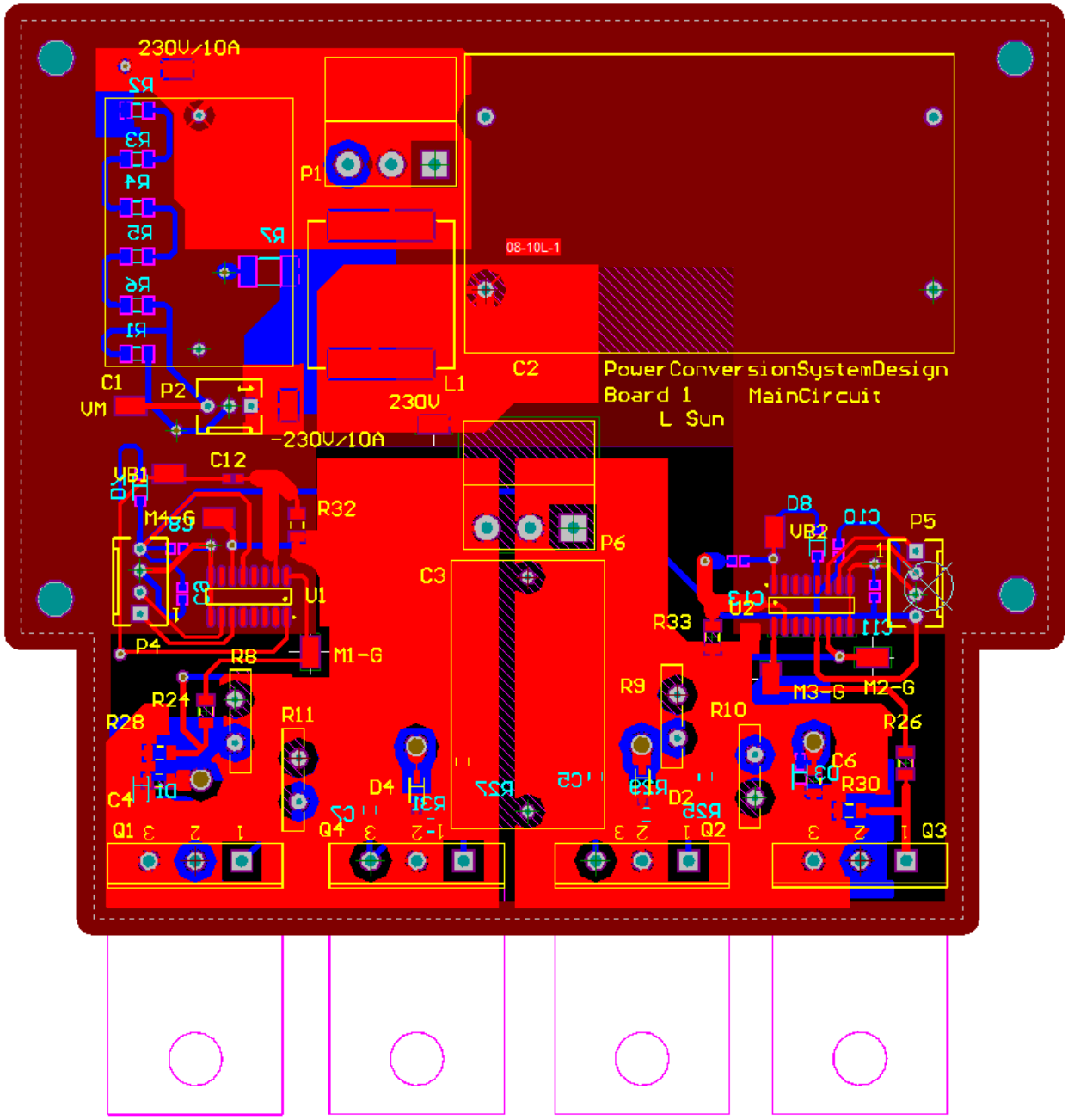

Figure A5-1: PCB layout diagrams of the top layer

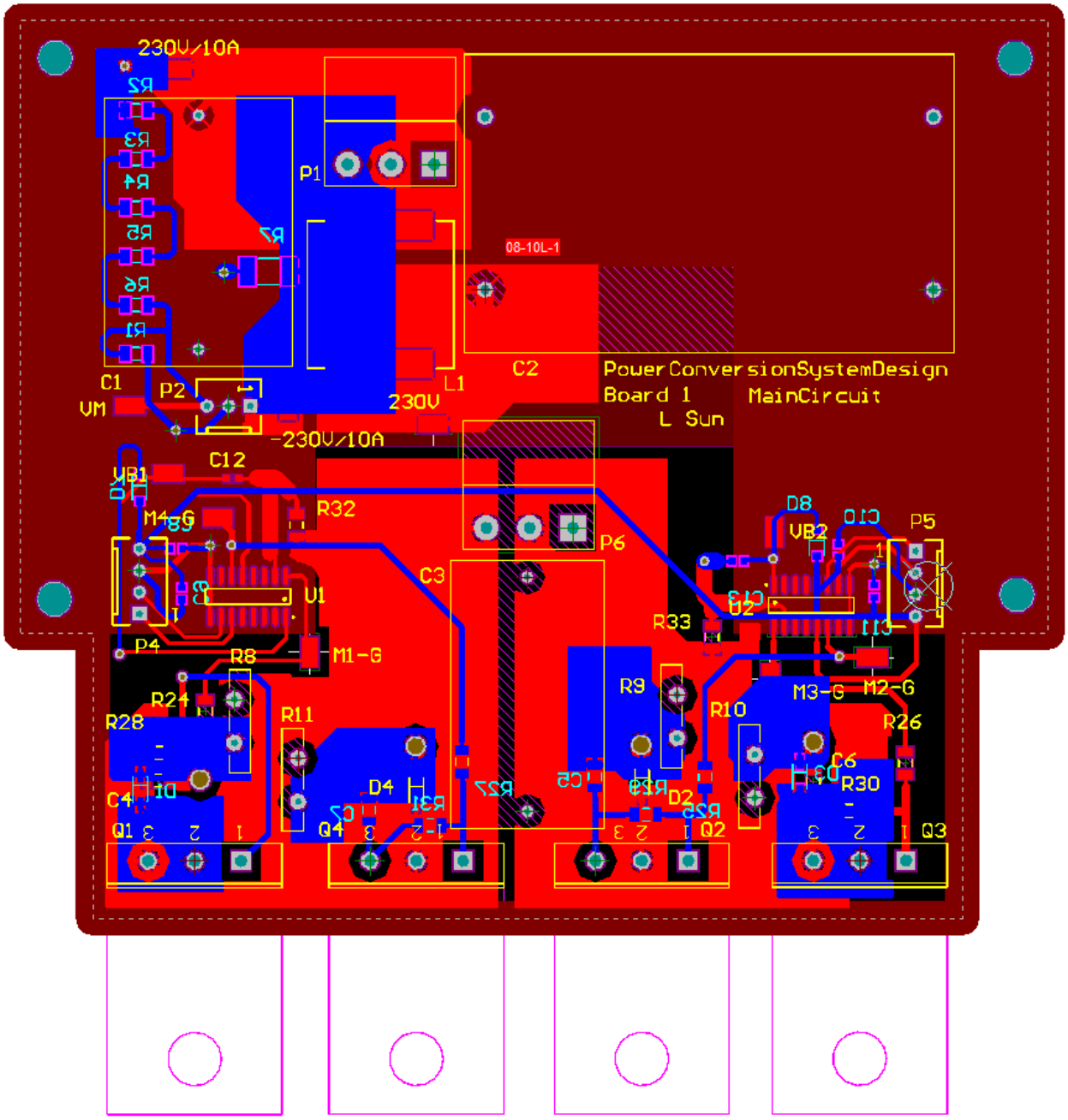

Figure A5-2: PCB layout diagrams of the bottom layer

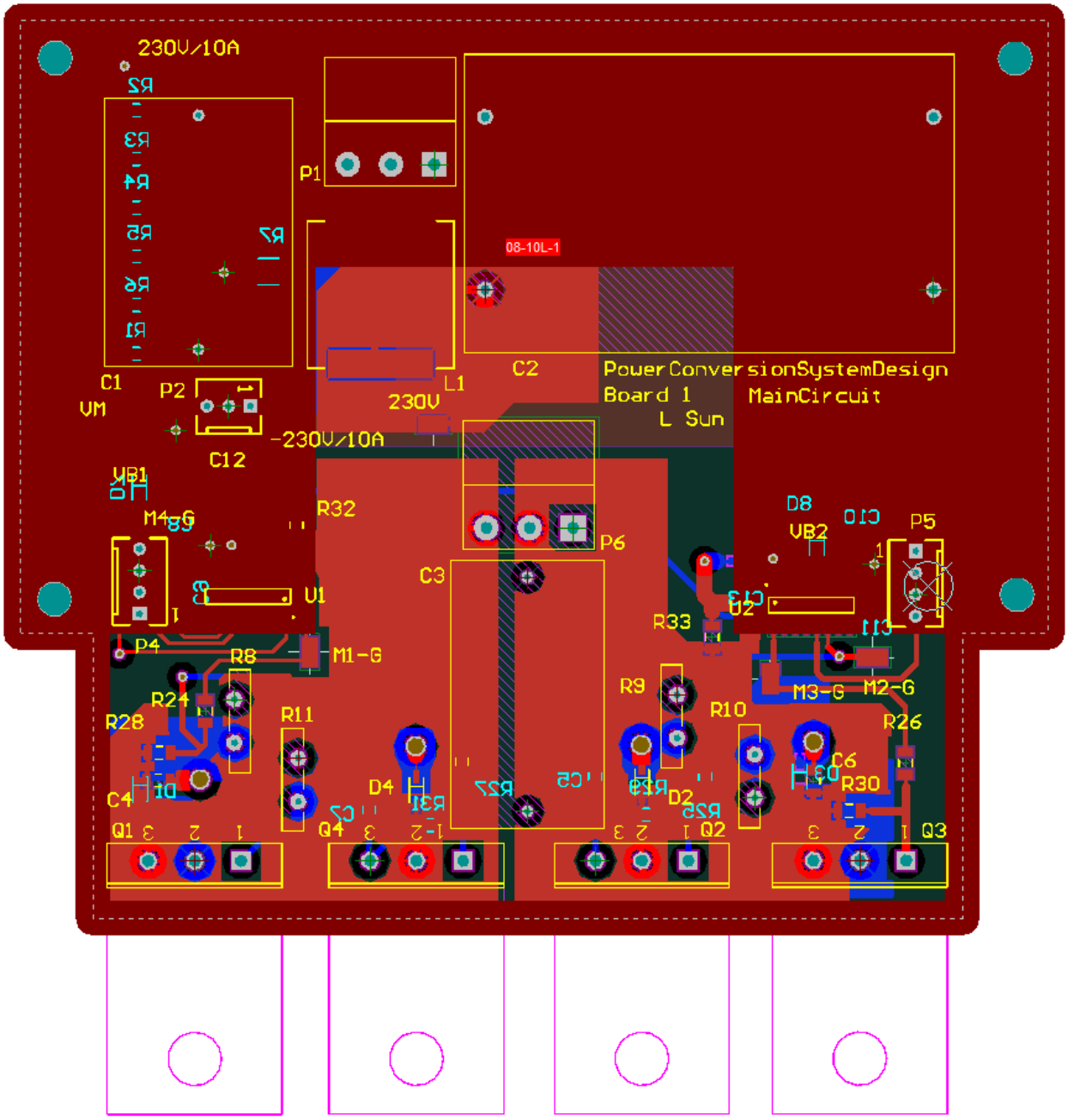

Figure A5-3: PCB layout diagrams of the internal plane power layer

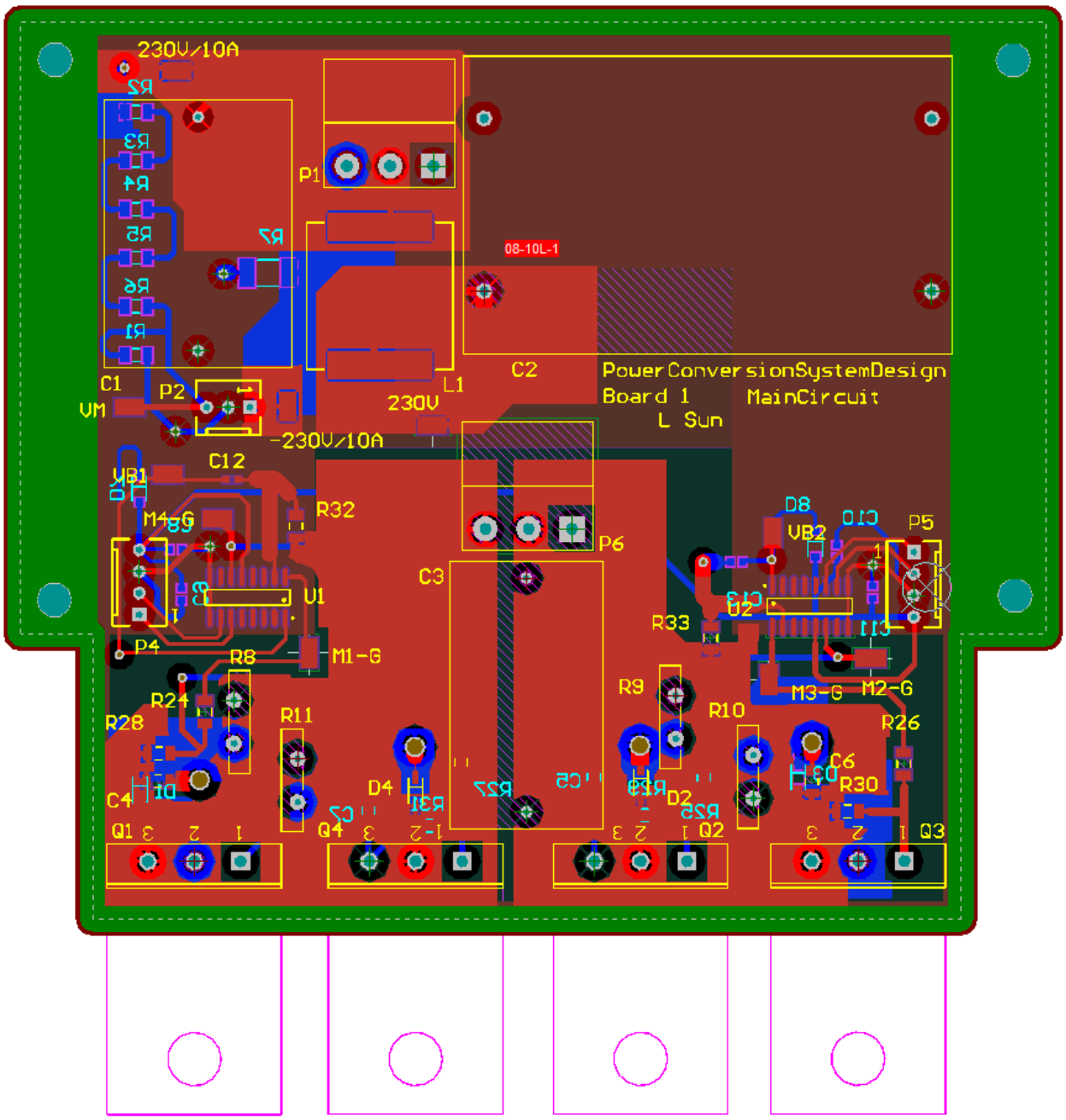

Figure A5-4: PCB layout diagrams of the internal plane ground layer (connection with GND)

Appendix 6: Arduino Boards

Operating Voltage	5V
Input Voltage (recommended)	7-12V
Input Voltage (limit)	6-20V
Digital I/O Pins	54 (of which 15 provide PWM output)
Analog Input Pins	16
DC Current per I/O Pin	20 mA
DC Current for 3.3V Pin	50 mA
Flash Memory	256 KB of which 8 KB used by bootloader
SRAM	8 KB
EEPROM	4 KB
Clock Speed	16 MHz
Length	101.52 mm
Width	53.3 mm
Weight	37 g

Figure A6-1 Technical specs of Arduino Mega2560

Operating Voltage	5V
Input Voltage (recommended)	7-12V
Input Voltage (limit)	6-20V
Digital I/O Pins	14 (of which 6 provide PWM output)
PWM Digital I/O Pins	6
Analog Input Pins	6
DC Current per I/O Pin	20 mA
DC Current for 3.3V Pin	50 mA
Flash Memory	32 KB (ATmega328P) of which 0.5 KB used by bootloader
SRAM	2 KB (ATmega328P)
EEPROM	1 KB (ATmega328P)
Clock Speed	16 MHz
Length	68.6 mm
Width	53.4 mm
Weight	25 g

Figure A6-2: Technical specs of Arduino UNO

Appendix 7: Driver IC

Unless otherwise noted, these specifications apply for an operating junction temperature range of -40°C ≤ Tj ≤ 125°C with bias conditions of V_{BIAS} (VCC or VBS) = 15V. The VIN, VTH parameters are referenced to VSS and are applicable to all logic input leads: HIN and LIN. The VO parameters are referenced to COM and are applicable to the respective output leads: HO or LO.

Symbol	Definition	Min	Typ	Max	Units	Test Conditions
V_{IH}	Logic "1" input voltage	2.5	---	---	V	V_{CC} = 9.8V – 20V
V_{IL}	Logic "0" input voltage	---	---	0.8		
V_{OH_2mA}	High level output voltage, V_{BIAS}-V_O	---	---	2.5		I_o= 2 mA
V_{OH_20mA}	High level output voltage, V_{BIAS}-V_O	---	---	3.3		I_o= 20 mA
V_{OL}	Low level output voltage, V_O	---	---	0.1		I_o= 2 mA
I_{LK}	Offset supply leakage current	---	---	50	µA	V_B = V_S = 600 V
I_{QBS}	Quiescent V_{BS} supply current	---	100	200		V_{IN} = 0V or 3.3V
I_{QCC}	Quiescent V_{CC} supply current	---	150	300		V_{IN} = 0V or 3.3V
I_{QBS18}	Quiescent V_{BS} supply current	---	180	300		V_{IN} = 0V or 3.3V V_{BS}=18V
I_{QCC18}	Quiescent V_{CC} supply current	---	300	450		V_{IN} = 0V or 3.3V V_{CC}=18V
I_{QBS20}	Quiescent V_{BS} supply current	---	850	1500		V_{IN} = 0V or 3.3V V_{BS}=20V
I_{QCC20}	Quiescent V_{CC} supply current	---	1500	2500		V_{IN} = 0V or 3.3V V_{CC}=20V
I_{IN+}	Logic "1" input bias current	---	3.5	7		V_{IN} = 3.3V
I_{IN-}	Logic "0" input bias current	---	---	1.0		V_{IN} = 0V
V_{BSUV+}	V_{BS} supply undervoltage positive going threshold	8.0	8.9	9.8	V	
V_{BSUV-}	V_{BS} supply undervoltage negative going threshold	7.4	8.2	8.8		
$V_{BSUVHYS}$	V_{BS} supply undervoltage hysteresis	0.3	0.7	---		
V_{CCUV+}	V_{CC} supply undervoltage positive going threshold	8.0	8.9	9.8		
V_{CCUV-}	V_{CC} supply undervoltage negative going threshold	7.4	8.2	9.0		
$V_{CCUVHYS}$	V_{CC} supply undervoltage hysteresis	0.3	0.7	---		
I_{O+}	Output high short circuit pulsed current (†)	2.6	3.5	---	A	V_O = 0 V, PW ≤ 10 µs, Tj = 25°C
I_{O-}	Output low short circuit pulsed current(†)	2.6	3.5	---		V_O = 15 V, PW ≤ 10 µs Tj = 25°C
I_{O+}	Output high short circuit pulsed current (†)	1.8	3.5	---	A	V_O = 0 V, PW ≤ 10 µs,
I_{O-}	Output low short circuit pulsed current(†)	1.8	3.5	---		V_O = 15 V, PW ≤ 10 µs

(†) Guaranteed by design

Appendix 8: Hardware

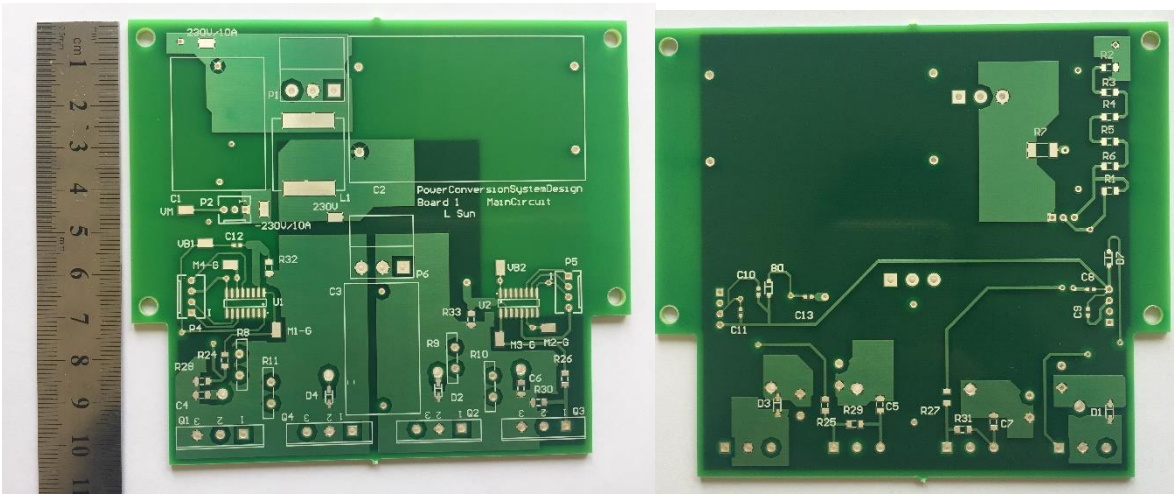

Figure A8-1: Top and bottom photos of PCB board

Figure A8-2: Cross-section view of PCB board

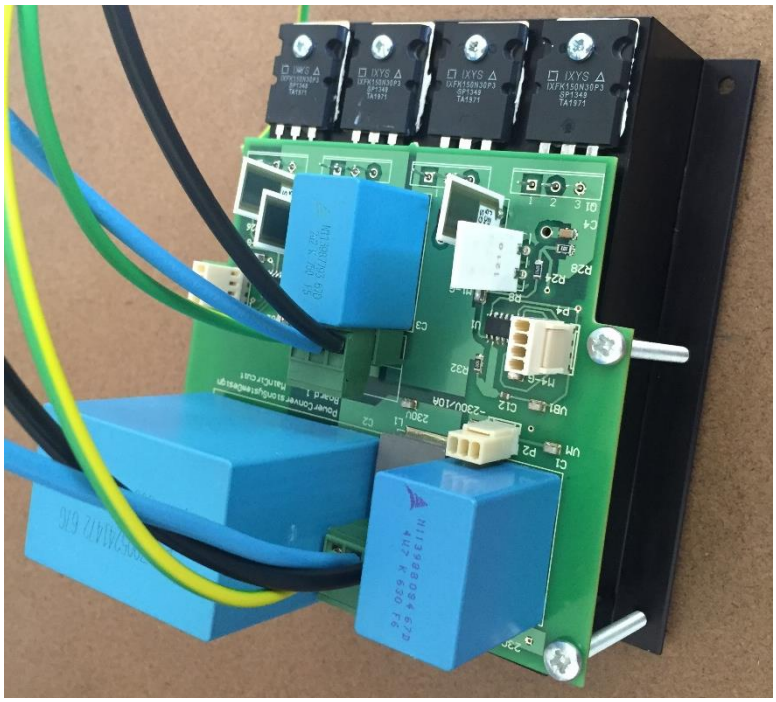

Figure A8-3: Top view of Main board

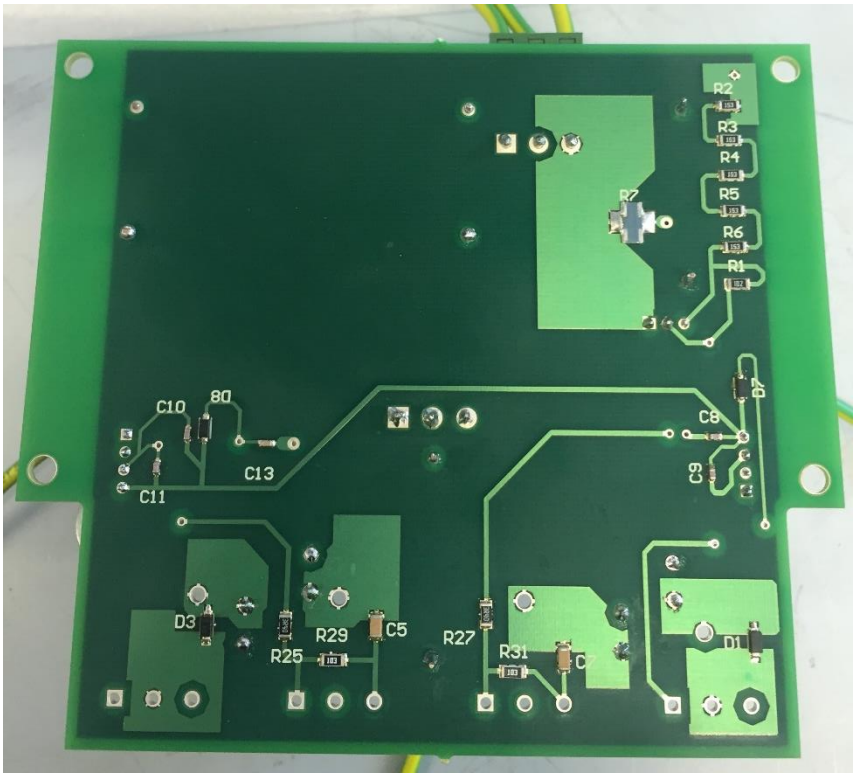

Figure A8-4: Bottom view of Main board